DOE/MC/10637--2827-Task-3.3

DE90 011400

COAL/CHAR REACTIVITY

Final Technical Report for the Period April 1, 1987-March 31, 1988
including the
Quarterly Technical Progress Report for the Period January through March 1988

By

Donald P. McCollor, Philip G. Sweeny, and Steven A. Benson

May 1988

Work Performed Under Cooperative Agreement No. DF-FC21-86MC10637

For
U.S. Department of Energy
Office of Fossil Energy
Pittsburgh Energy Technology Center
Pittsburgh, PA

By
University of North Dakota
Energy & Mineral Research Center
Box 8213, University Station
Grand Forks, ND 58202

DISCLAIMER

TABLE OF CONTENTS

LIST OF TABLES

LIST OF FIGURES

LIST OF FIGURES
(continued)

COAL/CHAR REACTIVITY

Project No.: 4848

Submitted by: M.L. Jones, Director,
Combustion and Environmental Systems Research Institute

Prepared by: D.P. McCollor
P.G. Sweeny
S.A. Benson

Assigned UNDEMRC Personnel: D.P. McCollor
P.G. Sweeny

1.0 EXECUTIVE SUMMARY

- The videomicroscope sizing system was designed and tested. This system is capable of obtaining images of particles concurrently with particle temperature measures. The images are recorded on a video recorder for later playback and image analysis. The actual size and shape of the particles can be used to determine combustion rate data.

- Chars were prepared for combustion testing in the single-particle reactor using a flame burner. The following coals have been prepared: Beulah-Zap (PSOC-1507), Lower Wilcox (PSOC-1443-D), New Mexico Blue (PSOC-1445-D), and Pittsburgh #8 (PSOC-1451-D). All coals, with the exception of Pittsburgh #8, have been demineralized and loaded with specific cations prior to char preparation and combustion testing.

- The morphologies of chars produced in the flame burner have been examined to determine changes as a result of demineralization and readdition of cations. Marked differences have been noted in the distribution of morphotypes between the chars produced from the demineralized coals as compared to the untreated coals. The demineralized coals have higher levels of cenospheres as compared to untreated and cation-loaded coals.

- Surface science studies using Auger and ESCA were performed on the suite of Beulah-Zap chars. The distribution of Na, Al, Si, S, Cl, K, Ca, Fe, C, and O were determined at the surface of the char particle. In addition, etching of the surface was performed to determine the abundance as a function of depth into the char particles. The chemical form of the selected elements was also determined using ESCA.

- The effect of various levels of sodium, potassium, and calcium on the burning rates of chars was examined. Sodium and potassium cations loaded onto the demineralized coal have little or no effect on the char burning rate either by direct catalytic promotion or by alterations in the char morphology when the char is produced. Calcium cation has an enhancing effect on the char burning rate at concentrations on the order of 4000 ppm. Higher loadings at the 27,000 ppm level do not show this effect.

- The ignition apparatus was completed and tested using Pittsburgh #8 (PSOC-1451) coal. The tests were successful, demonstrating the capability of measuring ignition delays and CO/CO_2 production rates from particles having volumes equivalent to those of spheres with diameters of 225 micrometers. Extrapolation of these results indicates a sensitivity limit of approximately 50 micrometer spheres.

- The effect of moisture on the ignition and combustion of the vitrain lithotype of Beulah lignite (PSOC-1507) was determined. No significant effect on the ignition delay or combustion rate was observed.

- The combustion behaviors of vitrain, attritus, and fusain lithotypes of Beulah lignite were examined at 650°C. These materials behaved similarly with the exception of fusain, which had a shorter ignition delay than the other two lithotypes.

- The effect of temperature on the ignition and combustion of the vitrain lithotype of Beulah lignite and Pittsburgh #8 coal was examined. Ignition delays were significantly longer for both materials at 650°C than at 1000°C. The combustion behavior of Pittsburgh #8 at 650°C differs dramatically from that at 1000°C, exhibiting two-stage combustion at 650°C as opposed to single-stage at 1000°C. The Beulah lignite results showed single-stage combustion at both temperatures.

- The effect of coal rank on combustion behavior was determined at both 650° and 1000°C. At 1000°C both lignite and bituminous coal behaved similarly. At 650°C these materials exhibited markedly different behavior, with the lignite being much more reactive.

2.0 GOALS AND OBJECTIVES

The overall objective of the coal/char reactivity project is to expand the fundamental combustion data base to support existing and advanced atmospheric combustion systems. The investigations will focus primarily on elucidating the burning rates of chars under realistic flame conditions as a function of fuel and system parameters. The chars are mainly derived from low-rank coals. The key issues include the relative contributions of inorganic constituents, and the surface and structural effects on the burning behavior of the low-rank coal-derived chars. Tests will be undertaken to ascertain the limits of bulk diffusion control of the burning rate.

A second objective is to perform fundamental investigations on the ignition mechanisms of single particles of low-rank coals by measuring rates of carbon monoxide and carbon dioxide production.

3.0 ASSESSMENT OF THE RELATIVE INFLUENCE OF CATALYTIC MINERAL MATTER EFFECTS AND PHYSICAL STRUCTURE ON THE COMBUSTION RATES OF HIGHLY REACTIVE CHARS

3.1 Equipment

3.1.1 Videomicroscope Particle Sizing System

A videomicroscope system designed to obtain direct particle images and obtain particle size and shape concurrently with temperature measurements, using three-color optical pyrometry, has been constructed and tested. The system provides a means of measuring size and aspect ratio of the same burning particle on which temperature measurements are made. Clear particle silhouettes suitable for analysis can be obtained for the majority of particles.

The optical components of the system consist of the following: a high-intensity microscope strobelight (Sage Instruments Model 550) fitted with an optical slit and lenses to focus the light onto the 1 mm x 1 mm pyrometer control volume, a long-range microscope (Questar Model M1), and a low-light-level black and white video camera (Panasonic Model WV 1550) attached to the camera port of the microscope. To provide sufficient magnification and to mate the camera to the microscope, an adapter was attached to the camera which holds a 2X Barlow lens and an 8 mm microscope eyepiece. If desired, a reticule may be inserted in the adapter between the Barlow lens and the eyepiece to provide a grid or arbitrary scale on the video image.

A diagram of the optical system is shown in Figure 1. The optical axis of the strobelight and microscope is aimed approximately 20 degrees off-axis from the pyrometer viewing axis, with the strobelight next to the pyrometer to minimize light from the strobelight being picked up by the pyrometer. To ascertain the possible interference of the strobelight on the pyrometer signal, tests were conducted using a stationary 150 micrometer nichrome wire as the target. These tests demonstrated that the pyrometer picked up only a weak signal reflected from the highly reflective wire on only the 550 nm channel, and that reflection from the quartz windows of the observation chimney had no effect.

In addition, four further tests, in which actual particle temperature data was obtained using the optical pyrometer with and without the strobelight operating, showed no significant change in either the mean particle temperatures or standard deviations in particle temperature. Therefore, the operation of the videomicroscope was found not to interfere with the particle temperature measurements.

A schematic of the videomicroscope sizing system is shown in Figure 2. While temperature measurements are being made in the laminar flow reactor, the picture from the videomicroscope is continually being recorded by a video recorder (Panasonic Model NV 8950) and displayed on a video monitor (Tandy Portavision Model 16-107). The picture is, of course, dark because of the high microscope magnification unless the strobelight fires. The detection of a particle in the pyrometer control volume by the coincidence detector starts signal acquisition by the waveform analyzer, which sends a trigger signal to the strobelight controller to fire the strobelight. Although the strobelight flash is much faster (less than 10 microseconds) than the camera video scan rate (30 Hz.), the camera vidicon tube acts as a storage device, holding the

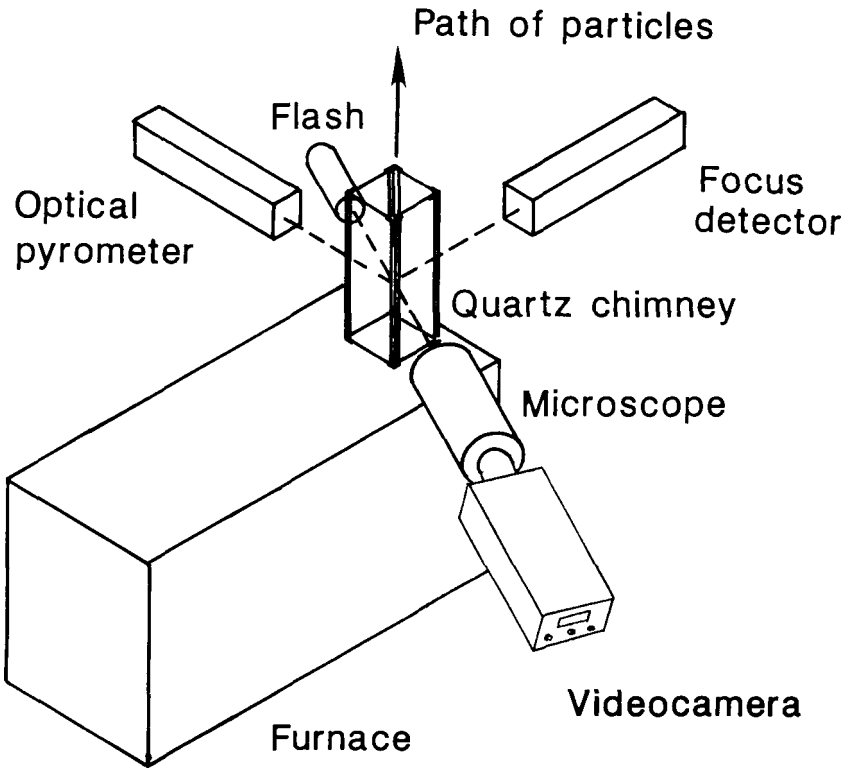

Figure 1. Diagram of the optical system of the videomicroscope particle sizing system.

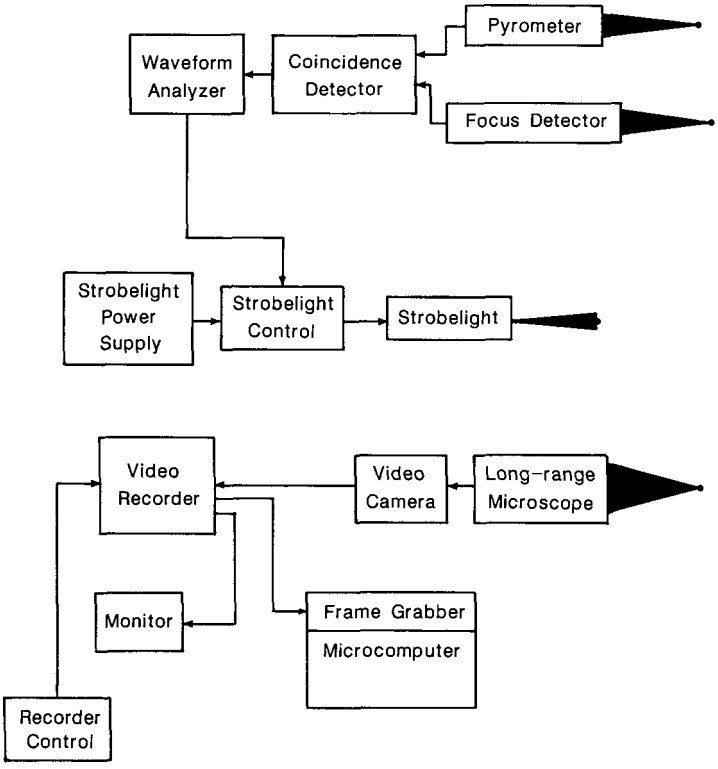

Figure 2. Schematic of the videomicroscope particle sizing system.

particle image for 1 to 3 frames, which are recorded by the VCR. By closely watching the video monitor, persistence of vision also allows one to see the brief particle image as the strobelight fires. If the pyrometer signal is acceptable, the video input signal is switched briefly from the videocamera to a color bar generator to place a visual marker on the videotape. The audio capability of the videotape is used to record particle number and comments.

After the test run, the videotape is scanned, the accepted particle images are found from the markers, and the best frame of each image is held with the freeze-frame capacity of the video recorder. The frame is then transferred to a microcomputer equipped with a video frame-grabber (Chorus Data Systems Model PC-1540 card). The captured image is manipulated, and particle size and shape are determined with image-processing software (Chorus Data Systems Imagepro).

Particle size may be determined in two ways, either from the particle area or by averaging manually selected major and minor axes. The area is determined by drawing a box around the particle and, since the particle is a dark silhouette against a light background, summing the number of pixels in the box which are below a selected intensity. The apparent particle diameter is then calculated from

$$d = 2\sqrt{A / pi} \qquad [1]$$

where A is the particle projected area determined from the video image, and d is the diameter of a spherical particle of the same projected area.

The average particle diameter may also be determined by manually selecting major and minor diameters on the particle image. The average diameter and aspect ratio is then calculated from

$$d = (d\ max + d\ min)/2 \qquad [2]$$

$$aspect\ ratio = d\ max/d\ min \qquad [3]$$

where d max and d min are the major and minor diameters, respectively, of the particle.

The system is calibrated by carefully positioning a thin wire of known diameter at the common focus of the pyrometer, focus detector, and videomicroscope prior to each run. The wire serves the dual purpose of a target to check that all the optics are at a common focus, and as a size calibration. The wire image is recorded on videotape and used to calibrate the x and y dimensions of the pixels of the video image.

3.1.2 Cold-Furnace Particle Detection With Laser Scattering

In order to perform sizing tests with the videomicroscope, it was desirable to have the capability to detect particles and obtain particle images without having the particles burning so that emitted light can be detected by the pyrometer and focus detector. Secondly, the capacity to detect particles without depending on emitted light would be a useful enhancement of the system.

Accordingly, the optical system of the laminar flow reactor was temporarily modified to test the feasibility of using laser light scattered at right angles to the particle to trigger the pyrometer and strobelight, similar to the one used by Sandia (1). The modified arrangement is shown in Figure 3. The focus detector is used to detect light from the small helium-neon laser (Spectraphysics Model 155, 0.95 mW) scattered from the particles. For these tests, the laser beam was not collimated, and no bandpass filter was used in the focus detector optics. It should be noted that in the configuration of Figure 3, the primary laser beam is aimed directly into the pyrometer. However, since the pyrometer narrow-bandpass filters reject the 632.8 nm beam, the only effect is an approximate doubling of the background noise level. Since the pyrometer was not used in these cold-flow tests, this was of no importance. If the pyrometer is to be used, a reconfiguration of the optical set-up would be necessary.

The cold-flow tests were successful in that there was a marked improvement in the number of acceptable particle images obtained by this triggering method. However, the rate of triggering by the particles was much lower than expected from the particle density in the observation chimney. This was probably due to the low power of the available laser. Overall, the tests demonstrated that the laser-scattering method was workable with the existing optical system and that, with improvements, it could be used as an alternative to the present emitted-light triggering method.

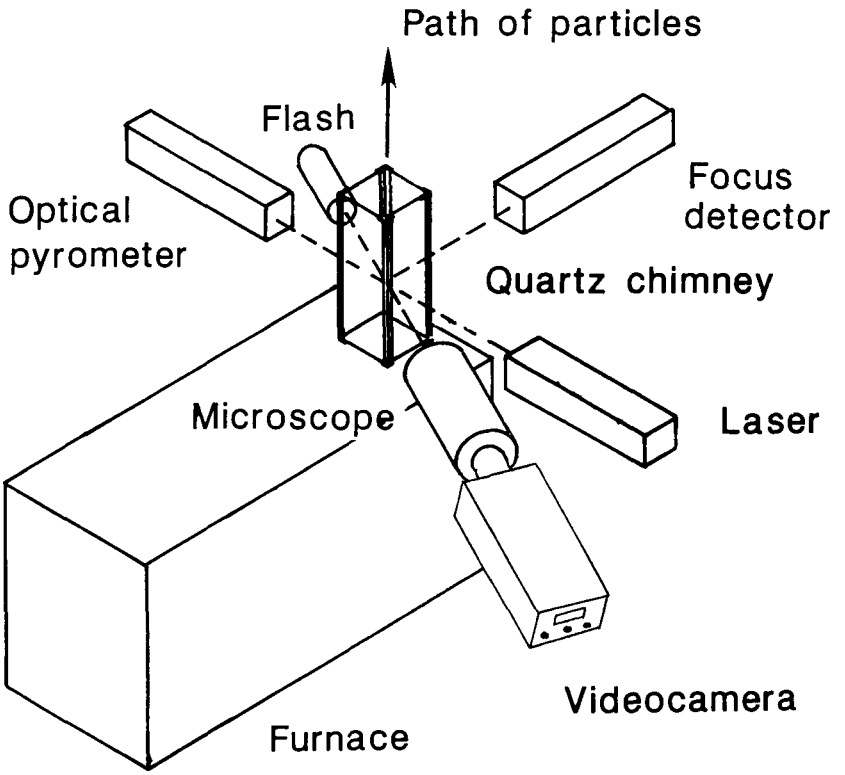

Figure 3. Modified trigger arrangement for the optical pyrometer.

3.2 Preparation and Characterization of Chars

3.2.1 Coal Samples

Samples of Beulah-Zap (ND) lignite, Lower Wilcox (TX) lignite, New Mexico Blue (NM) subbituminous coal, Smith-Roland (WY) subbituminous coal, and Pittsburgh (PA) #8 bituminous coal were obtained from the Pennsylvania State University coal sample bank. The identifying sample bank numbers are:

Beulah-Zap	PSOC-1507
Lower Wilcox	PSOC-1443-D
New Mexico Blue	PSOC-1445-D
Smith-Roland	PSOC-1520-D
Pittsburgh #8	PSOC-1451-D

The "-D" designation indicates air-classified samples prepared and distributed under the direction of the Pittsburgh Energy Technology Center, U.S. Department of Energy. It should be noted that the sample of Beulah-Zap lignite was obtained directly from the sample bank before the size-graded samples were available and does not bear the "-D" designation. The proximate and ultimate analyses of these coals are given in Table 1.

3.2.2 Preparation of Demineralized and Cation-Loaded Coals

Coals were demineralized by treatment in sequence with hydrochloric, hydrofluoric, and hydrochloric acids, followed by washing with water to remove residual acid. The detailed procedure is as follows:

(1) The coal was placed in a plastic beaker and 100 ml of concentrated HCl added and stirred for 1 hour at 50°C.

(2) The suspension was filtered using a vacuum millipore filter with HVLP filter paper. The filtrate was discarded and the residue washed once with 100 ml distilled water.

(3) The residue was removed from the paper, placed in a plastic beaker with 100 ml of concentrated HF, and stirred for 1 hour at 50°C.

(4) The suspension was filtered as in (2).

(5) The residue was removed from the filter paper and placed in a plastic beaker with 100 ml of concentrated HCL and stirred for one hour at 50°C.

(6) The suspension was filtered using a pressure millipore and HVLP filter paper. Approximately twelve 100 ml washes of distilled water were used until a test of the filtrate with $AgNO_3$ indicated that no residual chloride ion was present.

(7) The filtrate was discarded, and the residue either air-dried or dried under mild vacuum in a vacuum desiccator.

TABLE 1

PROXIMATE AND ULTIMATE ANALYSES OF THE TEST COALS

BEULAH-ZAP (PSOC 1507):

Proximate	As Received, Wt%	Ultimate	Dry Basis, Wt%
Moisture	33.57	Carbon	62.61
Volatile Matter	27.08	Hydrogen	4.41
Fixed Carbon	31.06	Nitrogen	0.83
Ash	8.30	Oxygen[a]	18.21
		Sulfur	1.43

NEW MEXICO BLUE (PSOC 1445D):

Proximate	As Received, Wt%	Ultimate	Dry Basis, Wt%
Moisture	10.30	Carbon	73.76
Volatile Matter	39.20	Hydrogen	5.54
Fixed Carbon	47.03	Nitrogen	1.23
Ash	3.46	Oxygen[a]	14.83
		Sulfur	0.76

LOWER WILCOX (PSOC 1443D):

Proximate	As Received, Wt%	Ultimate	Dry Basis, Wt%
Moisture	15.70	Carbon	56.43
Volatile Matter	36.24	Hydrogen	4.43
Fixed Carbon	32.26	Nitrogen	1.02
Ash	15.79	Oxygen[a]	18.53
		Sulfur	0.84

PITTSBURGH #8 (PSOC 1451D)

Proximate	As Received, Wt%	Ultimate	Dry Basis, Wt%
Moisture	1.50	Carbon	62.85
Volatile Matter	34.67	Hydrogen	4.50
Fixed Carbon	43.74	Nitrogen	1.11
Ash	20.07	Oxygen[a]	5.94
		Sulfur	5.19

[a] Determined by difference.

The demineralization removes essentially all mineral matter except for small amounts of iron sulfides and traces of aluminosilicate clay material.

Portions of the demineralized coals were then cation-loaded with either calcium, potassium, or sodium cations by ion-exchanging the coal in a solution of the corresponding acetate using a procedure derived from that used to determine carboxyl groups (2). The detailed procedure for cation-loading the demineralized coal is as follows:

(1) Approximately 20 grams of the demineralized coal is placed in a large flask and 1000 ml of a 1.1 M solution of the desired acetate added (i.e., calcium, potassium, or sodium acetate). The suspension is stirred for 20 hours at room temperature, and then filtered.

(2) The filtrate is discarded, and the residue washed with 100 ml of distilled water to remove residual acetate solution.

(3) The residue is removed from the filter paper and air dried or dried under mild vacuum in a vacuum desiccator.

Demineralized, calcium-loaded, potassium-loaded, and sodium-loaded samples of the Beulah-Zap, Lower Wilcox, New Mexico Blue, and Pittsburgh #8 coals. Approximately 90 g of each coal was demineralized, and portions of this reloaded with each cation, yielding approximately 20 g of demineralized and 20 g of each cation-loading for each coal. Since the "-D" designated coals were supplied in several size fractions, equal amounts of each size fraction for these coals were combined before demineralization to ensure that a sufficient amount of the size fractions of interest would be obtained after the demineralization, cation-loading, and char preparation processes. Table 2 lists the size ranges used, amounts used, and sonic sieve analysis of the coals. Table 3 gives the calcium, potassium, and sodium concentrations in the coal samples as determined by inductively coupled-plasma emission spectroscopy (ICP) analysis.

3.2.3 Char Nomenclature

A substantial number of coal and char samples have been prepared, several using "nonstandard" procedures. As the investigation proceeded, the naming of the samples evolved to cover new circumstances. In addition, the inclusion of data from Young et al. (3) and Young and Niksa (4), and combustion tests on samples used in those studies make a unification of the nomenclature used to identify the char samples necessary. The nomenclature which will be used is given in Table 4. Occasionally, the full designation (i.e., demineralized Beulah char) will be used instead of the abbreviated designation.

TABLE 2

SIZE RANGES, AMOUNTS USED, AND SONIC SIEVE ANALYSIS OF THE TEST COALS

Coal	Size Range Used (microns)	Mean Coal Size (microns)	Coal Used for Char Production (grams)
BEULAH-ZAP:			
Untreated	53-106	76	6.4531
Demineralized	53-106	84	24.6019
Calcium-loaded	53-106	80	18.8872
Potassium-loaded	53-106	75	19.5330
Sodium-loaded	53-106	83	14.5396
NEW MEXICO BLUE:[a]			
Untreated	53-106	102	15.5576
Demineralized	53-106	103	24.4427
Calcium-loaded	53-106	82	30.7315
Potassium-loaded	53-106	94	28.6122
Sodium-loaded	53-106	99	29.5846
LOWER WILCOX:[b]			
Untreated	53-106	80	22.5389
Demineralized	53-106	100	26.8769
Calcium-loaded	53-106	77	27.1439
Potassium-loaded	53-106	96	29.8705
Sodium-loaded	53-106	90	27.9925
PITTSBURGH #8:[b]			
Untreated	53-106	80	26.8493

[a] 100 g of each of the following size fractions were combined: 45-63 microns, 63-75 microns, 75-106 microns. The mixture was sieved to separate the 53-106 micrometer fraction.

[b] 100 g of each of the following size fractions were combined: 53-63 microns, 63-75 microns, 75-106 microns.

TABLE 3

CATION CONCENTRATIONS IN THE TEST COALS
(PPM DRY COAL BASIS)

	Calcium	Potassium	Sodium
BEULAH-ZAP:			
Untreated	32,000	820	7,900
Demineralized	<220	<220	420
Calcium-loaded	34,000	<250	<250
Potassium-loaded	<2,500	45,000	3,300
Sodium-loaded	<400	<400	26,000
BEULAH-ZAP 2:[a]			
Demineralized	1,500	<600	<1,000
Calcium-loaded	40,000	<600	<1,000
Potassium-loaded	<500	57,000	<1,000
NEW MEXICO BLUE:			
Untreated	700	<600	<1,000
	900	<500	<500
Demineralized	<200	<600	<1,000
Calcium-loaded	10,000	<500	<500
Potassium-loaded	200	21,000	<500
Sodium-loaded	<200	<600	11,000
LOWER WILCOX:			
Untreated	17,000	<550	<1,000
Demineralized	7,000	<500	<500
Calcium-loaded	59,000	<500	<500
Potassium-loaded	1,600	40,000	<1,000
Sodium-loaded	900	<500	32,000

[a] Second preparation, referred to as Beulah 2 in text

TABLE 4

CHAR NOMENCLATURE

Char	Explanation
LNB	Low-sodium Beulah lignite char used by Young, et al. (3) and Young and Niksa (4). This char was prepared by pyrolysis in the laminar flow reactor in nitrogen at 1000K gas temperature and 111 ms residence time.
B1	First preparation of char from the Pennsylvania State University Coal Sample Bank sample of Beulah lignite coal (PSOC-1507). This sample was obtained before the DOE "-D" sized coal samples were available and does not carry the "-D" designation. The char was prepared in an air-natural gas flame burner at approximately 3% excess oxygen and a residence time of approximately 110 ms.
B2	Second preparation of char from Beulah-Zap lignite. (PSOC-1507). Char was prepared in the same manner as the B1 char.
NMB	Char prepared from the DOE-supplied sized sample of New Mexico Blue subbituminous coal from the Pennsylvania State University Coal Sample Bank (PSOC-1445-D). The char was prepared in the same manner as the B1 char.
LWX	Char prepared from the DOE-supplied sized sample of Lower Wilcox lignite from the Pennsylvania State University Coal Sample Bank (PSOC-1443-D). The char was prepared in the same manner as the B1 char.
P8	Char prepared from the DOE-supplied sized sample of Pittsburgh #8 bituminous coal from the Pennsylvania State University Coal Sample Bank (PSOC-1451-D). The char was prepared in the same manner as the B1 char.
B1(UT) B2(UT) NMB(UT) LWX(UT) P8(UT)	Designates char prepared from the parent coal without any pretreatment or cation loading.

TABLE 4 (continued)

CHAR NOMENCLATURE

Char	Explanation
LNB(DM) B1(DM) B2(DM) NMB(DM) LWX(DM)	Designates that the parent coal was demineralized using concentrated hydrochloric and hydrofluoric acids before the char was produced.
LNB(HCl) B1(HCl)	Designates that the parent coal was partially demineralized with concentrated hydrochloric acid only before the char was produced.
B1(CA), B1(K), B1(NA) B2(CA), B2(K), B2(NA) NMB(CA), NMB(K), NMB(NA) LWX(CA), LWX(K), LWX(NA)	Designates that the parent coal was demineralized with concentrated hydrochloric and hydrofluoric acids and the demineralized coal reloaded with the respective cation by an ion-exchange process before the char was produced.
B2(DM-RDM) B2(CA-RDM) B2(K-RDM) B2(NA-RDM)	Designates that the char was "redemineralized" with 1 M hydrochloric acid after the char was produced.

3.2.4 Char Preparation

Chars of the complete sample suites (untreated, demineralized, calcium-loaded, potassium-loaded, and sodium-loaded samples) have been prepared in the flame burner for the Beulah-Zap, Lower Wilcox, and New Mexico Blue coals. Char from the untreated sample of Pittsburgh #8 has also been prepared. Each char was produced in a small excess of oxygen, normally 2% to 4%. Oxygen concentration was determined using gas chromatography or non-dispersive IR analysis.

The flame burner is a small laminar flame burner fired with air-natural gas designed to produce small amounts of char samples under realistic flame conditions. A schematic of the flame burner is shown in Figure 4. The gas temperatures, corrected for radiation, range from approximately 1500K (1370K uncorrected) at the coal injection point to approximately 1050K (1020K uncorrected) at the char collection point. The char is collected with a nitrogen-quenched extraction probe 200 mm above the injection point, corresponding to an estimated residence time of 150 ms.

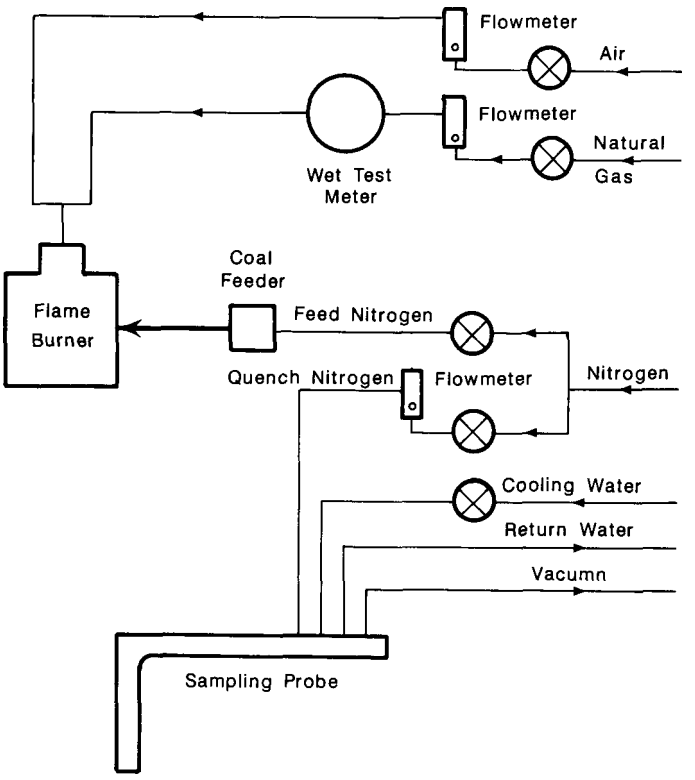

Figure 4. Schematic of the flame burner used to prepare char samples.

The collected chars were sized with the sonic sieve to obtain a particle size distribution, and to separate size fractions of each char for subsequent combustion tests. Table 5 gives the preparation conditions and sieve analysis for the chars. Table 6 gives the cation concentrations in the chars as determined by flame atomic absorption analysis (flame AA).

3.2.5 Special Char Preparations

Several char samples were prepared under "nonstandard" conditions rather than the procedures used in 3.2.2 and 3.2.4. To avoid confusion, these special preparation conditions are described, since combustion data concerning them appears in Appendix I.

(1) A sample of demineralized Beulah-Zap lignite char was produced in 8% oxygen instead of the nominal 2%-4% oxygen. Several combustion tests were performed on this char before it was decided to produce another char sample at lower excess oxygen. This char is listed in the Appendix as B(DM-8.0%).

(2) A sample of the Beulah-Zap lignite was partially demineralized using only HCl instead of the normal HCl and HF. This char is listed as B(HCl-2.3%) in the Appendix.

TABLE 5

PREPARATION CONDITIONS AND SIEVE ANALYSIS OF THE CHARS

Char	Size range Used (microns)	% O_2	Burner Temp. 0mm (degrees C)	Burner Temp. 200mm (degrees C)	Net Char Produced (grams)	% Char Produced	Mean Char Size (microns)	% >106 (microns)
BEULAH-ZAP:								
Untreated	53-106	1.90	1147	850	3.7770	38.8	56.0	1.4
	53-106[a]	2.50	1108	875	2.4543	38.0	67.0	1.9
Demineralized	53-106	2.50	1050	840	2.8214	54.3	63.0	--
	53-106[a]	2.25	1081	800	7.2055	29.3	92.0	18.1
Calcium-loaded	53-106	3.70	1120	820	4.8936	41.4	75.0	3.5
	53-106[a]	2.75	1167	812	5.6577	30.0	87.0	10.5
Potassium-loaded	53-106	2.75	1140	845	3.2816	31.0	93.0	26.1
	53-106[a]	2.00	1108	905	5.605	29.0	72.0	6.7
Sodium-loaded	53-106	2.76	1139	850	2.8597	25.9	72.0	6.5
	53-106[a]	1.60	1125	860	3.1714	21.8	79.0	9.5
NEW MEXICO BLUE:								
Untreated	45-106	2.90	1170	915	4.0282	25.9	84.0	4.2
Demineralized	53-106	1.80	1100	770	8.3914	34.3	63.0	1.1
Calcium-loaded	53-106	2.20	1083	760	10.5177	34.2	83.0	0.1
Potassium-loaded	53-106	2.20	1123	835	9.5461	33.4	90.0	2.5
Sodium-loaded	53-106	2.20	1098	863	13.8450	46.8	96.0	10.6
LOWER WILCOX:								
Untreated	53-106	2.10	1105	800	9.2822	41.2	74.0	0.1
Demineralized	53-106	3.30	1080	815	7.4110	27.6	84.0	1.6
Calcium-loaded	53-106	2.80	1078	775	10.7560	39.6	66.0	0.1
Potassium-loaded	53-106	2.00	1148	745	10.9108	36.5	82.0	1.6
Sodium-loaded	53-106	2.10	1105	805	2.2837	8.2	53.0	0.7
PITTSBURGH #8:								
Untreated	53-106	3.50	1142	715	8.0355	29.9	58.0	1.1

[a] Referred to as Beulah 2 in the text, determined from a second preparation.

TABLE 6

CATION CONCENTRATIONS IN THE BEULAH-ZAP CHARS
ANALYSIS OF 75-90 MICRON CHARS

Char	Concentration[a] Calcium (ppm)	Potassium (ppm)	Sodium (ppm)
LNB(DM)	356	82	182
B1(DM)	288	777	138
B2(DM)	4,220	66	287
B2(CA)	65,200	420	469
B2(K)	699	66,900	409
B2(NA)	327	93	51,700
B2(DM-RDM)	1,990	12	49
B2(CA-RDM)	27,100	35	33
B2(CA-RDM-2)[b]	28,300	15	25
B2(K-RDM)	417	596	82
B2(NA-RDM)	254	31	495

[a] Determined by flame AA.
[b] Second demineralization of B2(CA) with 1 M HCl for three hours.

(3) An older char, LNB(N2), produced from another low-sodium Beulah lignite by pyrolysis in nitrogen in the laminar flow reactor, was examined to confirm that previous mean particle temperature measurements could be reproduced.

(4) A "practice" sample of Beulah lignite obtained from a pilot-plant combustion test ongoing at the time in the particulate test combustor (PTC), was used in the flame burner to check the reproducibility of char preparation and any effect of char preparation in the flame burner on combustion behavior in the laminar flow reactor.

(5) Several char samples were treated with dilute hydrochloric acid to "redemineralize" them by removing their cation loadings and other residual minerals. These have a suffix "-RDM" and will be dealt with in greater detail later.

3.3 Physical Properties of Chars

3.3.1 Changes in Particle Size Distribution During Char Production

Prior to producing the chars in the flame burner, the size distributions of the input coals were determined by sieve analysis using a sonic sieve. The 53-106 micrometer fraction of the coal was used to prepare the corresponding char. A sieve analysis of the char was then performed to determine the char size distribution, as well as to separate the individual sieve size fractions for subsequent experiments.

Table 5 gives the mean particle size by mass of the input coals and the char produced from each coal. The mass fraction of each char >106 micrometers is also given. Since the input coals were in the size range 53-106 micrometers, the presence of a significant amount of char of size >106 micrometers is evidence of agglomeration and/or swelling behavior during the char formation process. A comparison of mean particle sizes of the input coal and the coal char should be treated with caution, since the char recovery is not quantitative, and burn-out of finer material will tend to shift the mean size to a higher value.

Although the variation between the first and second preparations of the Beulah-Zap chars is substantial, the maximum amount of >106 micrometer char in the samples gives a rough indication of the relative swelling/agglomeration behavior. The untreated Beulah-Zap char showed little or no evidence of swelling/agglomeration, while the calcium-loaded and sodium-loaded char gave moderate swelling/agglomeration. Extensive swelling/agglomeration was seen for the demineralized and potassium-loaded chars. The change in mean particle size between the Beulah-Zap coals and coal chars approximately parallels this, with the the mean char particle size decreasing slightly from that of the parent coal for the untreated, calcium-loaded, and sodium-loaded samples, while the demineralized and potassium-loaded mean char size increases markedly.

The behaviors of the New Mexico Blue and Lower Wilcox chars are strikingly different than those of the Beulah-Zap chars. The demineralized and potassium-loaded New Mexico Blue chars had less material in the >106 micrometer size range than did the untreated char. The sodium-loaded New Mexico Blue char had the only significant amount of char in the >106 micrometer size range, while none of the Lower Wilcox chars had significant material in this size range. Further, the mean particle sizes of these chars decreased from or remained the same as that of the parent coals.

The behavior of the untreated Pittsburgh #8 char is rather interesting, as there was virtually no char material produced that was in the >106 micrometer size range, and the mean particle size decreased drastically from that of the parent coal.

3.3.2 Terminology Used in Char Morphology Analysis

Standard terminology uses three general classifications in describing char morphology: 1) cenospheres, 2) honeycomb, and 3) unfused. While examining the chars produced from the lower-rank coal samples, subdivisions or possibly new types were identified. The descriptions of the important char

types are given below. The new terms, while primarily given here for the purposes of this report, have also been given as part of a presentation (5). Figure 5 illustrates the different char morphotypes.

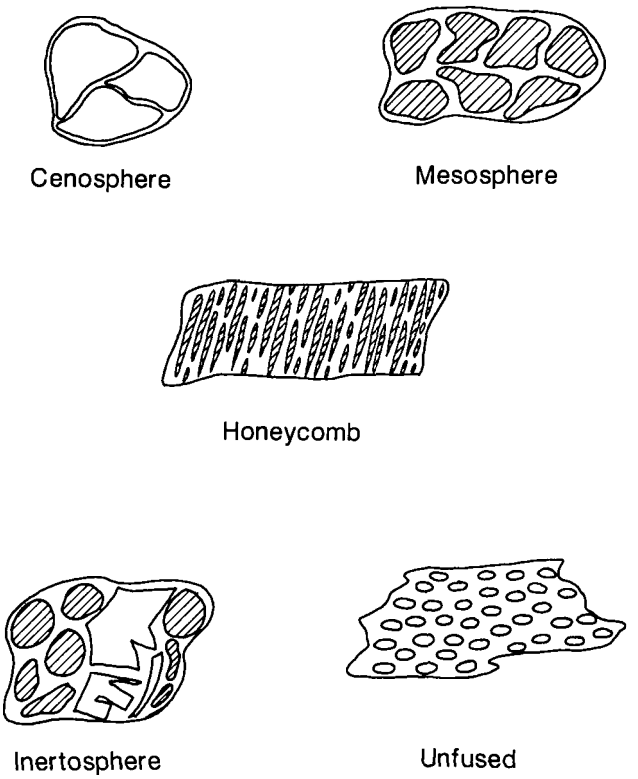

Figure 5. Sketches of major morphotypes.

Cenosphere: Typically has more pore (void) space than wall material. The overall shape of the particle is spherical. Well-developed cenospheres have three or less major pore openings which may account for up to 90% of the volume of the particle. The walls enclosing the pores are generally thin and commonly broken. The walls are typically free of smaller (secondary) pores. The pore morphology is round to slightly "umbrella" shaped.

Mesosphere (new term): Typically has more than three major pores which account for most of the porosity. The walls are three to five times thicker than those in the cenospheres and commonly contain secondary pores. The pores and wall material are approximately equal in total particle volume. The walls appear to be very solid and generally do not show signs of breakage. The particle shape is moderately spherical, but can occur in an irregular shape with subangular edges. All solid material within the particle appears to be homogeneous.

Honeycomb A: The pore-to-solid ratio of these particles is less than one. The particles are typically rectangularly shaped (2:1 length-to-width ratio), but can occur with a very rectangular outline. The pores are elongated and are normally subparallel to parallel to the short side. The walls contain a few, widely dispersed secondary pores. The solid portion of the particle commonly appears to be heterogeneous, with fragments of higher reflecting material.

Honeycomb B: Same morphological type as above, but having a significantly lower reflectance.

Inertosphere (new term): These particles always having an irregular shape, and are typically angular with many sides. The pores make up approximately 30% of the total volume and have an elongated-to-very-spherical morphology with no distinct orientation pattern. The most distinctive feature of this type is the heterogeneity of the solid portion. As in the honeycomb type, included fragments have a significantly variable reflectance value. Unlike the honeycomb type, these fragments have recognizable inertinite maceral remnants from the original coal. Some of these particles appear to be agglomerates of very fine, unfused char particles (<5 micrometers).

Unfused A: This type occurs as a massive particle with few to no pores. The particle outline is rectangular to irregular. Some particles have what appear to be desiccation cracks. The particles appear to be homogeneous in composition, but typically have a mottled reflectance. This type almost always resembles inertinite maceral morphology, such as fusinite, macrinite, and sclerotinite.

Unfused B: This type has the same characteristics as the Unfused A type with the exception that the reflectance value is much lower.

Mineral-Rich: This type is extremely similar to the Inertosphere with the exception of the presence of a high percentage of either pyrite or clay-type minerals. The minerals typically occur in bands approximately 20 micrometers thick. The inorganic phases (minerals) constitute more than 30% of the particle volume. Any particle with less than 34% minerals was not included in this group; therefore the percentage of mineral-rich char is not a true representation of the total mineral content of the sample.

For purposes of the following discussion, no distinction is made between subtypes (i.e., Honeycomb A and Honeycomb B and Unfused A and Unfused B) to simplify the data presented.

3.3.3 Morphology of Chars

The morphology of the suites of chars produced from the Beulah, New Mexico Blue, and Lower Wilcox coals has been examined. Since only a limited amount of sample was available, the standard preparation technique of preparing the sample in epoxy plugs was modified to concentrate a small amount of sample in one region of the plug (6). Char morphology analyses were performed using both reflected white-incident and fluorescent light microscopy. Quantitative analyses were performed using standard petrographic

point-counting techniques (7). A total of 100 char particles were identified for each sample. Each char morphotype was reported as a volume percent of the total sample. For the Beulah chars, char residues were also collected at 100, 150, and 200 mm above the particle injection point in the laminar flow reactor chimney, corresponding to residence times of 56, 83, and 111 ms, respectively. The morphology of the Beulah char residues have been reported previously (7).

Description and sketches of the morphotypes were given in Section 3.2.2 and Figure 5, respectively. The results of the morphology analyses of the Beulah-Zap, New Mexico Blue, and Lower Wilcox chars are given in Table 7.

TABLE 7

CHAR MORPHOLOGY ANALYSES
(VOLUME %)

Morphotype	Untreated	Demineralized	Ca-loaded	K-loaded	Na-loaded
BEULAH-ZAP:					
Cenosphere	2.0	40.0	2.8	7.8	8.0
Mesosphere	38.0	41.6	46.8	64.0	60.8
Honeycomb	43.6	5.4	39.4	14.2	16.4
Inertosphere	7.2	2.8	3.8	4.8	8.2
Unfused	1.6	8.2	5.8	7.4	5.6
Mineral-rich	7.4	2.0	1.4	1.8	1.0
NEW MEXICO BLUE:					
Cenosphere	57.0	77.0	3.0	5.0	15.0
Mesosphere	30.0	16.0	44.0	72.0	69.0
Honeycomb	3.0	2.0	35.0	13.0	8.0
Inertosphere	3.0	1.0	9.0	5.0	5.0
Unfused	6.0	4.0	9.0	5.0	3.0
Mineral-rich	1.0	0.0	0.0	0.0	0.0
LOWER WILCOX:					
Cenosphere	3.0	28.0	3.0	7.0	4.0
Mesosphere	11.0	59.0	30.0	47.0	65.0
Honeycomb	37.0	2.0	38.0	20.0	9.0
Inertosphere	27.0	5.0	19.0	22.0	11.0
Unfused	13.0	6.0	6.0	4.0	11.0
Mineral-rich	9.0	0.0	4.0	0.0	0.0

The demineralized chars show a dramatic increase in the number of cenospheres and mesospheres over the untreated chars, with the cenospheres predominating in the Beulah-Zap and New Mexico Blue demineralized chars, and the mesospheres predominating in the Lower Wilcox demineralized char. The calcium-loaded chars have a morphology approximating those of the untreated chars, except for a moderate increase in the number of mesospheres. However, the sodium- and potassium-loaded chars show a large increase in the number of mesospheres, apparently at the expense of the cenosphere and honeycomb populations.

The mineral matter in New Mexico coals consists mainly of discrete mineral phases with little or no organically bound cations. Thus demineralization of the New Mexico Blue coal would have little effect on its behavior during char preparation. Addition of the calcium cation to the demineralized New Mexico Blue coal also had little effect. However, the addition of potassium and especially sodium cations increased the swelling/agglomeration tendency of this coal.

The char morphology analysis of the New Mexico Blue chars in Table 7 shows that the untreated and demineralized chars are comprised primarily of cenospheres and mesospheres, with the cenospheres predominating. The calcium-loaded char shows a modest increase in mesospheres and a drastic increase in cenospheres. In fact, the morphology of the calcium-loaded New Mexico Blue char closely resembles that of the untreated and calcium-loaded Beulah chars. It is interesting to note that, although cenospheres and mesospheres predominate in the untreated and demineralized New Mexico Blue chars, very little swelling/agglomeration behavior was seen, as was the case in the demineralized Beulah-Zap char.

The Texas lignite coals also produced very little char in the >106 micrometer size range during char preparation, and all chars (untreated, demineralized, and cation-loaded) showed a decrease in mean particle size from the input coal. Here, the presence or absence of organically bound cations appeared to have little effect on the charring process, and no swelling/agglomeration was seen for any of the chars. The morphology of the Texas lignite chars shown in Table 7 generally supports this, with the untreated and calcium-loaded chars having mesosphere populations similar to that of the untreated Beulah char, but also having significant numbers of honeycomb, inertosphere, and unfused structures. The demineralized, sodium-loaded, and potassium-loaded chars show a substantial increase in mesospheres similar to that of the corresponding Beulah chars, but do not seem to exhibit the same gross swelling/agglomeration behavior.

Several conclusions can be drawn from the combined sieve analyses and char morphologies:

(1) The demineralization process increases the number of cenospheres and, secondarily, mesospheres at the expense of the honeycomb structures. It is suggested that the cenospheres either form from mesospheres and mesospheres from honeycomb structures during the char formation, or all form from a common coal precursor, the relative number of each depending on cation content of the coal.

(2) The presence of organically bound calcium, potassium, or sodium ions inhibits cenosphere formation, favoring instead mesosphere formation (or preservation) instead. Furthermore, sodium and potassium ions increase the number of mesospheres at the expense of the honeycomb structures. In contrast, calcium ions produce (or maintain) roughly equal numbers of mesospheres and honeycomb structures at the expense of cenospheres. The calcium ion appears to be the ion responsible for inhibiting swelling behavior by inhibiting the formation of large numbers of cenospheres and/or mesospheres.

(3) The unfused and inertosphere structures are more or less unaffected by demineralization or cation loading.

3.3.4 Surface Analysis of Coals and Chars

The results of a scanning electron microscope (SEM) energy dispersive x-ray analysis of untreated, demineralized, calcium-, sodium-, and potassium-loaded Beulah-Zap chars are given in Table 8. The SEM analysis represents a sample volume to a depth of 1 micrometer (10,000 angstroms) into the char. Area scans were obtained to examine a random array of particles. This relatively deep analysis should approximate a bulk analysis. Comparison with the flame atomic absorption measurements in Table 6, however, indicates that either the SEM technique underestimates the Ca, Na, and K concentrations or that the surface layer of the char is depleted in these elements. The average concentration for the five SEM analyses is also given in Table 8. The results indicate that the demineralization step removes essentially all the sodium and calcium from the B1(DM) char. The sodium-loaded B1(NA) sample had a sodium content similar to that of the untreated B1(UT) char, while the calcium enrichment in the B1(CA) char was about twice that of the untreated char. The potassium enrichment of B1(K) was 0.271 atomic percent. The untreated B1(UT) char contained no significant amount of potassium.

TABLE 8

SEM ANALYSIS OF BEULAH LIGNITE CHARS[a]

	Atomic % of Elements[b]									
Sample	Na	Mg	Al	Si	S	Cl	K	Ca	Fe	C
Untreated	0.21	0.15	0.14	0.20	0.06	0.01	0.01	0.37	0.07	98.8
Demineralized	0.01	0.0	0.0	0.02	0.04	0.01	0.0	0.01	0.02	99.9
Sodium-loaded	0.25	0.0	0.0	0.01	0.03	0.01	0.0	0.0	0.02	99 7
Calcium-loaded	0.01	0.01	0.0	0.01	0.06	0.04	0.0	0.8	0.03	99.0
Potassium-loaded	0.01	0.0	0.0	0.01	0.27	0.01	0.27	0.0	1.0	98.4

[a] Area scans results normalized with C.
[b] Average values of five.

The results of ESCA (electron spectroscopy for chemical analysis) survey scans are given in Table 9 for the five char samples along with a survey scan of the raw Beulah coal in Table 10 as a reference. ESCA provides an analysis for a very shallow volume of the sample, penetrating only about 50 angstroms into the sample. Thus the technique is a surface analysis.

TABLE 9

ESCA SURVEY SCANS OF BEULAH LIGNITE CHARS

	Atomic % of Elements[a]									
Sample	Na	Al	Si	S	Cl	K	Ca	Fe	C	O
Untreated	3.9	0.9	0.4	0.7	ND	ND	1.2	0.0	78.0	14.5
Demineralized[b]										
Sodium-loaded	12.7	ND	0.1	0.9	ND	ND	0.1	ND	68.2	17.7
Calcium-loaded	0.3	0.4	0.0	0.6	0.2	ND	4.6	ND	71.4	20.8
Potassium-loaded	0.5	0.2	0.0	1.4	0.5	6.3	0.1	0.0	68.2	22.3

ND = Not Detected.
[a] One determination.
[b] No results could be obtained for this sample.

TABLE 10

ESCA SURVEY SCAN OF BEULAH COAL

	Atomic % of Elements[a]									
Sample	Na	Al	Si	S	Cl	K	Ca	Fe	C	O
Raw Coal:										
Beulah-Zap	0.9	2.2	1.7	0.0	0.0	ND	0.2	0.0	71.3	23.1

ND = Not Determined.
[a] One determination.

The sodium-loaded B1(NA) sample had a sodium surface enrichment (by ESCA) of 12.7 atomic percent, approximately four times the surface concentration of sodium on the untreated B1(UT) char. A surface sodium concentration of approximately 1 atomic percent was observed for the raw Beulah coal.

The surface concentration of calcium was less than that for sodium in the B1(UT) char and increased to approximately 5 atomic percent on the surface of the calcium-loaded B1(CA) char sample. Potassium was not detectable on the surface of the B1(UT) char and was approximately 6 atomic percent on the surface of the potassium-loaded B1(K) char. The calcium-, sodium-, and potassium-loaded chars all displayed an increase in the outermost surface concentration of their respective cation, a small decrease in carbon concentration, and a small increase in oxygen concentration.

The next step in the ESCA analysis was to follow the concentrations of elements as a function of depth into the samples. This is accomplished by etching the sample with an ion beam for specified periods of time, followed by an ESCA scan of the newly exposed surface. The depth to which a particular sample is etched away is highly dependent on the sample; however, the chars examined are physically similar. Thus the depths of etching for a given etching time are expected to be similar, although the absolute depth of etching is less certain.

The results of the depth profiles for the untreated sodium-loaded and potassium-loaded chars are summarized in Tables 11 a-c. The untreated char had a slightly lower concentration of sodium and calcium on the outermost surface, but the concentration remained constant in the depth range of approximately 200-600 angstroms. The sodium-loaded sample displayed a small increase in sodium after the outermost surface was removed and a continuous decrease in oxygen concentration with increasing depth. The potassium-loaded sample showed the largest concentration on the outermost surface, and the oxygen concentration also decreased with increasing penetration into the sample.

TABLE 11a

ESCA DEPTH PROFILE OF UNTREATED BEULAH CHAR

	Atomic % of Elements[a]							
Etch Time (min)[b]	Na	S	Cl	K	Ca	Fe	C	O
None	3.9	0.7	ND	ND	1.2	0.0	78.0	14.5
60	6.0	0.3	1.4	ND	1.6	0.2	79.2	9.1
130	6.1	0.3	1.7	ND	1.4	0.3	80.3	7.8
190	6.3	0.2	1.7	ND	1.5	0.2	80.5	7.3

ND = Not Determined.
[a] One determination.
[b] 60 min = approximately 200 Angstroms.

TABLE 11b

ESCA DEPTH PROFILE OF SODIUM-LOADED BEULAH CHAR

Etch Time (min)[b]	Atomic % of Elements[a]							
	Na	S	Cl	K	Ca	Fe	C	O
None	12.7	0.7	ND	ND	0.1	ND	68.2	17.7
60	16.3	1.2	1.5	ND	0.0	0.2	68.9	11.2
120	16.9	1.1	2.5	ND	ND	0.2	70.7	8.0
180	19.1	0.8	3.4	ND	ND	0.2	69.5	6.3
240	17.1	0.8	3.6	ND	ND	0.1	72.4	5.5

ND = Not Determined.
[a] One determination.
[b] 60 min = approximately 200 Angstroms.

TABLE 11c

ESCA DEPTH PROFILE OF POTASSIUM-LOADED BEULAH CHAR

Etch Time (min)[b]	Atomic % of Elements[a]							
	Na	S	Cl	K	Ca	Fe	C	O
None	0.5	1.4	0.5	6.3	0.1	0.0	68.2	22.3
60	ND	1.2	2.2	4.7	0.2	0.3	79.8	11.2
130	ND	1.0	2.5	4.2	0.1	0.3	84.7	7.0
190	ND	0.9	3.1	4.0	0.2	0.3	85.2	5.9

ND = Not Determined.
[a] One determination.
[b] 60 min = approximately 200 Angstroms.

Finally, an attempt was made to obtain detailed ESCA scans on the outermost 50 angstroms of the chars. In principle, ESCA has the ability to provide chemical information about the elements present because of the sensitivity of chemical shifts to oxidation state and chemical environment. Unfortunately, the chemical shifts obtained do not correspond to those which are well-established in the literature. A summary of these results is listed in Table 12. The complexity of the solid chars makes it difficult to interpret these results without running a large number of known reference standards in a similar matrix, which would involve a great deal of time and expense.

TABLE 12

DETAILED ESCA SCAN OF BEULAH LIGNITE CHARS

Sample	Element	Chemical Shift (eV)	Comment
Untreated	Carbon	284.6 (57.2% of C)	Aromatic. Normal contamination from pump oil.
		285.9 (35.5% of C)	Ether or hydroxyl
		290.0 (7.3% of C)	Carboxyl
	Oxygen	532.4	Unknown; perhaps a ring structure
	Sodium	1072.87	Unknown
		264.6	Unknown
	Sulfur	169.8	Unknown
	Calcium	348.0	Unknown; perhaps $CaSO_4$
		351.6	
Na-loaded	Carbon	284.6 (48.9% of C)	Aromatic. Normal contamination from pump oil.
		285.9 (36.5% of C)	Ether or hydroxyl
		290.1 (14.5% of C)	Carboxyl
	Oxygen	532.7	Unknown; perhaps a ring structure
	Sodium	1073.2	Unknown
		264.1	Unknown
K-loaded	Carbon	284.6 (60.7% of C)	Aromatic. Normal contamination from pump oil.
		285.5 (39.3% of C)	Ether or hydroxyl
	Oxygen	532.3	Unknown; perhaps a ring structure
	Sulfur	169.3	SO_4^{-2}
	Potassium	293.3	Unknown
		296.0	
Ca-loaded	Carbon	284.6 (86.2% of C)	Aromatic. Normal contamination from pump oil.
		287.8 (10.4% of C)	Carbonyl
		290.6 (3.4% of C)	Carboxyl
	Oxygen	532.5	Unknown; perhaps a ring structure
		348.7	Unknown

3.3.5 Surface Area Measurements of Chars

An attempt was made to determine the surface area of the cation-loaded Beulah lignite chars by both standard and modified BET analysis. Difficulty was experienced in that the samples would not come to equilibrium in the sample cell in any reasonable time, but seemed to keep adsorbing nitrogen for hours or even days. Accordingly, a modified two-point technique was tried to limit the analysis time necessary. Further, the samples of sodium-loaded and potassium-loaded chars were inadvertently mixed prior to the analysis of the sodium-loaded char. Lack of sample material allowed only the potassium-loaded and mixed char to be analyzed.

The results of the surface area measurements for the 75-90 micrometer fraction of the potassium-loaded and mixed chars are given in Table 13. Although these results are somewhat imprecise, they indicate that the cation-loaded Beulah chars have a quite high surface area, indicative of high porosity.

TABLE 13

BET AND LANGMUIR SURFACE AREAS

Char	BET Surface Area	Langmuir Surface Area
B1(K) 75-90 microns	249 m^2/g	334 m^2/g
B1(Ca) 75-90 microns	85 m^2/g	--
Mixed B1 char 75-90 microns	358 m^2/g	534 m^2/g

3.4 Burning Rates of Chars

3.4.1 The Laminar Flow Reactor

Char burning rates were examined in a bench-scale laminar flow reactor with optical and extractive sampling techniques in an environment in which the gas temperature and composition can be closely controlled. The distinguishing features of the laminar flow reactor are: 1) the particles are burned in a flameless gaseous environment enclosed by a vertical quartz observation chimney, 2) gas composition and temperature can be widely varied and independently controlled, 3) particle temperatures are monitored by a three-color optical pyrometer, and 4) particle sizes can be obtained with a video-microscope concurrently with the temperature measurements. The system is depicted schematically in Figure 6.

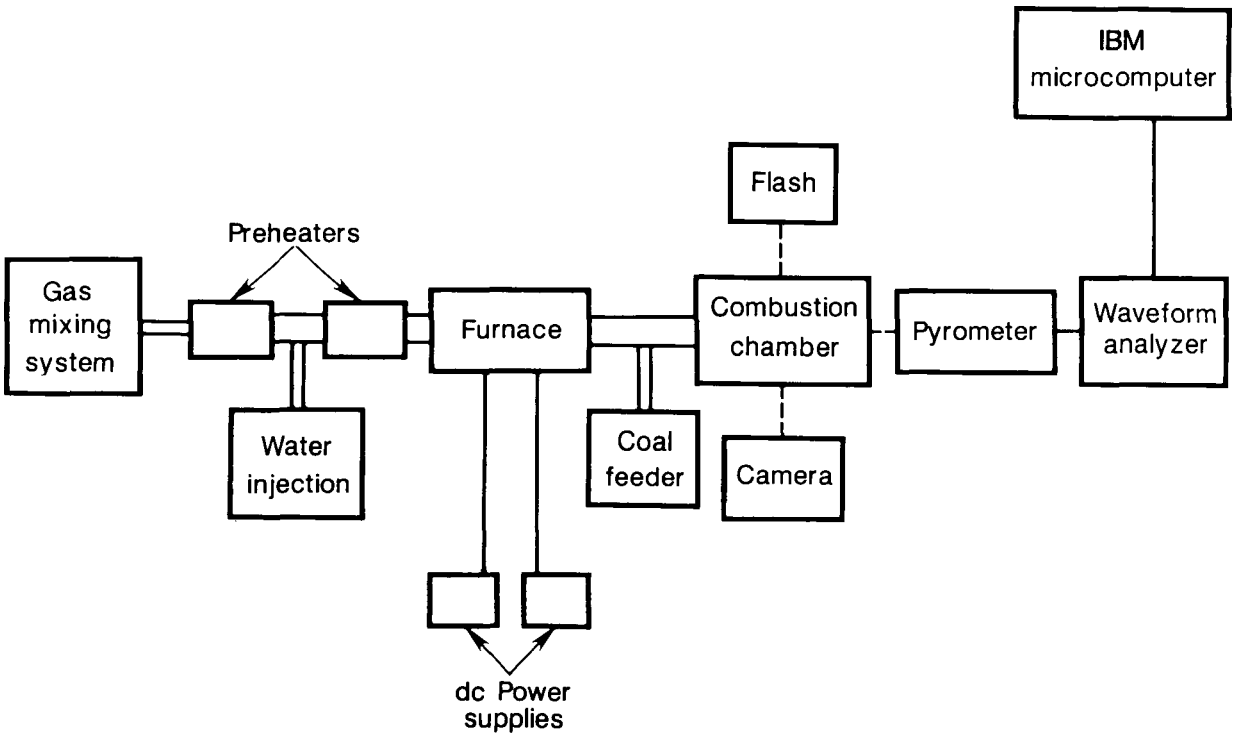

Figure 6. Schematic of the laminar flow reactor.

During operation, a mixture of oxygen (0-50 L/min) and nitrogen (0-100 L/min) is prepared with mass flow controllers, with a metering accuracy within 1% of the full-scale flow rate of each gas. If desired, carbon dioxide, sulfur dioxide, and water can be included in the gas stream to simulate a combustion gas mixture. The total gas flow rate is normally 100 L/min. A small amount of the gas leaving the mass flowmeters is diverted to the feeder to entrain the particle sample; the bulk is preheated to 775 K before entering the high-temperature section of the furnace. Here the gas passes over 48 molybdenum disilicide electric heating elements and is heated to a maximum 1100 K exit temperature before entering the quartz observation chimney.

The observation chimney, 8.6 cm x 8.6 cm x 30.5 cm high, allows optical pyrometry and videomicroscopy of the burning particles perpendicular to the particle trajectory. The gas stream passes through a nichrome screen flow straightener at the base of the chimney and flows vertically upward. To reduce radiation loss, the first 6 cm of the chimney consists of 2.5-cm-thick high-temperature insulation. At the top exit of the chimney, a tapered flow restricter fits over the chimney, sloping in at a 45-degree angle to a final 5.4-cm-square exit opening. The dilute particle stream is fed intermittently into the chimney through a water-cooled feed tube and enters the gas stream just above the flow straightener at the base of the chimney.

The optical instruments shown in Figure 1 consist of a three-color optical pyrometer and right-angle focus detector, and a videomicroscope and strobelight. The videomicroscope was described previously in Section 3.1.1. The optical head of the pyrometer is focused on a 1 mm x 1 mm area on the chimney centerline at the selected observation height. Light from the burning particles passing through this control volume is focused on the end of a trifurcated fiber optics cable and transmitted to three narrow bandpass filters (10 nm bandpass) centered at 550, 700, and 800 nm into three photomultiplier tubes. The focus detector is similar to the pyrometer, with the optical head connected by a fiber optics cable to a forth photomultiplier assembly, but without the filter.

The photomultiplier signals are amplified with combination socket/wide band amplifiers and captured by a digital waveform analyzer. The signals are low-pass filtered and stored by the analyzer. A circular convolution procedure is then applied to the signals to smooth noise. Particle signals are then manually accepted if the pyrometer and focus detector signals are coincident and if no multiple peaks or overranging of the pyrometer occurs. The signals are then stored in their entirety on floppy disk for subsequent processing.

Calibration of the pyrometer is carried out using a tungsten strip lamp and pinholes of known size (41, 93, 113, and 190 micrometers), which are either stationary or located on a rotating chopper wheel. In the case of the stationary pinholes, light passing through them is chopped to simulate an incandescent moving particle. The temperature of the lamp is measured using a disappearing-filament optical pyrometer. The calibration procedure involves collecting up to eight sets of 16 signals which are processed using an algorithm for determining peak height, area, and background. A least-squares analysis of the data is carried out, and the regression equation is subsequently used to calculate each particle temperature and its prediction interval.

Three peak height or peak area ratios can be determined for each particle measured, two of which are independent. The ratios of peak area of 550/700 nm and 700/800 nm were selected as they have been found to give the most reliable temperature data. Two particle temperatures are thus determined for each particle signal, and the validity of each particle temperature is tested by determining whether it falls within the 95% confidence interval of the mean calculated on the basis of the predicted response. Finally, the mean temperature for all acceptable signals in the data set is calculated.

Gas temperatures in the observation chimney are measured using a Pt/Pt-Rh thermocouple positioned 1 cm above the control volume. When a particle triggers the pyrometer, the gas temperature is automatically read. For each acceptable particle observation, the gas temperature is recorded to disk.

In addition to the optical measurements, particle samples can be extracted from the observation chimney using a nitrogen-quenched sampling probe, which collects the sample in an in-line cyclone. Sampling is done at a high anisokinetic flow rate which ensures collection of virtually all particulate material injected into the chimney during the sampling period.

Because the sampling probe occupies the position where the thermocouple to measure gas temperature normally is, collection of particulates is done as a separate experiment from temperature measurements.

3.4.2 Combustion Test Matrix

The goal of the combustion tests of the chars in the laminar flow reactor is to determine overall particle burning rates of the chars as a function of char type, concentration of calcium, potassium, and sodium cations in the chars, particle size, oxygen concentration, and gas temperature.

The text matrix was set up to examine the untreated, demineralized, and the three cation-loaded char samples for each coal type. Measurements would be made on three particle size ranges of each sample (53-63, 63-75, and 75-90 micrometers), three oxygen concentrations (0.05, 0.10, and 0.15 mole fraction oxygen), and two gas temperatures (900 and 1000 K). To obtain comparative data for the coal types and cation loadings, the tests concentrated on obtaining measurements at one gas temperature (1000 K).

The original plan was to obtain measurements at a single height (150 mm) above the particle injection point in the chimney. This was changed in the course of the tests to concentrate on a single particle size (63-75 micrometers) and to make measurements at 100, 150, and 200 mm above the particle injection point to obtain data at several points in the particle burning history. This was found to be nonproductive, and measurements were resumed at the 150 mm level.

Additional tests were also made to reconfirm the steady-state burning region in the observation chimney and to reproduce the temperature measurements on chars used by Young, et al. (3) and Young and Niksa (4).

3.4.3 Combustion Tests

Temperatures of single char particles were obtained using the laminar-flow reactor and three-color optical pyrometer. After the videomicroscope-sizing system became operational, particle images were obtained along with the temperature measurements. All combustion tests were conducted at atmospheric pressure (nominally 0.97 atm.). The gas temperature was 900 or 1000 K at a total flow rate into the furnace of 100 liters/minute. The gas composition for most measurements was 0.05 (or 0.06), 0.10, or 0.15 mole fraction oxygen, with the balance nitrogen. Particle temperature measurements were made at 100, 150, and 200 mm above the particle injection point, corresponding to residence times of 56, 83, and 111 ms, respectively.

3.4.4 Data Reduction

Combustion rates were calculated from the measured particle temperatures by applying a steady-state heat analysis to the burning particles. In this analysis, it is assumed that the particles are in thermal equilibrium with the local surroundings. It is further assumed that the primary reaction product is carbon monoxide. Thus, the heat balance is given by Equation 4.

$$\rho\Delta H = \frac{2\lambda}{d}\ (T_p - T_g) + \varepsilon\sigma(T_p^4 - T_w^4) \qquad [4]$$

where ρ is the overall burning rate, ΔH is the heat of reaction (~2300 cal/mole at 1500 K for CO formation), Nu is the Nusselt number (taken as 2), λ is the gas thermal conductivity, and d is the particle diameter. Tp, Tg, and Tw are the particle, bulk gas, and wall temperatures, respectively; ε is the particle emissivity (taken as 0.9); and σ is the Stefan-Boltzmann constant.

A small correction is required for Equation 4 due to Stefan flow (4,10) which arises from the net outflow of molecules from the boundary layer around each particle. The corrected form of Equation 4 is given by Equation 5.

$$\chi\rho_m \Delta H = \frac{2\lambda}{d}\ (T_p - T_g)\ \frac{\ell n\ (1 + {}^{X^\infty}O_2)}{{}^{X^\infty}O_2\ [1-(\frac{1-\chi}{2})/Le)\ {}^{X^\infty}O_2]} + \varepsilon\sigma\ (T_p^4 - T_w^4) \qquad [5]$$

where $$\chi = \rho/p_m \qquad [6]$$

and $$Le = \frac{\lambda}{\bar{C}_{pg} DC} \qquad [7]$$

The χ factor is the ratio of the overall burning rate to the diffusion-limited rate ρ_m which is defined by

$$\rho_m = \frac{4M_C\ DC}{d}\ \ell n\ (1 + {}^{X^\infty}O_2) \qquad [8]$$

for the conversion to carbon monoxide. Here M_C is the molecular weight of carbon and ${}^{X^\infty}O_2$ is the mole fraction of oxygen in the bulk gas. Equation 7 defines the Lewis number and C_{pg} is the mean heat capacity of O_2 and CO, D is the bulk diffusion coefficient for oxygen in nitrogen (equivalent to CO in nitrogen), and C is the total molar concentration (equal to P_t/RT_m) where P_t is the total pressure, R is the universal gas constant, and $T_m = (T_p + T_g)/2)$, i.e., the mean temperature in the boundary layer around the particle.

3.4.5 Discussion of Burning Rates

A summary of the data obtained to date from the combustion tests is given in Appendix I. The data given in the Appendix and discussed here have the following caveats:

- The values of chi and rho are corrected for Stefan flow and assume conversion to carbon monoxide only.
- The particle size used in the calculation is taken as the midrange size of the char size fraction used.

Calculations and discussion of chi and rho values calculated differently will be explicitly stated as such in the subsequent text.

It should be noted that particle temperature and rate data previously reported for the untreated Pittsburgh #8 char have been removed from the Appendix. Subsequent combustion tests with the Pittsburgh #8 char gave good reason to suspect that the data that had been obtained for this char was unreliable, since the bulk of the char did not appear to be igniting. This has been confirmed by experiments at Sandia National Laboratories (10). The Pittsburgh #8 data should, therefore, not be used. It should be further noted that the brief comparison of the P8 (UT) data with that obtained by Sandia Laboratories on page 9 of the July-September 1987 Quarterly Report and Figure 2 of that report (11) is incorrect and should not be used.

3.4.6 Reproducibility of Previous Temperature Measurements

Since the Beulah-Zap chars produced from the Pennsylvania State University coal sample bank coal differed in reactivity in some cases from that of the LNB chars used in the studies of Young et al. (3) and Young and Niksa (4), combustion tests were run in the laminar flow reactor to determine if the mean particle temperatures could be reproduced. A sample of the older LNB(UT) char and a sample of the older LNB(DM) char were reexamined. The mean particle temperatures obtained are shown in Table 14 and Figure 7. In both cases, the old and new mean particle temperatures for the same oxygen concentrations and gas temperatures are in good agreement, indicating that the char particle temperature measurements are reproducible.

3.4.7 Reconfirmation of Steady-State Burning Conditions

In order for the analysis used with the single-particle temperature measurements to provide meaningful char burning rates, the particle temperatures must be measured under steady-state burning conditions. Previous assessment of the steady-state burning region was reported in (4) and the temperature measurements standardized at 150 mm above the particle injection point. To reconfirm that steady-state burning conditions prevail at the 150 mm measurement point, further tests were made in the laminar flow reactor. The 75-90 micrometer fraction of the B2(DM) char was burned at 1000 K gas temperature and 0.10 mole fraction oxygen. Sets of single-particle temperature measurements were obtained at 25 mm height intervals from 100 to 200 mm above the particle injection point. The mean particle temperatures obtained are tabulated in Table 15. For this material, the mean particle temperature is nearly constant from 125 mm to 175-200 mm, indicating that steady-state burning occurs in this region and that temperature measurements made at the 150 mm point are at steady-state conditions.

TABLE 14

REPRODUCIBILITY OF MEAN PARTICLE TEMPERATURE DATA

Char	Size (microns)	$[O_2]$ (mole fraction)	T_p	T_g	Chi	Rho
LNB(UT)[a]	63-75	0.05	1370	1016	1.37	0.0097
			1378	1013	1.38	0.0100
	63-75	0.10	1633	1009	1.19	0.0182
			1632	1011	1.19	0.0182
			1578	1016	1.09	0.0163
			1611	1029	1.12	0.0171
			1592	1010	1.12	0.0168
LNB(UT)[b]	63-75	0.05	1387	1016	1.43	0.0102
		0.10	1594	1016	1.13	0.0168
LNB(DM)[a]	63-75	0.08	1503	1005	1.18	0.0140
	63-75	0.10	1569	1010	1.06	0.0161
			1574	1016	1.06	0.0161
			1584	1018	1.07	0.0164
	63-75	0.15	1659	1005	0.85	0.0193
			1692	1010	0.88	0.0203
			1676	1020	0.84	0.0196
LNB(DM)[b]	63-75	0.08	1510	995	1.21	0.0144
B2(DM)[c]	63-75	0.10	1622	1012	1.16	0.0178
	63-75	0.15	1736	1012	0.94	0.0219

[a] Earlier data from References 3 and 4.
[b] Data produced from redoing experiment.
[c] Data from present study.

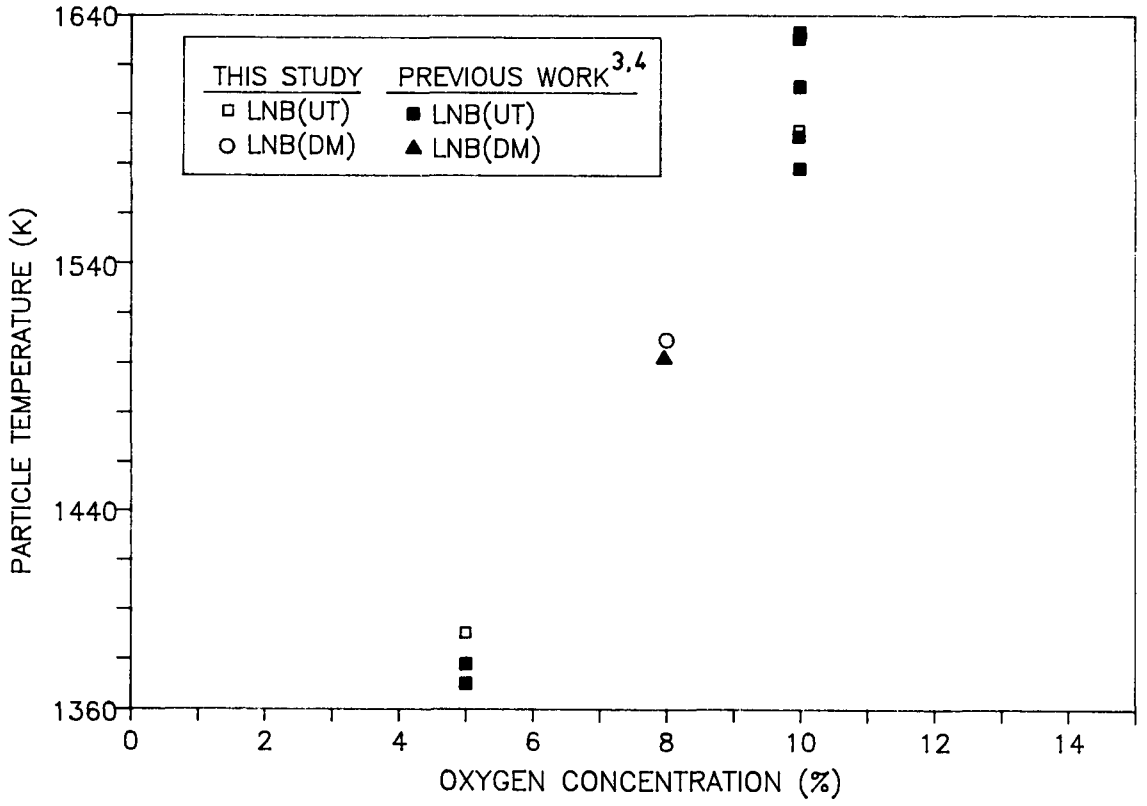

Figure 7. Reproducibility of particle temperatures for 63-75 micron chars.

TABLE 15

VALIDATION OF STEADY-STATE BURNING CONDITIONS
(Char is B2(DM) 75-90 micron size range at $[O_2]$=0.10.)

Height	$[O_2]$ (mole fraction)	T_p	T_g	Chi	Rho
100 mm	0.10	1637	1009	1.26	0.0159
125 mm	0.10	1651	1005	1.32	0.0164
150 mm	0.10	1668	1009	1.32	0.0168
175 mm	0.10	1666	1005	1.35	0.0168
200 mm	0.10	1650	1009	1.28	0.0163
200 mm	0.10	1663	1005	1.34	0.0167

3.4.8 Overall Observations of Char Burning Rates

A summary of the data obtained to date of mean particle temperatures and char burning rates is given in Appendix I. With the exception of the Pittsburgh #8 char, which is not reported for reasons described in Section 3.4.5, the chars tested show high reactivity, burning under diffusion control below approximately 0.10 mole fraction oxygen. Further, examination of the χ values show that the burning rates under these conditions frequently exceed the theoretical diffusion-controlled burning rate ($\chi > 1$) assuming CO is the reaction product under these conditions. In general, the overall burning behavior is similar to that reported previously (3,4).

The effect of particle size on burning rate is shown in Figures 8a-c for two of the Beulah-Zap chars. The figures show an inverse relationship between particle size and burning rate, as expected. The other Beulah chars for which burning rates have been measured for more than one particle size show similar trends.

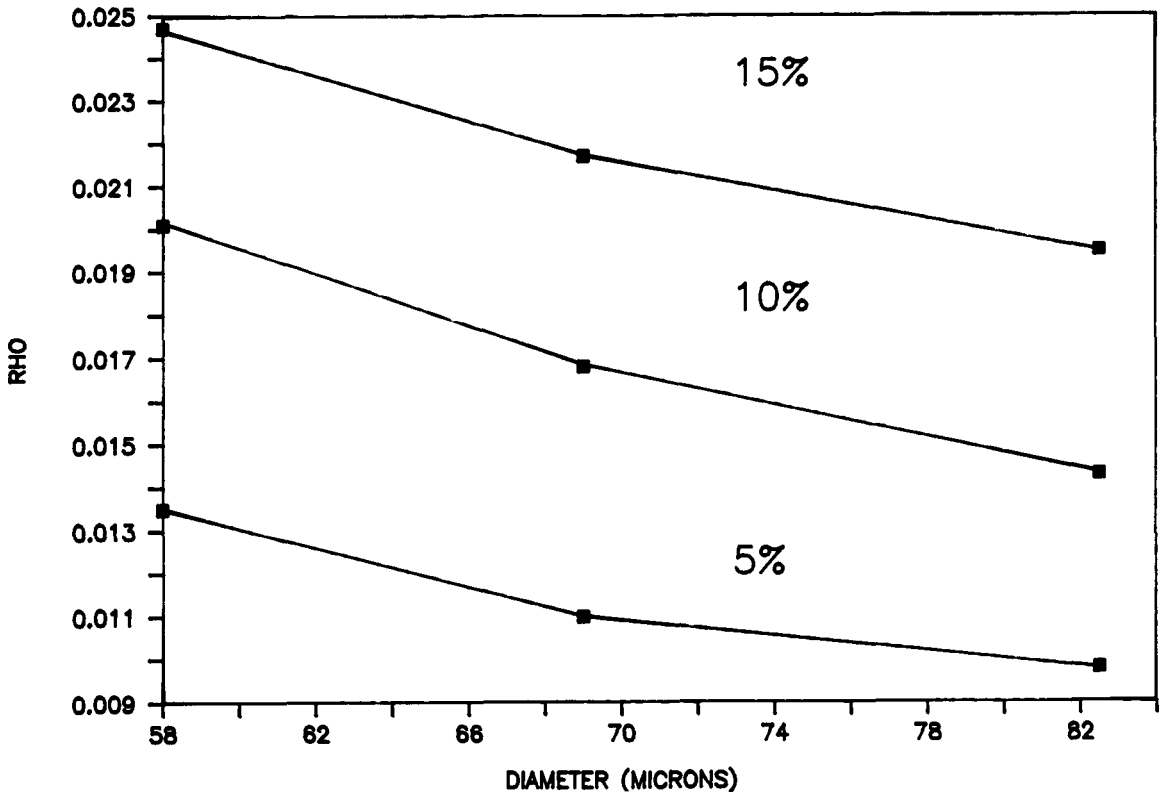

Figure 8a. Rho versus particle diameter for untreated Beulah lignite char (B1(UT)) at three oxygen concentrations.

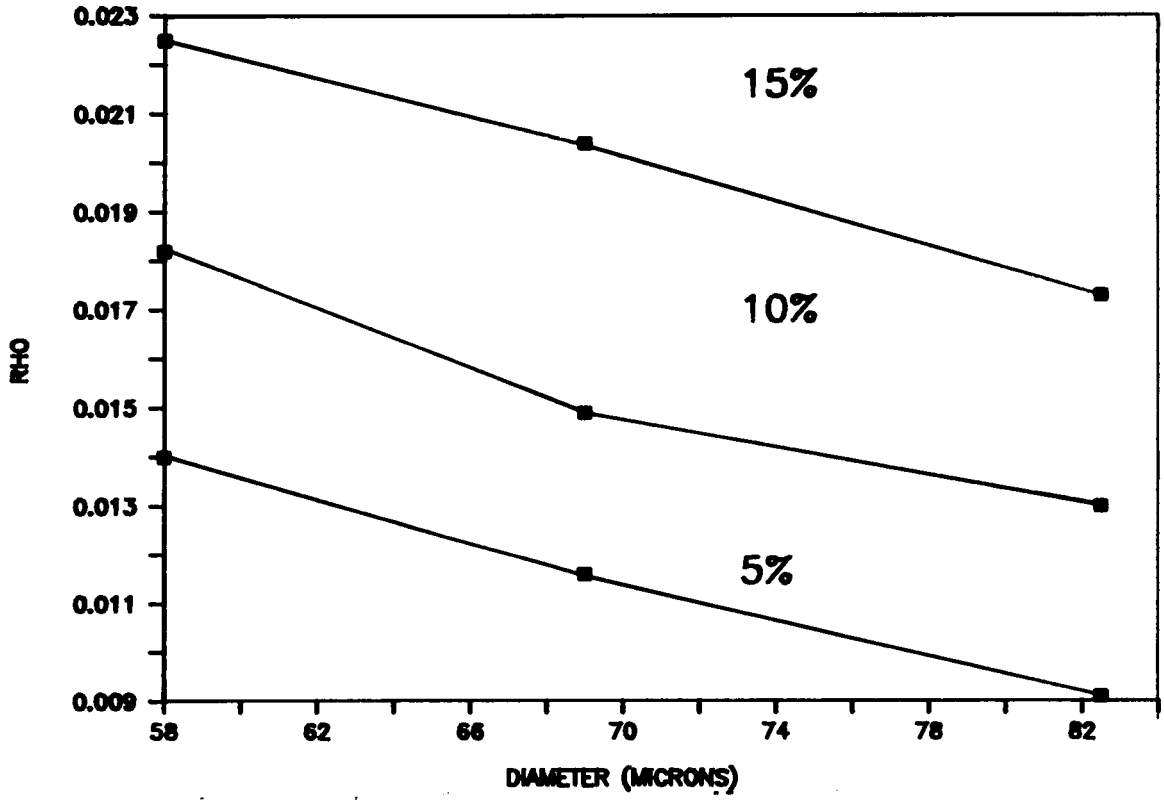

Figure 8b. Rho versus particle diameter for demineralized Beulah lignite char (B1(DM)) at three oxygen concentrations.

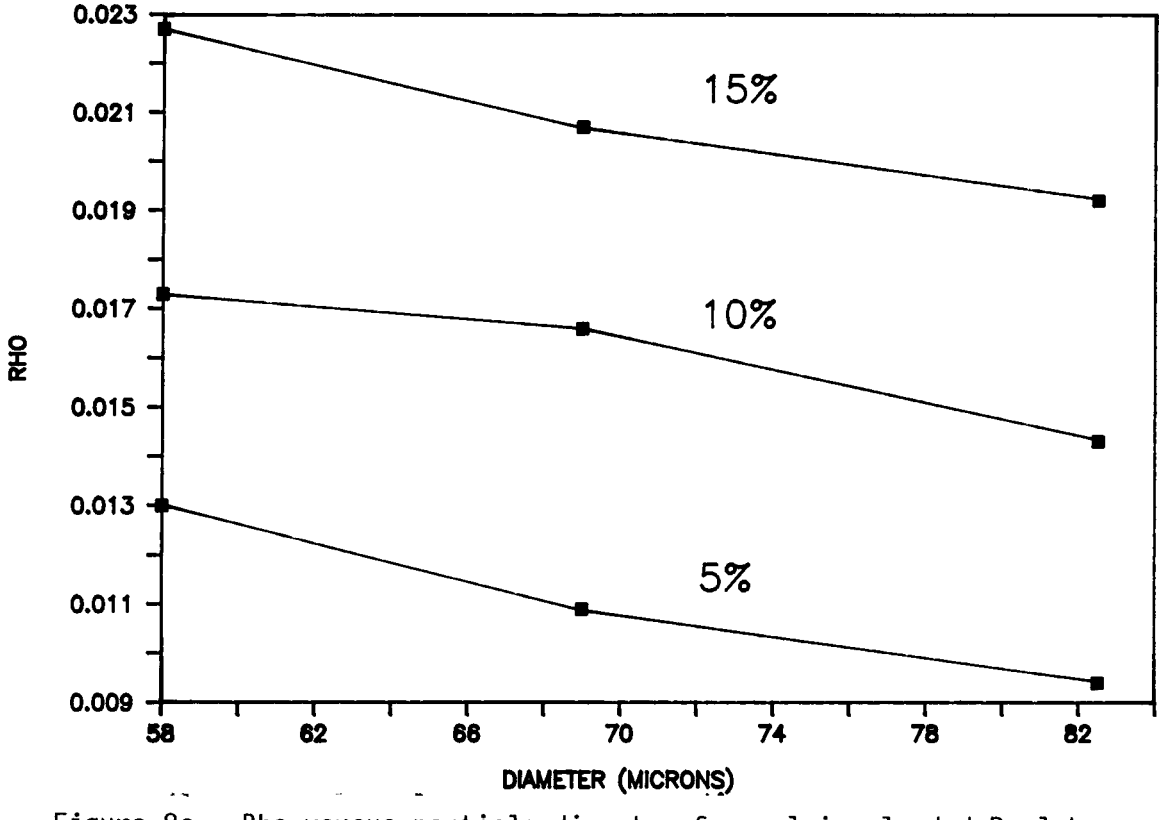

Figure 8c. Rho versus particle diameter for calcium-loaded Beulah lignite char (B1(CA)) at three oxygen concentrations.

3.4.9 Effect of Cations on Char Burning Rates

Low-rank coals contain appreciable amounts of inorganic constituents associated with organic ion-exchange sites rather than as discrete mineral phases (12). Calcium, potassium, and sodium cations are found to bind to these ion-exchange sites in appreciable amounts. These cations are known to catalyze carbon dioxide formation in gasification processes at low temperatures (13,14,15,16,17). The present study is a systematic effort to determine the extent of promotion of char combustion by inorganic constituents--specifically organically bound calcium, potassium, and sodium cations--and to quantify these effects.

The first evidence to be presented regarding the catalytic enhancement of the char burning rate by organically bound mineral matter is a comparison, in Figure 9 and Table 16, of the mean particle temperature data for LNB(DM) char from references (3) and (4), and the remeasured LNB(DM) data with that of the two separate preparations of demineralized B1(DM) and B2(DM) char. The higher mean particle temperature for the B2(DM) char is a real effect, as this char was run immediately after the tests confirming that the LNB(DM) char particle temperatures could be reproduced. Examination of the cation concentrations shown for the coals and coal chars in Table 3 and Table 17 suggests that the enhanced reactivity of the B2(DM) char may be due to the significant amount of

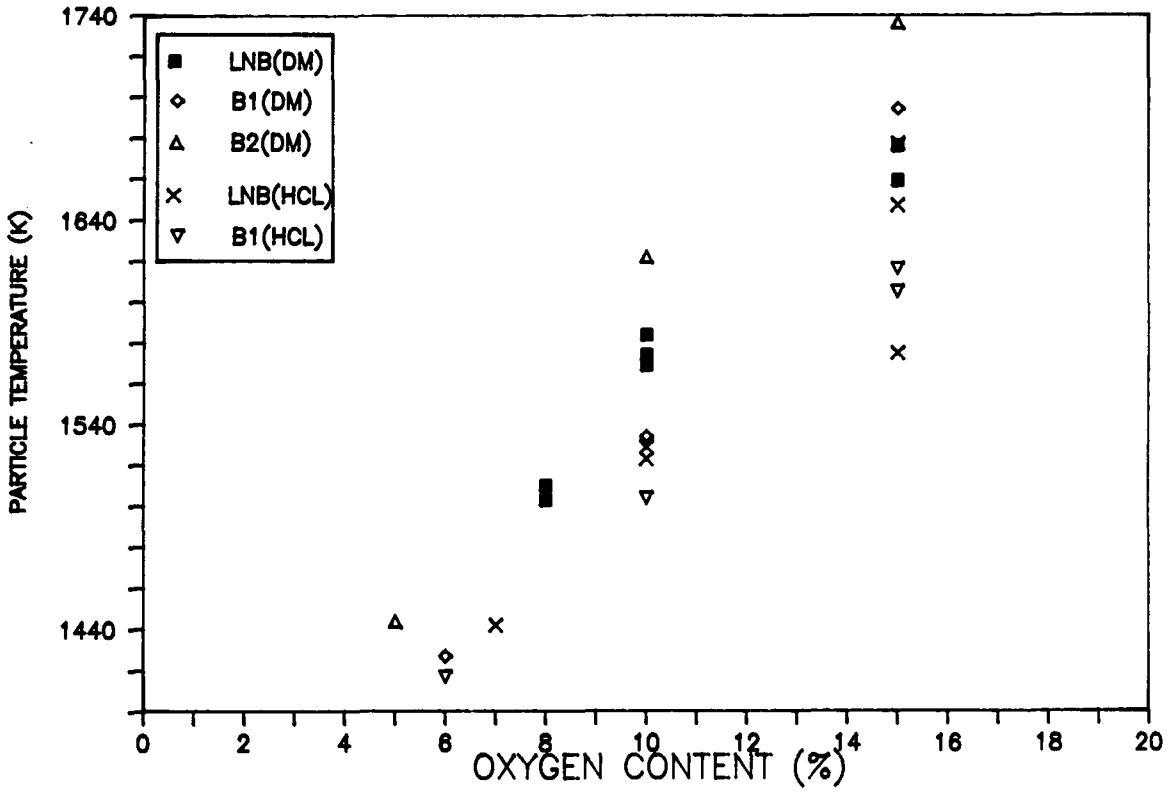

Figure 9. Comparison of 63-75 micron demineralized chars.

calcium remaining in the coal after the demineralization process. The B2(DM) char, with significantly higher residual calcium compared to the LNB(DM) and B1(DM) chars, exhibits markedly higher mean particle temperatures than either the LNB(DM) or B1(DM) chars. This strongly suggests that, in this case, the calcium cation is responsible for the enhanced reactivity of the B2(DM) char.

TABLE 16

COMPARISON OF HCl-EXTRACTED AND DEMINERALIZED CHARS
(Char size is 63-75 microns.)

Char	$[O_2]$ (mole fraction)	Tp	Tg	Chi	Rho
LNB(DM)	0.08	1503	1005	1.18	0.0140
	0.08	1510	995	1.21	0.0144
	0.10	1569	1010	1.06	0.0161
	0.10	1574	1016	1.06	0.0161
	0.10	1584	1018	1.07	0.0164
	0.15	1659	1005	0.85	0.0193
	0.15	1676	1020	0.84	0.0196
B1(DM)	0.06	1427	1009	1.31	0.0116
	0.10	1534	1010	--	--
	0.15	1694	1010	0.91	0.0204
B2(DM)	0.05	1444	1012	1.61	0.0120
	0.10	1622	1012	1.16	0.0178
	0.15	1736	1012	0.94	0.0219
LNB(HCl)	0.07	1442	1013	1.17	0.0120
	0.10	1529	1001	1.00	0.0149
	0.10	1523	983	0.98	0.0151
	0.15	1575	1003	0.74	0.0165
	0.15	1677	1022	0.86	0.0196
	0.15	1647	1003	0.85	0.0189
B1(HCl)	0.06	1417	992	1.34	0.0116
	0.10	1504	1005	0.95	0.0174
	0.15	1605	1005	0.78	0.0174
	0.15	1616	1009	0.79	0.0177

TABLE 17

COMPARISON OF CATION-LOADED AND REDEMINERALIZED CHARS
(Char sizes are 75-90 microns.)

Char	$[O_2]$ (mole fraction)	T_p	T_g	Chi	Rho
B2(K)	0.08	1522	1012	1.25	0.0125
	0.10	1566	1013	1.10	0.0137
B2(K-RDM)	0.08	1522	1003	1.29	0.0126
	0.10	1543	1004	1.08	0.0132
B2(NA)	0.06	1459	1004	1.47	0.0109
	0.08	1499	1001	1.22	0.0120
	0.10	1557	1014	1.08	0.0135
B2(NA-RDM)	0.06	1418	1005	1.34	0.0098
	0.08	1503	1011	1.23	0.0120
	0.10	1551	1005	1.10	0.0134
B2(CA)	0.06	1423	1000	1.38	0.0100
	0.08	1519	1001	1.27	0.0126
	0.10	1574	1002	1.15	0.0141
B2(CA-RDM)	0.06	1452	1003	1.47	0.0107
	0.08	1542	1005	1.32	0.0132
	0.10	1616	1010	1.21	0.0152
B1(DM)	0.06	1400	1024	1.23	0.0091
	0.10	1531	999	1.05	0.0130
LNB(DM)	0.08	1503	1005	1.18	0.0140
	0.08	1510	995	1.21	0.0144
	0.10	1569	1010	1.06	0.0161
	0.10	1574	1016	1.06	0.0161
	0.10	1584	1018	1.07	0.0164
B2(DM)	0.06	1472	1009	1.57	0.0119
	0.08	1599	1003	1.45	0.0149
	0.10	1668	1009	1.32	0.0168
B2(DM-RDM)	0.08	1584	1003	1.40	0.0145
	0.10	1657	1001	1.28	0.0166

Table 16 and Figure 9 also include data for the LNB(HCL) and B1(HCL) chars which were "demineralized" with hydrochloric acid only. In the course of examining the LNB(DM) char with the SEM/electron microprobe, it was observed that, although very little calcium, potassium, or sodium remained, the cations were uniformly distributed throughout the char structure, and did not appear to be associated with residual iron, silicon, or aluminum. Although the demineralization with concentrated hydrofluoric and hydrochloric acids was effective in removing nearly all calcium, sodium, and potassium, the treatment appeared to disperse what remained uniformly throughout the coal structure. This dispersement would enhance any catalytic activity to to these lations. Conversely, treatment with only hydrochloric acid removes these cations, unless they are incorporated into silicates or clays, and would be expected to leave them as discrete mineral grains in the coal structure. Such inclusions would not be expected to be as effective in catalytically enhancing the char burning rate. Although the data is not conclusive, the particle temperatures for LNB(HCl) and B1(HCl) are comparable, as are the temperatures for LNB(DM) and B1(DM), as shown in Table 16. However, the particle temperatures for the HCl-extracted chars are lower than the particle temperatures for the demineralized chars, consistent with the above argument.

The demineralized and cation-loaded chars exhibited significant and striking differences in the distribution of morphotypes. In order to separate direct catalytic effects of the cations (i.e., effects due to the cations in the char) from indirect effects due to alterations in the char structure during the char preparation process, portions of the B2 chars were "redemineralized" with 1M hydrochloric acid. The cations in the chars were expected to be organically bound or in the form of oxides, hydroxides, or carbonates which would be readily removable with the dilute acid.

Table 6 gives the concentration of calcium, sodium, and potassium in the original demineralized and cation-loaded Beulah chars and in the chars after the "redemineralization" treatment. The calcium concentration of the calcium-loaded char was reduced to half of the original level, while the cation levels of the potassium- and sodium-loaded chars were reduced by approximately two orders of magnitude. A second sample of the calcium-loaded char was treated with 1M HCl for four hours instead of one hour, but the residual calcium level was similar to that of the first sample.

Examination of the χ values in Table 17 and the mean particle temperature data in Figure 10 for the cation-loaded B2(K) and B2(NA) chars with those of the "redemineralized" B2(K-RDM) and B2(NA-RDM) chars does not show differences in mean particle temperature commensurate with the huge change in cation loading between these cation-loaded and redemineralized chars. Further, the two sets of chars are quite similar to each other and to the B1(DM) char in mean particle temperature. It is concluded that potassium and sodium cations have little or no effect on the char burning rate, and the difference in char morphology due to the presence of sodium or potassium cations during the char preparation process has little effect on the char burning rates for the Beulah chars.

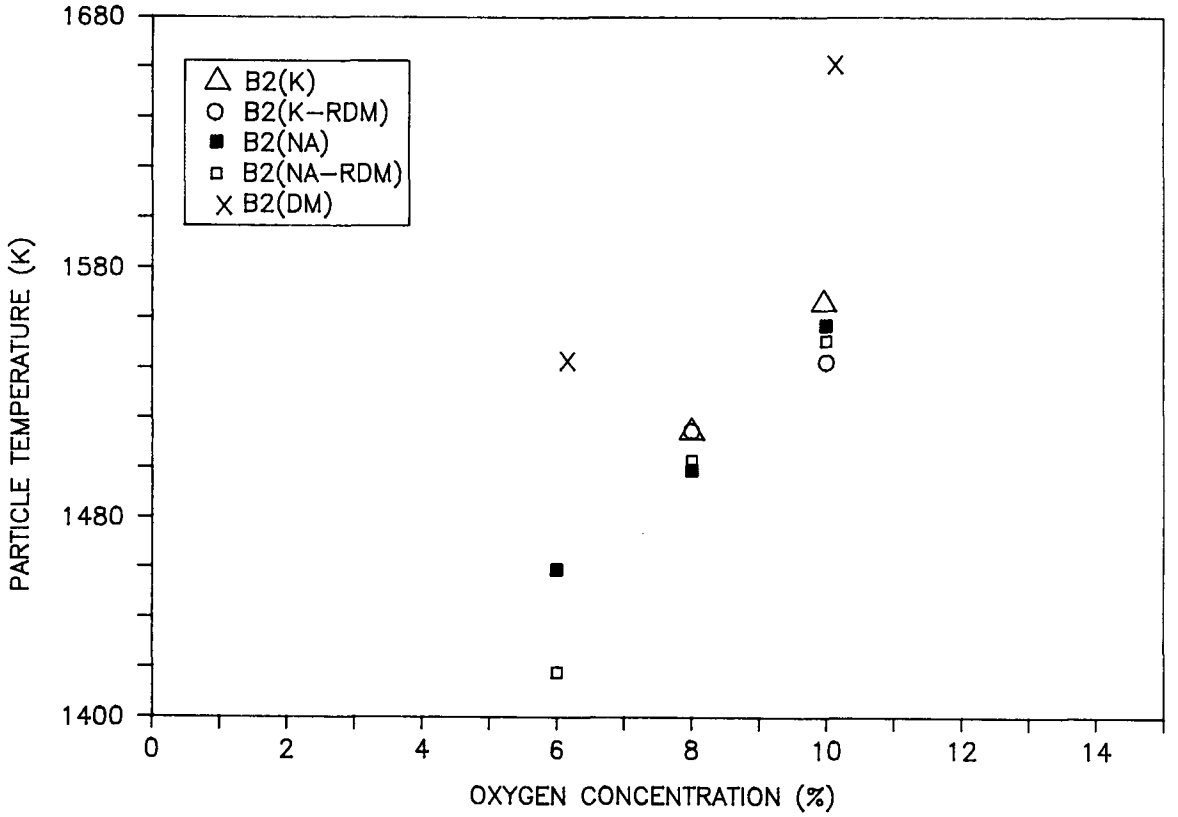

Figure 10. Comparison of 75-90 micron cation-loaded and demineralized chars.

The calcium ion did appear to enhance the char burning rates at low calcium concentration. Figures 11 and 12 are plots of mean particle temperature and χ values, respectively, versus an calcium concentration for several 75-90 micrometer Beulah chars. These figures show a clear trend of increasing particle temperature and χ value with calcium concentration to at least the 4000 ppm level. The effect of calcium then decreases until the mean particle temperature and χ value of the B2(CA-RDM) char at 27,000 ppm calcium are close to those of the very lightly loaded chars.

The initial cation loadings of the B1 and B2 chars were done under saturation conditions, i.e., nearly all the possible ion-exchange sites were loaded with the respective cations to maximize any catalytic effect. However, in retrospect, there is no reason to expect that the relationship of cation catalytic activity is linear with calcium concentration. At some loading, the effect of the cation may plateau and additional loading would have no further effect. It is suggested that at high loadings, the cations (probably as the oxide under char combustion conditions) could form a layer, or "skin," on the outer surface of the char particle, physically preventing oxygen from reaching and reacting with a significant portion of the carbon surface.

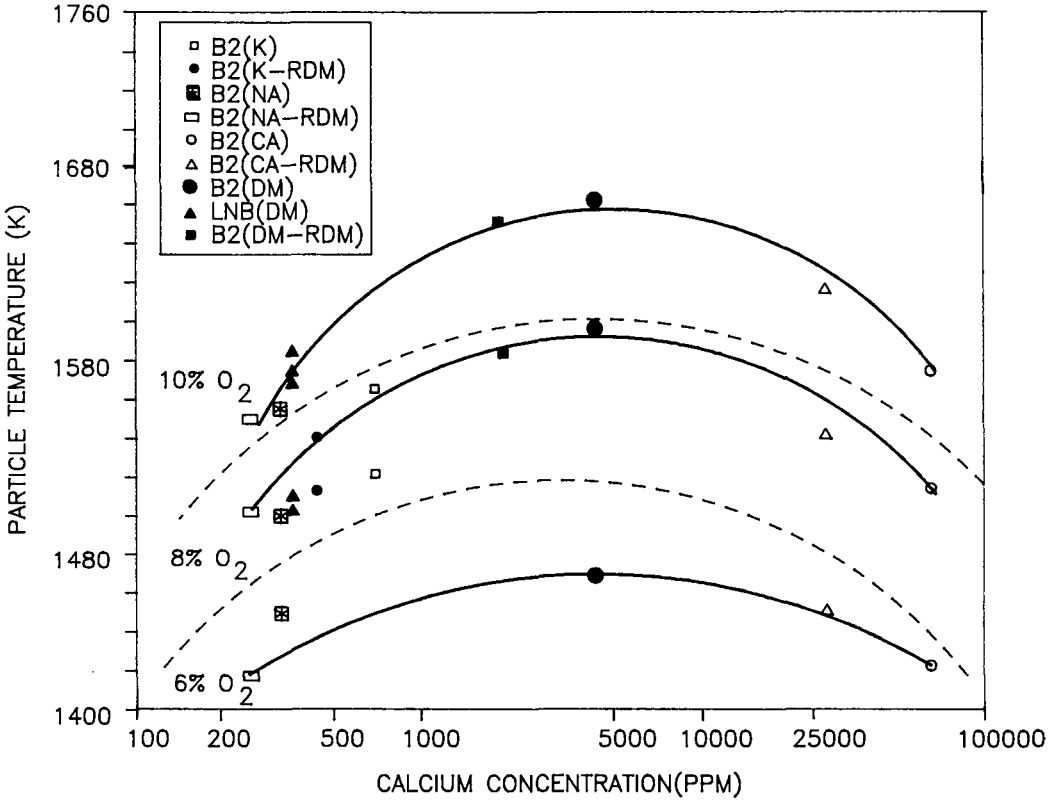

Figure 11. Comparison of 75-90 micron cation-loaded and demineralized chars. Dashed lines separate data for each oxygen concentration.

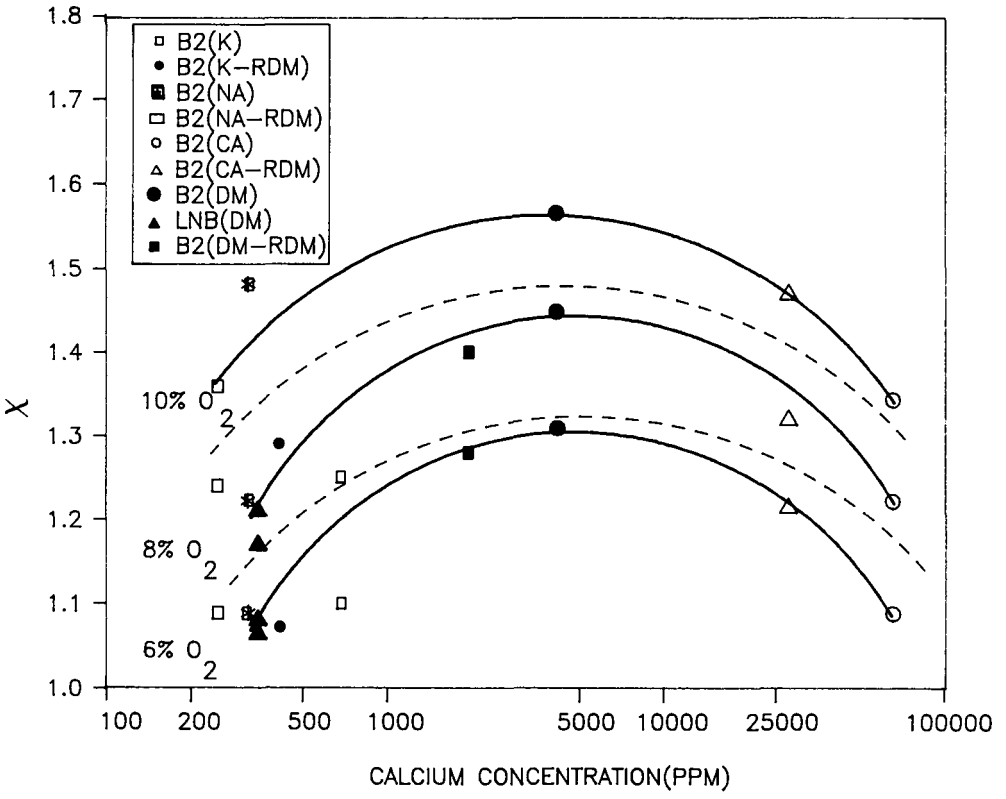

Figure 12. Comparison of 75-90 micron cation-loaded and demineralized chars. Dashed lines separate data for each oxygen concentration.

3.4.10 Mass Flux Calculations

Particles have been traditionally treated as spheres in burning rate calculations and modeling. The treatment of heat and mass flux to a sphere is an attractively simple and easily solved case, particularly when no data are available about the actual particle shape. The direct particle imaging with the videomicroscope allows two dimensions of the particle to be discerned and fitted to non-spherical shape approximations. With this data, an evaluation of the more intractable non-spherical mass flux equations is in order.

The maximum rate of diffusion-controlled reaction to a spherical particle is given by:

$$\rho_m = (48D/dRT_m)\ (P), \qquad [9]$$

where D is the diffusion coefficient (cm^2/sec) of oxygen evaluated at the mean temperature of the particle and the gas, d is the particle diameter (cm), R is the gas constant (82.056 cm^3 atm/mole K), and P is the partial pressure (atm) of oxygen in the bulk gas. The equation is the result of integrating the mass conservation equation

$$(1/r^2)\ D[(d/dr)(r^2(dc/dr)] = 0 \qquad [10]$$

together with the boundary conditions $c=c_o$ at $r=\infty$ and $c=0$ at $r=r_o$.

If these boundary conditions are changed to $c=c_o$ at $r=\delta$ and $c=0$ at $r=r_o$, the boundary layer becomes finite and the mass flux equation becomes

$$\rho_m = (48D/dRT_m)\ (1/(\delta/\delta-r_o))P \qquad [11]$$

This serves to increase the mass flux. For example, if δ is taken to be twice the radius of the particle, then the flux is doubled.

If the particles are cylindrical in shape (and infinitely long), the flux to the surface again depends on the choice of a boundary condition. The mass balance in cylindrical coordinates is

$$(1/r)\ [d/dr(rD(dc/dr))] = 0 \qquad [12]$$

and the boundary conditions are $c=c_o$ at $r=\delta$ and $c=o$ at $r=r_o$. Integration yields the formula

$$\rho_m = (48D/RT_m)(1/\ln(\delta/r_o))P \qquad [13]$$

For boundary layers that are close to the surface, the maximum reaction rate is increased. Table 18 lists the enhancement factor, defined as the maximum oxygen diffusion rate divided by the maximum rate for a sphere with an infinite boundary layer. From Table 18, it is apparent that the reaction rate increases dramatically as the boundary layer thickness is decreased to the same order of magnitude as the particle radius.

TABLE 18

ENHANCEMENT FACTORS FOR SPHERICAL AND CYLINDRICAL FINITE BOUNDARY LAYERS

Geometry	Boundary Layer Extent	Enhancement Factor, e[a]
Cylinder	$1.05r_o$	21.0
Cylinder	$1.1r_o$	10.0
Cylinder	$1.5r_o$	2.5
Cylinder	$2.0r_o$	1.4
Cylinder	$10.0r_o$	0.43
Sphere	$1.05r_o$	21.0
Sphere	$1.1r_o$	11.0
Sphere	$1.5r_o$	3.0
Sphere	$2.0r_o$	2.0
Sphere	10.0_r	1.1
Spheroid[b], a/b=1	$3.57r_{o_c}$[c]	1.00
Spheroid[b], a/b=2	$3.57r_{o_c}$	1.20
Spheroid[b], a/b=3	$3.57r_{o_c}$	1.36
Spheroid[b], a/b=4	$3.57r_{o_c}$	1.49

[a] Ratio of the maximum rate of oxygen diffusion for a given geometry to the maximum rate of diffusion for a sphere immersed in an infinite fluid (infinite boundary layer).

[b] Estimation for prolate spheroid by "infinite cylinder" approximation with 250 radius points; a and b are the major and minor axes, respectively, of the ellipsoid of revolution.

[c] Boundary layer was chosen to give an enhancement factor of 1.0 for a sphere (a=b).

It should be pointed out that the mass flux equation can be solved rigorously only for a sphere with an infinite boundary layer. All other solids require a finite value for the boundary layer thickness. As seen in Table 18, the value assumed for the boundary layer thickness can have a profound effect on the mass flux rate. As may be expected, experimental measurements of boundary layer thickness of burning solids in the <200 micrometer size range are sparse.

If the particles are elliptical in shape, the mass balance equation is written in elliptical coordinates (18).

$$(\eta-\zeta)\, R_{\S}\frac{d}{d\S}\left(R_{\S}\frac{dc}{d\S}\right) + (\zeta-\S)\, R_{\eta}\frac{d}{d_{\eta}}\left(R_{\eta}\frac{dc}{d_{\eta}}\right) + (\S-\eta)\, R_{\zeta}\frac{d}{dc}\left(R_{\zeta}\frac{dc}{d_{\zeta}}\right) = 0 \qquad [14]$$

where $R_{\zeta} = [(\S + a^2)(\S + b^2)(\S + c^2)]^{1/2}$

Solutions are frequently expressed in terms of elliptic integrals,

$$c(\S) = A_1 \int_{\S}^{\infty} \frac{d\S}{R_{\S}} + B \qquad [15]$$

Such integrals appear frequently in problems involving potential theory (19) and heat transfer (20). An elongated particle can be modeled as a prolate spheroid (an ellipse rotated about the major axis) and the elliptic integral form of the mass flux equation solved numerically. The mass flux rate is dependent on the values chosen for the boundary layer thickness, and on the aspect ratio (ratio of the lengths of the major and minor axes). Particle size and shape data obtained with the videomicroscope for the Lower Wilcox char and for the Pittsburgh #8 char indicate significant deviation from sphericity, as shown in Table 19. The Lower Wilcox char is seen to be much more elongated than the Pittsburgh char.

3.4.11 Discussion of Particle Size Measurements

Particle size and shape data has been obtained using the videomicroscope for combustion tests with the Lower Wilcox and Pittsburgh #8 chars. Particle temperatures and χ values are presented for the Lower Wilcox char only, and not for the Pittsburgh #8 char, since the temperature data for the latter is unreliable, as described previously. The results for the Lower Wilcox char is given in Table 19 and Figures 13 and 14. The particle diameters have been calculated from both particle areas and manually selected major and minor axes. The mean diameters given in Figures 13 and 14 are those obtained from the measurement of the major and minor axes. Chi values in Figure 14 were calculated individually using each particle's measured temperature and average diameter.

From the figures, it is seen that there is a fair scatter in the particle temperature and chi values, and there is no simple correlation of these with diameter or aspect ratio. The aspect ratios given in Table 19 show that the particles are quite elongate, with an average aspect ratio of 1.97.

TABLE 19

PARTICLE-SIZING DATA FOR LOWER WILCOX 63-75 MICRON CHAR

Diameter 1[a] (microns)	Diameter 2[b] (microns)	Aspect Ratio	Particle Temperature (degrees K)	Chi
42	51	1.57	1619	0.75
72	78	1.93	1714	0.80
77	64	4.8	1679	0.86
--	62	1.82	1510	0.64
68	62	2.52	1610	0.72
70	62	2.25	1687	0.86
54	54	2.2	1687	0.84
63	72	1.81	1609	0.78
44	44	2.43	1645	0.76
42	45	2.87	1659	0.78
50	57	1.72	1662	0.82
53	52	1.02	1653	0.79
83	75	1.59	1582	0.75
62	68	1.22	1658	0.84
51	53	1.6	1658	0.80
38	43	1.19	1775	0.91
59	61	2.45	1533	0.66
81	67	2.16	1624	0.79
44	48	1.59	1627	0.75
66	56	1.7	1649	0.80
47	45	1.58	1565	0.67
47	53	1.65	1726	0.88
67	68	1.83	1594	0.75

[a] Diameter 1 was calculated using area measurements.
[b] Diameter 2 was calculated using maximum x and y axis measurements.

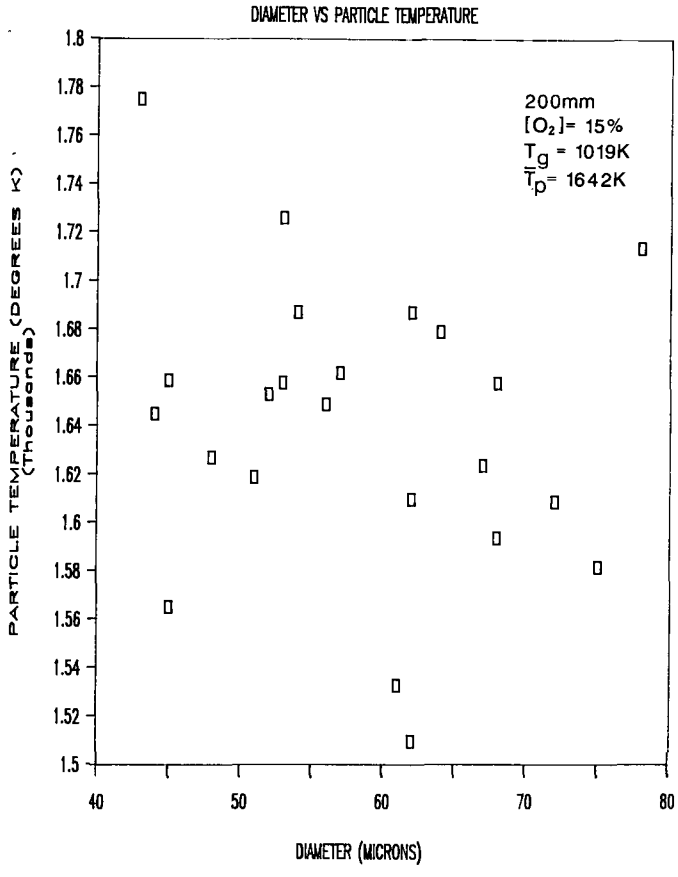

Figure 13. Particle temperature versus particle size for Lower Wilcox char.

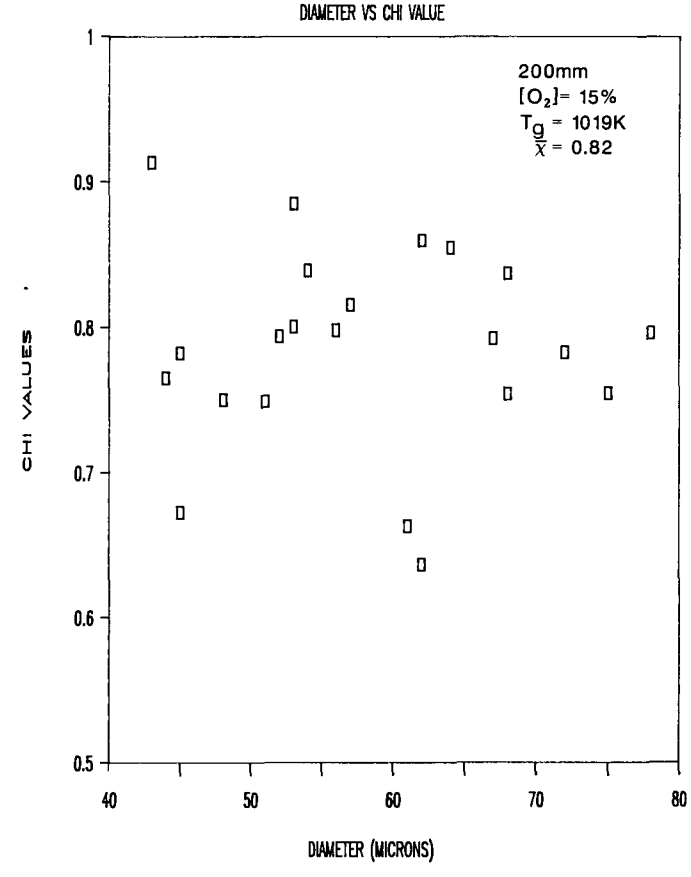

Figure 14. Chi value versus particle size for Lower Wilcox char.

3.5 Future Work

1. The Lower Wilcox and New Mexico Blue chars will be examined to determine char cation content. They will also be redemineralized and further combustion tests conducted to show that the same dependence of particle temperature and burning rate on calcium concentration applies to these chars.

2. Beulah lignite and other chars which have been carefully loaded with a systematic range of calcium concentrations of 0-10,000 ppm will be prepared and combustion tests will be performed.

4.0 IGNITION BEHAVIOR

4.1 Introduction

An important consideration in designing any combustion system is the ignition delay. The ignition delay can generally be defined as the time from the combination of a fuel/oxidant mixture with an activation energy source and the beginning of this mixture's exothermic transition. In the field of coal combustion, knowledge of the ignition characteristics of a given coal is important in the prevention of spontaneous ignition, in the production of stable flames, and in the establishment of optimum combusting fluidized bed temperatures.

Reviews of coal combustion behavior are available that include summaries of the present understanding of coal ignition processes (21,22,23). Rank, volatiles concentration, and surface area have all been reported to affect the ignition behavior and combustion rates of coals, lignites, and chars. Ignition delays of coals have been shown to increase with increasing rank (24), as have ignition temperatures (25). The chars of lignites have also been shown to be more reactive than their higher-rank counterparts (4). The inherent mineral matter in low-rank chars has also been indicated to enhance combustion rates of coals and their chars (4,21,26). Volatile matter has been demonstrated to affect the ignition mechanisms of both subbituminous and bituminous coals (27,28). Others have emphasized the effects of surface area (29).

The objective of this study is to define the effects of basic coal compositional parameters such as moisture content, lithotype, volatile matter concentration, and mineral matter distribution on the ignition delays and combustion rates of single coal particles. In addition, particle temperatures and sizes will be monitored throughout combustion for selected studies. These investigations will focus on lignites, which have been studied far less extensively than high-rank coals.

The most commonly monitored events used to determine coal ignition points are light production, mass loss, heat production, and combustion product detection. The detection of CO_2 and CO evolution was chosen as the primary means of determining ignition for the present study. This procedure was selected since it is relatively unresponsive to the production of volatile pyrolysis products and allows a carbon mass balance to be performed on the overall combustion process. Experiments in which light emission will be monitored are also planned.

Apparent activation energies and Arrhenius preexponential factors can be calculated from the ignition temperatures and delays of particles undergoing heterogeneous ignition (24,30,31). Heterogeneous ignition is defined as the point at which the heat gained by the particle is equivalent to the heat lost, and the rate of heat gain equals the rate of heat loss. A modification of this procedure is presently being used to calculate these kinetic parameters for the materials studied.

4.2 Experimental Equipment and Procedures

A schematic of the ignition apparatus is shown in Figure 15. A listing of the major components is presented in Table 20. All components of this apparatus are operational; however, the optical pyrometer and video system, which are available for use as needed, have not yet been integrated into the system. These two pieces of equipment are described in Section 3.0.

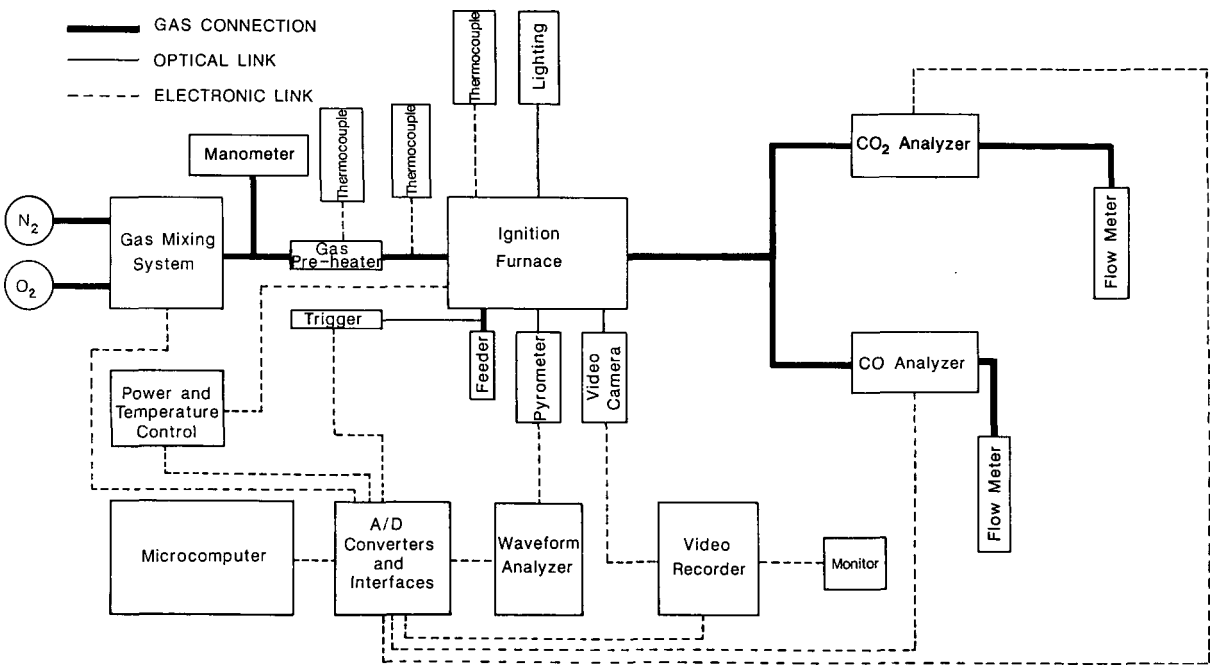

Figure 15. Layout of ignition apparatus.

TABLE 20

PARTS LIST FOR IGNITION APPARATUS

1. Beckman model 868 non-dispersive infrared CO analyzer with 36.48 cm^3 detection chamber

2. Beckman model 868 non-dispersive infrared CO_2 analyzer with 18.24 cm^3 detection chamber

3. Standard 286 microcomputer

4. Gas mixing system:
   a) Brooks N_2 mass flow controller model 5851
   b) Brooks O_2 mass flow controller model 5851
   c) Brooks control and readout model 5876

5. A/D converter (Techmar Incorporated)

6. Omega model 660 thermocouple thermometer

7. Omega model 6000 furnace controller

8. Omega model CN-2010 programmable furnace controller

9. Type S thermocouples

10. Trigger:
    a) Micronta low-voltage DC power supply
    b) Infrared emitting diode MFOE71 (Radio Shack)
    c) Photodetector MFOD72 (Radio Shack)
    d) Type 324 quad operational amplifier

The combustion zone furnace is detailed in Figures 16 and 17. Gas temperatures were measured by a thermocouple inserted into the sample zone. Wall temperatures were measured by a thermocouple glued to the quartz tube directly under the position of the particle. The wall temperature is reported in the text. The gas temperatures were within 1% of the wall temperatures.

The particle drop tube was modified from that initially used (32). The present design consists of a stainless steel tube having a quartz window glued into a position that coincides with the optical trigger. The steel portion of the tube is grounded. This modification prevents the coal particles from sticking to the drop tube as a result of static charging.

The operational procedure for the ignition apparatus is as follows. The coal particle is picked up with a suction bulb attached to a capillary tube and sized under a microscope. It is then placed in the 0.5 mm O.D. syringe needle. The needle is inserted into the airtight chamber containing the top of the 1 mm I.D., 2 mm O.D. drop tube, as shown in Figures 16 and 17. The

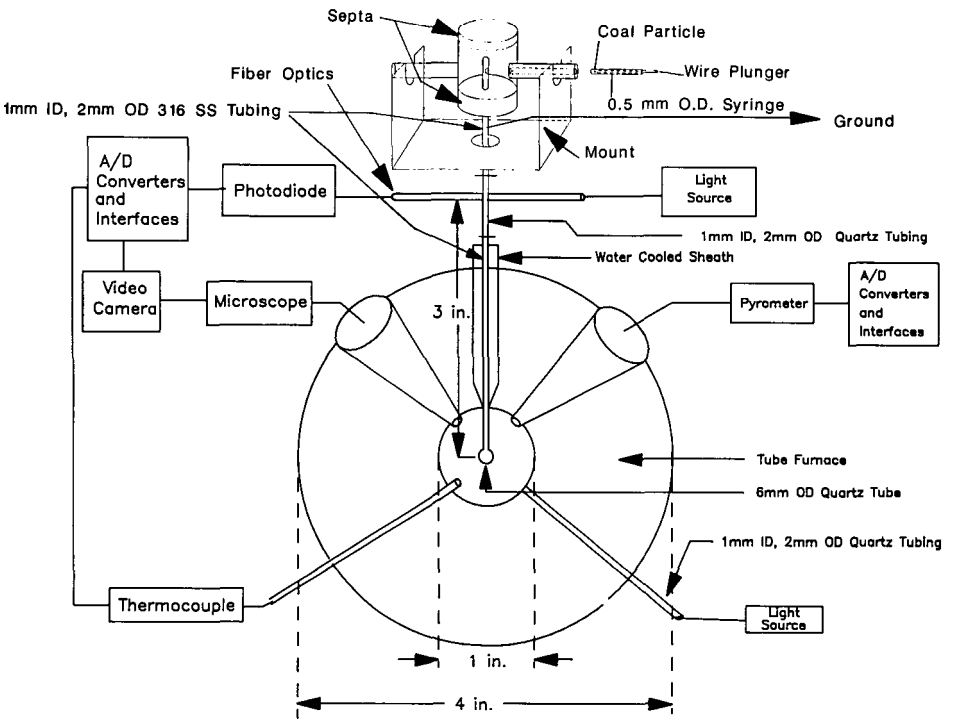

Figure 16. Detailed front view of the combustion zone of the ignition apparatus.

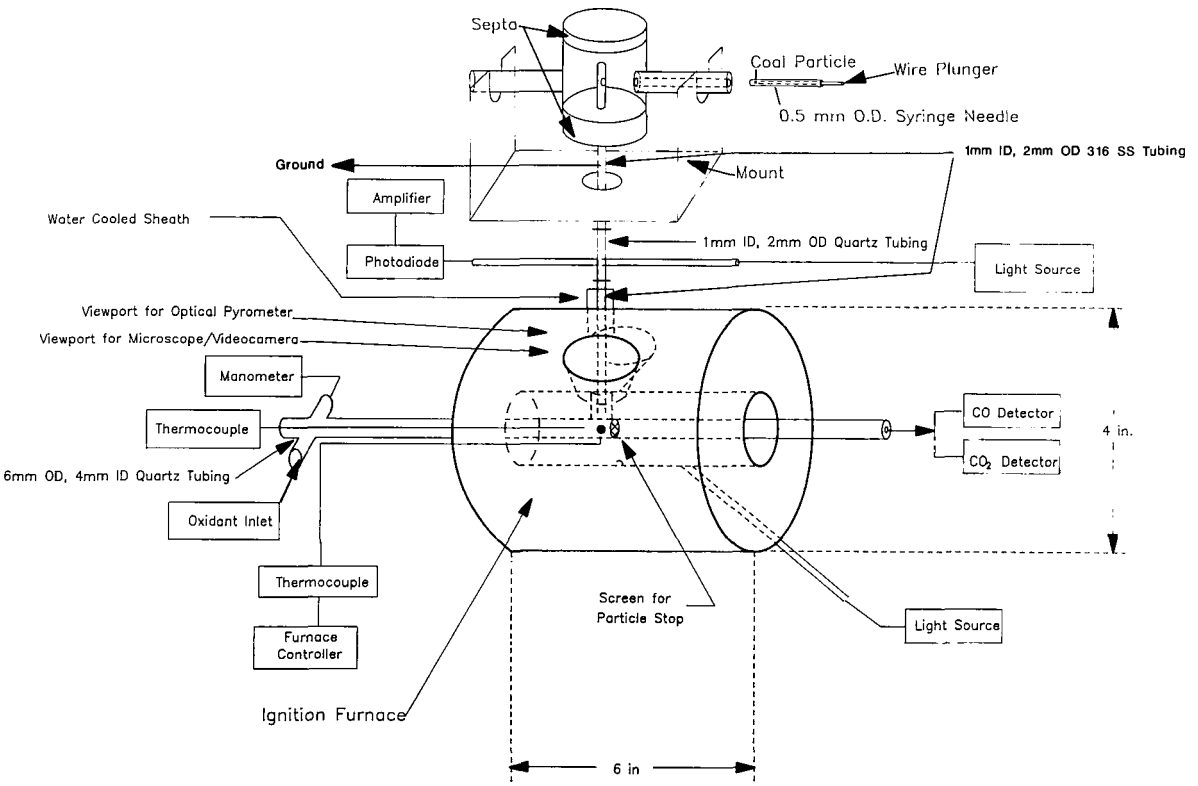

Figure 17. Detailed side view of the ignition apparatus.

particle is pushed into the tube with a wire plunger and falls through the drop tube into the flowing oxidant gas stream. The particle comes to rest at the spot determined by the particle stop screen shown in Figure 17. Passage of the particle through the detection system triggers data accumulation from the CO and CO_2 analyzers.

The flow rate through the combustion zone was 200±1 mL/min; the gas composition was 80% N_2 and 20% O_2. The pressure in the combustion zone was 102 kPa (14.8 psi) for the 650°C runs and 103 kPa (14.9 psi) for the 1000°C runs. The flow rates through the CO_2 and CO analyzers were 100±0.5 mL/min. The linear velocity through the sample zone was 26 cm/sec.

The time scale used to collect the CO and CO_2 analyses was based on the A/D conversion board clock which was calibrated with a sine wave generator.

The coal samples used, Beulah lignite (PSOC-1507) and Pittsburgh #8 (PSOC-1451), were obtained from the Pennsylvania State Sample Bank. The original samples consisted of pieces <0.25 inches in diameter. These pieces were separated according to lithotype using the following criteria. Vitrain was categorized by its hard texture and glassy appearance, attritus by its hard texture and grainy appearance, and fusain by its brittleness and tendency to fracture into needlelike fragments.

The moisture content of the particles was established by storage either over water or concentrated sulfuric acid at 30°C for a period of two weeks or greater. This procedure establishes the relative moisture content as 100% or 0%, respectively (33).

Each particle was sized under a microscope immediately preceding combustion. Due to the asymmetrical nature of the coal particles, three axes per particle were measured. The reported particle volumes were based on this data by assuming a rectangular shape. The particle aspect ratios were calculated by dividing the length of the longest axis by the average of the two smaller.

Diffusional distortion, produced during the transition of the gas samples from the combustion zone to the gas analyzers, can cause significant differences between the recorded analyzer responses and the events originally occurring in the combustion zone. In order to correlate the analyzer responses to actual combustion zone events, the analyzers were calibrated with gas samples of known volume and concentration using the flow system calibrator shown in Figure 18.

The operational procedure for the flow system calibrations was as follows. The calibrator was substituted for the combustion zone furnace with the outlet positioned to mimic the particle position in the ignition studies. The CO/CO_2 cell, the region between the top two solenoid valves pictured in Figure 18, was filled with specific concentrations of CO and/or CO_2, while the gas stream passed through the zero gas cell, the region between the bottom two solenoid valves of Figure 18. The gas stream was then switched to flow through the CO/CO_2 cell while simultaneously triggering the data acquisition. The same oxidant gas flow rate and composition used in the ignition studies was employed during the calibrations. The volume of the standard gas plugs were varied as necessary.

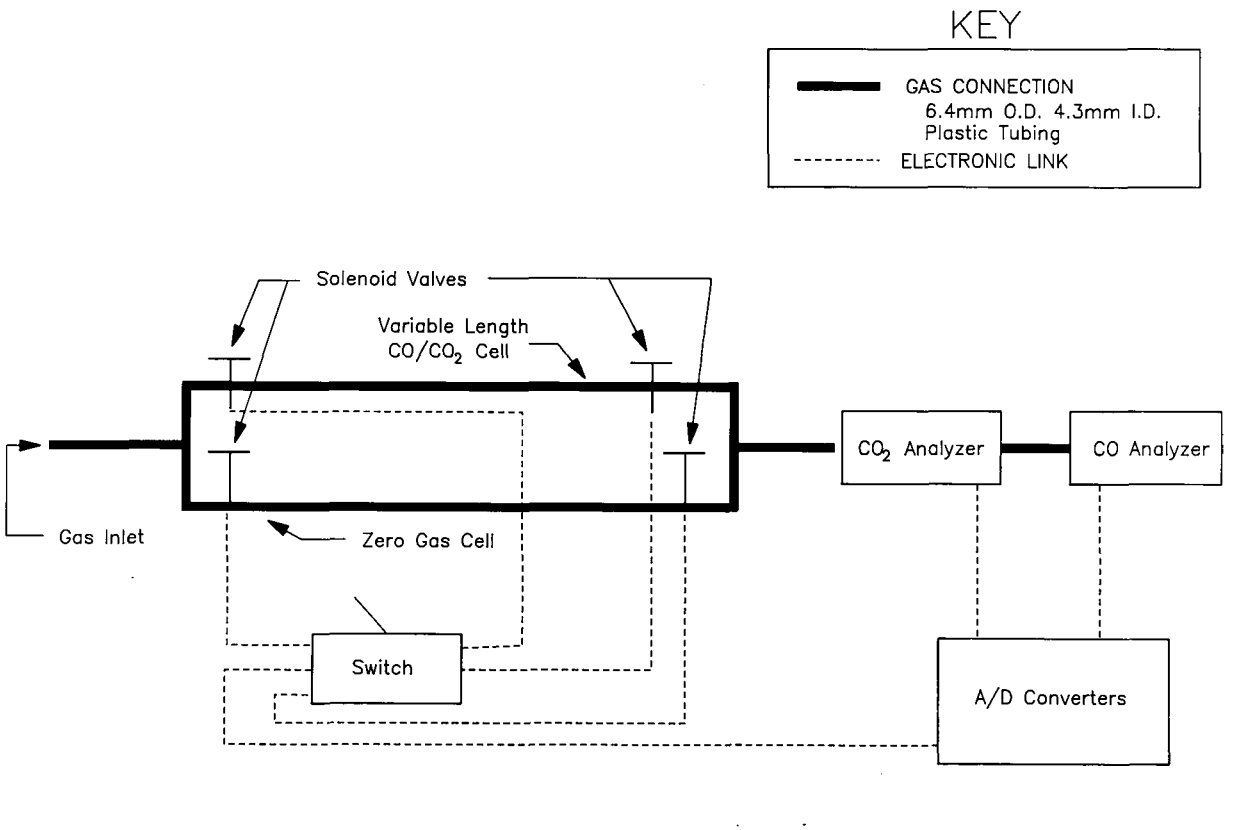

Figure 18. Flow system calibrator for the ignition apparatus.

In order to determine the ignition delay times of the coal particles, a method for quantitating the software delay, the flow system delay, and particle drop time was necessary (see Figure 19). Originally it was envisaged to determine the flow system delay with the flow system calibrator and the particle drop time with a prototype of the particle injector (11). The software delay was easily determined using a sine wave generator. Due to the fact that the flow system delays were discovered to be a function of the furnace temperature and that large cumulative errors were produced in the ignition delays due to separate measurement of the flow system delays and particle drop times, an alternative method for defining the ignition delay was established.

The modified procedure for calculating the ignition delay consisted of using malonic acid particles to define a single operational constant for the ignition apparatus (see Figure 20). Malonic acid particles were injected into the ignition apparatus and the delay between the trigger and initial CO_2 detection was measured. Since malonic acid decarboxylates at the relatively low temperature of 140°C, it was assumed that the decarboxylation time (time E in Figure 20) was essentially zero. Subtraction of the malonic acid response time from the total delays of the various coal particles yielded their ignition delays. This procedure also assumed that the malonic acid particles have drop times equivalent to those of the coal particles; hence, malonic acid particles similar in size to the coal particles were used for the calibrations. The malonic acid response times measured at 650° and 1000°C were 4.241 ± 0.013 sec and 4.205 ± 0.042 sec, respectively. The ignition delays were calculated from the CO_2 analyses and not the CO because of the fourfold greater sensitivity of the CO_2 analyzer.

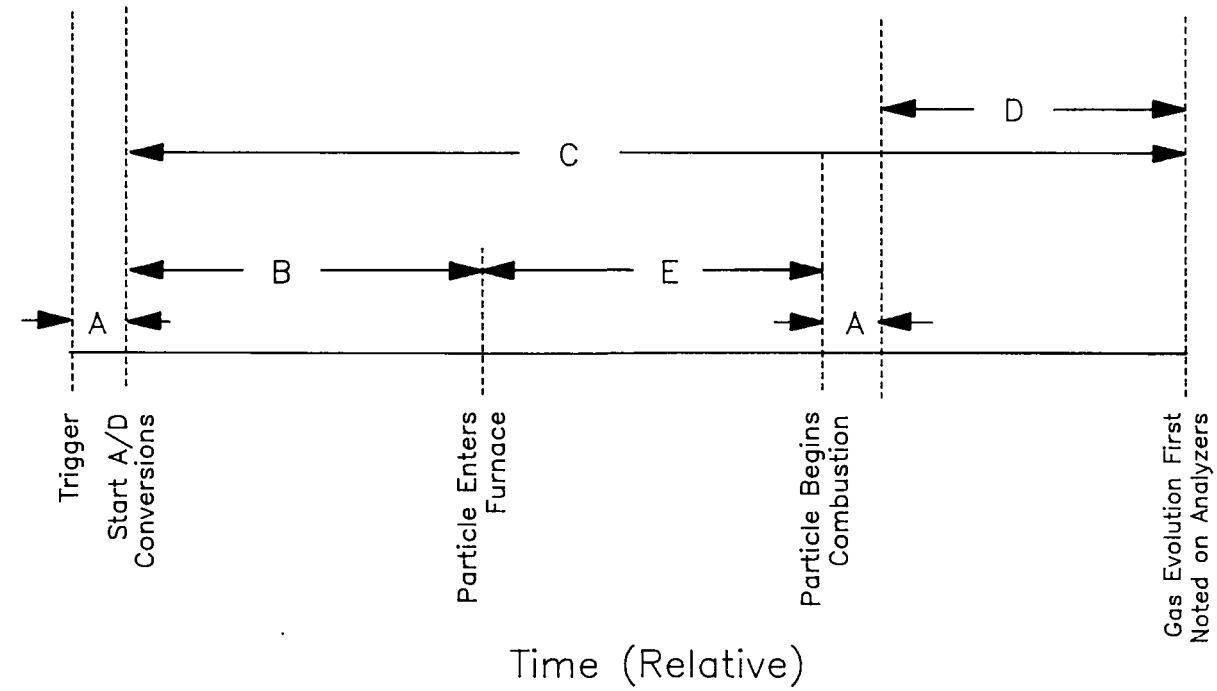

Figure 19. Original timing chart. A) software delay, B) particle drop time, C) total delay, D) flow system delay, and E) ignition delay = C-B-A-D.

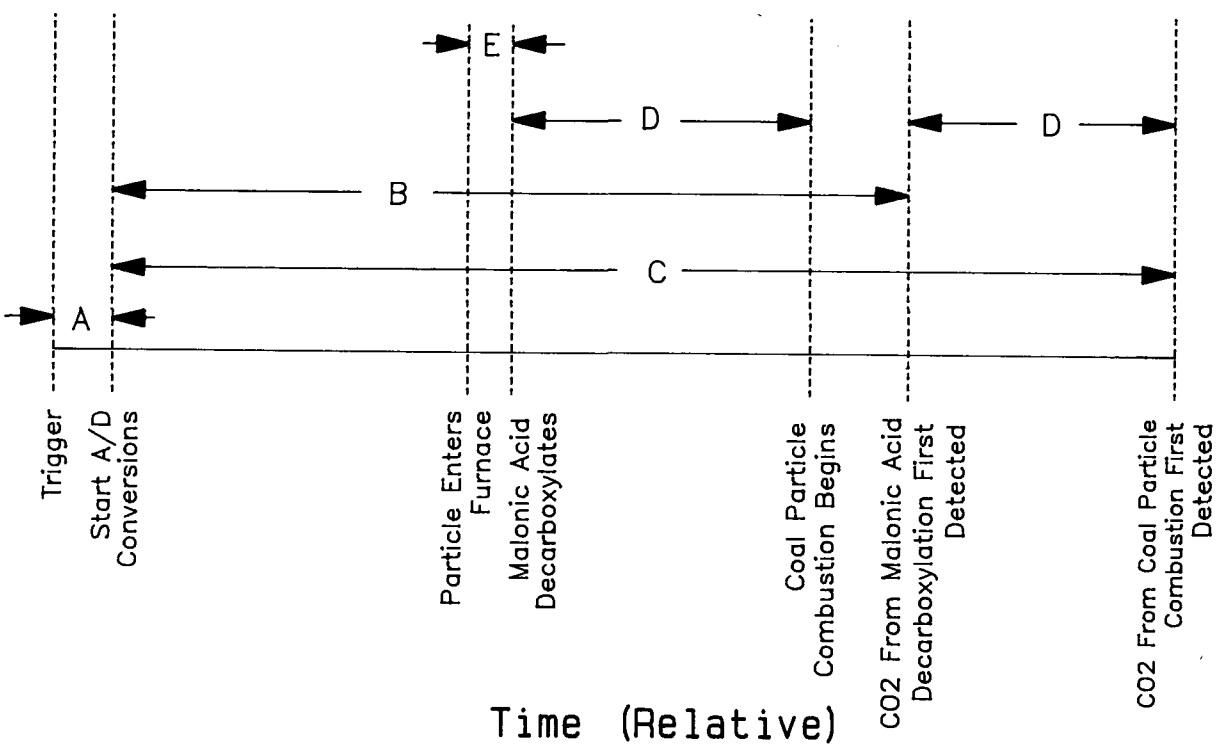

Figure 20. Modified timing chart. A) software delay, B) malonic acid response time, C) total coal delay, D) coal particle ignition delay = C-B, and E) decarboxylation delay.

4.3 Data Analysis

Four separate pieces of information can be directly extracted from the CO and CO_2 analyzer responses; these are the ignition delay, the total moles of CO and CO_2 produced, the duration of combustion, and the maximum rate of CO and CO_2 production. The ignition delay is defined as the time from injection of a particle into the furnace until its initial production of CO_2. The procedure for calculating this value has been described in the experimental section.

In order to determine the other three parameters, moderate manipulation of the initially recorded detector responses is necessary. Figure 21 describes the response of an integral detector to the movement of sample plug through its detection chamber (23). From this result it can be seen that the total moles of the sample plug can be calculated from the peak deflection of the analyzer. Tests performed with the flow system calibrator resulted in the establishment of equations capable of accurately (±5%) quantifying the amount of CO_2 and CO present in a sample as small as 2×10^{-8} moles. These calculations are valid as long as the sample time does not exceed the detection chamber residence time. The flow system calibrator results indicated that the residence time of a sample in the smaller, and therefore limiting, CO_2 detection chamber was approximately 6.5 seconds at the employed flow rate. Most of the coal particles studied had total burnout times less than 6.5 seconds. The one data set which did not meet this criteria (PVLB) did produce a lower-than-average mass recovery (see Table 21).

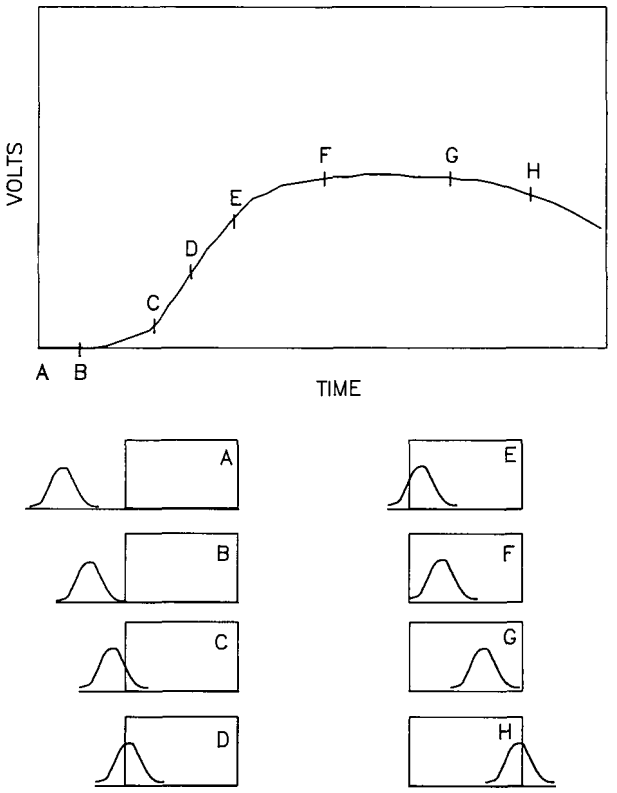

Figure 21. Response of an integral detector to a pulse-type signal.

TABLE 21

IGNITION AND COMBUSTION PARAMETERS OF BEULAH LIGNITE AND PITTSBURGH #8 BITUMINOUS COAL

Data Set	No. of Particles	Coal[a]	Litho-type[b]	T (^{o}C)	Moisture (%)	Particle Volume (cm^3)	Aspect Ratio	Grams of Carbon Detected	Mass Recovery (%)
BVLB	7	B	V	650	100	$8.3 \pm 1.5 \times 10^{-6}$	1.60 ± 0.33	$2.9 \pm 1.1 \times 10^{-6}$	63 ± 25
BVLA	11	B	V	650	0	$5.4 \pm 1.3 \times 10^{-6}$	1.70 ± 0.36	$3.7 \pm 0.1 \times 10^{-6}$	121 ± 29
BFLA	7	B	F	650	0	$6.7 \pm 1.9 \times 10^{-6}$	1.81 ± 0.46	$4.7 \pm 1.1 \times 10^{-6}$	127 ± 30
BALA	9	B	A	650	0	$9.8 \pm 5.1 \times 10^{-6}$	2.10 ± 0.85	$7.2 \pm 3.8 \times 10^{-6}$	109 ± 27
BVHA	8	B	V	1000	0	$6.9 \pm 2.0 \times 10^{-6}$	1.68 ± 0.43	$3.8 \pm 0.8 \times 10^{-6}$	102 ± 32
PVHB	7	P	V	1000	0	$6.2 \pm 1.8 \times 10^{-6}$	1.38 ± 0.16	$3.9 \pm 1.6 \times 10^{-6}$	108 ± 36
PVLB	8	P	V	650	0	$6.5 \pm 2.9 \times 10^{-6}$	1.68 ± 0.51	$2.1 \pm 0.9 \times 10^{-6}$	$61^{c} \pm 26$

[a] B = Beulah lignite (PSOC-1507); P = Pittsburgh #8 (PSOC-1451)

[b] V = Vitrain; F = Fusain; A = Attritus

[c] Underestimated due to long burnout.

TABLE 21 (continued)

IGNITION AND COMBUSTION PARAMETERS OF BEULAH LIGNITE AND PITTSBURGH #8 BITUMINOUS COAL

Data Set	CO_2:CO Product Ratio	Maximum Carbon Conversion Rate (g/sec)	Carbon Conversion Rate Constant (k) ($g/cm^2 sec$)	CO_2:CO Rate Ratio	Total Combustion Duration (sec)	First-Stage Combustion Duration (sec)	Ignition Delay (sec)
BVLB	0.99 ± 0.21	$3.9 \pm 1.1 \times 10^{-6}$	$1.55 \pm 0.53 \times 10^{-3}$	0.74 ± 0.14	0.749 ± 0.267	0.749 ± 0.267	0.376 ± 0.062
BVLA	0.84 ± 0.16	$4.5 \pm 1.1 \times 10^{-6}$	$2.35 \pm 0.60 \times 10^{-3}$	0.59 ± 0.13	0.976 ± 0.578	0.976 ± 0.578	0.419 ± 0.051
BFLA	0.88 ± 0.33	$6.3 \pm 1.4 \times 10^{-6}$	$2.77 \pm 0.53 \times 10^{-3}$	0.60 ± 0.17	0.830 ± 0.122	0.830 ± 0.122	0.302 ± 0.051
BALA	0.78 ± 0.25	$7.2 \pm 2.7 \times 10^{-6}$	$2.42 \pm 0.68 \times 10^{-3}$	0.54 ± 0.16	1.240 ± 0.416	1.240 ± 0.416	0.371 ± 0.036
BVHA	1.19 ± 0.36	$5.3 \pm 1.2 \times 10^{-6}$	$2.45 \pm 0.62 \times 10^{-3}$	0.89 ± 0.31	0.757 ± 0.140	0.757 ± 0.140	0.137 ± 0.038
PVHB	2.01 ± 0.53	$4.5 \pm 1.8 \times 10^{-6}$	$2.14 \pm 0.74 \times 10^{-3}$	1.53 ± 0.41	1.109 ± 0.329	1.109 ± 0.329	0.120 ± 0.079
PVLB	$0.62^c \pm 0.10$	$9.9 \pm 2.5 \times 10^{-7}$	$4.74 \pm 1.14 \times 10^{-4}$	1.59 ± 0.26	$6.9^c \pm 0.5$	0.670 ± 0.094	0.480 ± 0.034

[a] B = Beulah lignite (PSOC-1507); P = Pittsburgh #8 (PSOC-1451)

[b] V = Vitrain; F = Fusain; A = Attritus

[c] Underestimated due to long burnout.

The grams of detected carbon reported in Table 21 are the sum of the moles of CO and CO_2 detected multiplied by the molecular weight of carbon. The mass recovery is the percent of injected carbon detected by the gas analyzers. The amount of injected carbon was calculated from the particle volume, average coal density, and carbon percentage of the coal.

In order to obtain the combustion duration and maximum CO_2 and CO production rates, the initial analyzer responses were converted to moles of gas detected and differentiated with respect to time. This procedure was used to generate Figures 22-29. The time constants used in the differentiation of the CO_2 and CO analyses were 100 and 400 ms, respectively. The larger differentiation time used for the CO analyses is a result of its lower sensitivity. The noise level present in the CO results is also much greater than that present in the CO_2 results.

The result of differentiating the analyzer response from a standard gas plug is compared with the initial plug shape in Figure 29. It can be seen that the analyzer response and initial plug shape differ in length and peak height. From this and similar results, a diffusion broadening constant was defined to subtract from the analyzer deflection duration to produce the combustion duration. This procedure is accurate ($\pm$0.2 sec) down to combustion durations of 0.543 sec.

The combustion durations reported in Table 21 represent the duration of CO_2 production from the burning coal particles. Two times are reported since two-stage combustion was observed for some particles. For these later particles, the total duration of combustion exceeds that of the initial oxidation step.

By comparing the known CO_2 and CO concentrations of sample plugs with the peak height of the differentiated analyzer responses, as shown in Figure 29, equations were defined which were capable of yielding the initial plug concentrations from the peak rate of the analyzer responses. This procedure was straightforward for long samples, since the central portions of such samples are not greatly changed in their transition from the sample zone to the detection chamber. However, when the plug is short, a condition mimicking rapidly burning coal particles, the maximum detected concentration becomes a function of sample length. Calibrations producing accurate ($\pm$5%) quantitation of plug concentrations were established down to total deflection times of 2.135 seconds, which corresponds to an initial plug length of 0.543 seconds.

The calibration equations established from the standard gas plug concentrations were used to calculate the maximum rates of CO_2 and CO production from the combusting coal particles. This analysis is valid for sample lengths between 6.5 seconds and 0.543 seconds and assumes a rapidly established constant particle combustion rate. The maximum carbon conversion rates reported in Table 21 are the sums of the peak CO_2 and CO production rates corrected for diffusional distortion. A rate constant (k) was calculated from the carbon conversion rate according to Equation 16.

$$-dm/dt = k\ A_s \qquad [16]$$

where A_s is the initial surface area of the particle, m is the mass of carbon, and t is time. These values are also reported in Table 21.

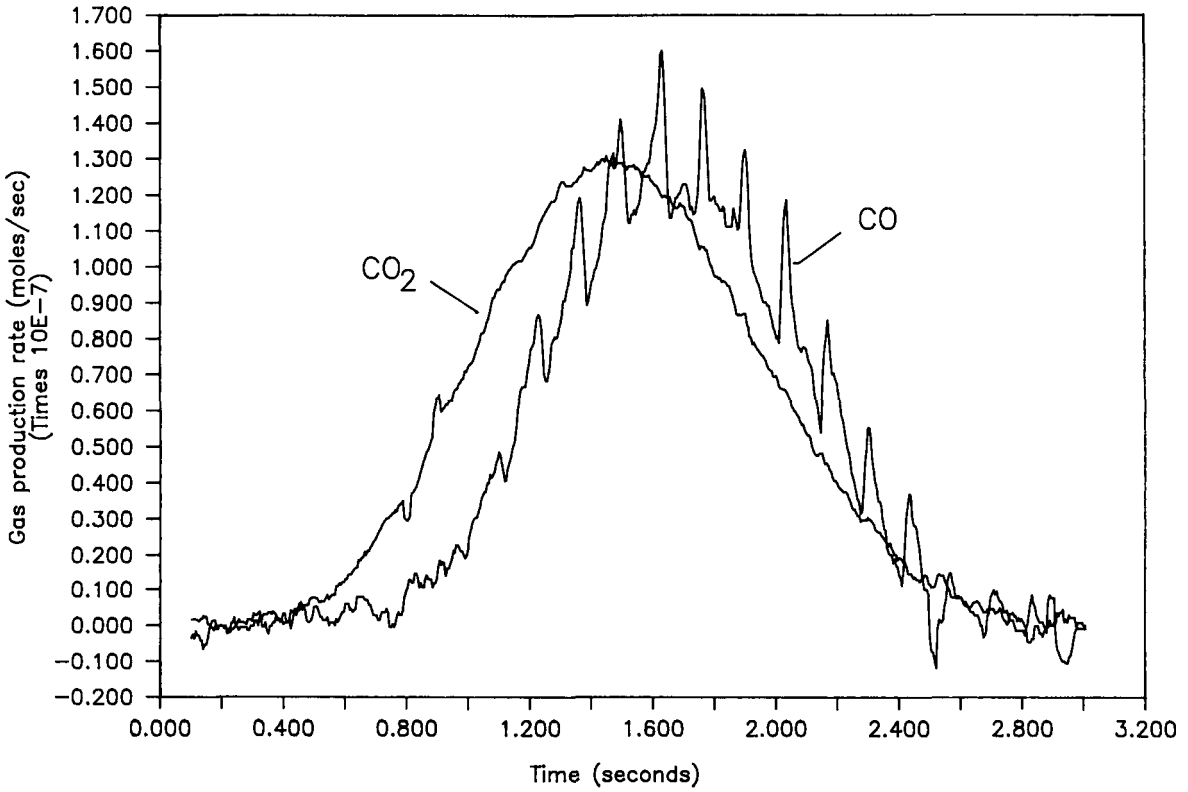

Figure 22. Rates of CO and CO_2 production from moist Beulah lignite vitrain at 650°C.

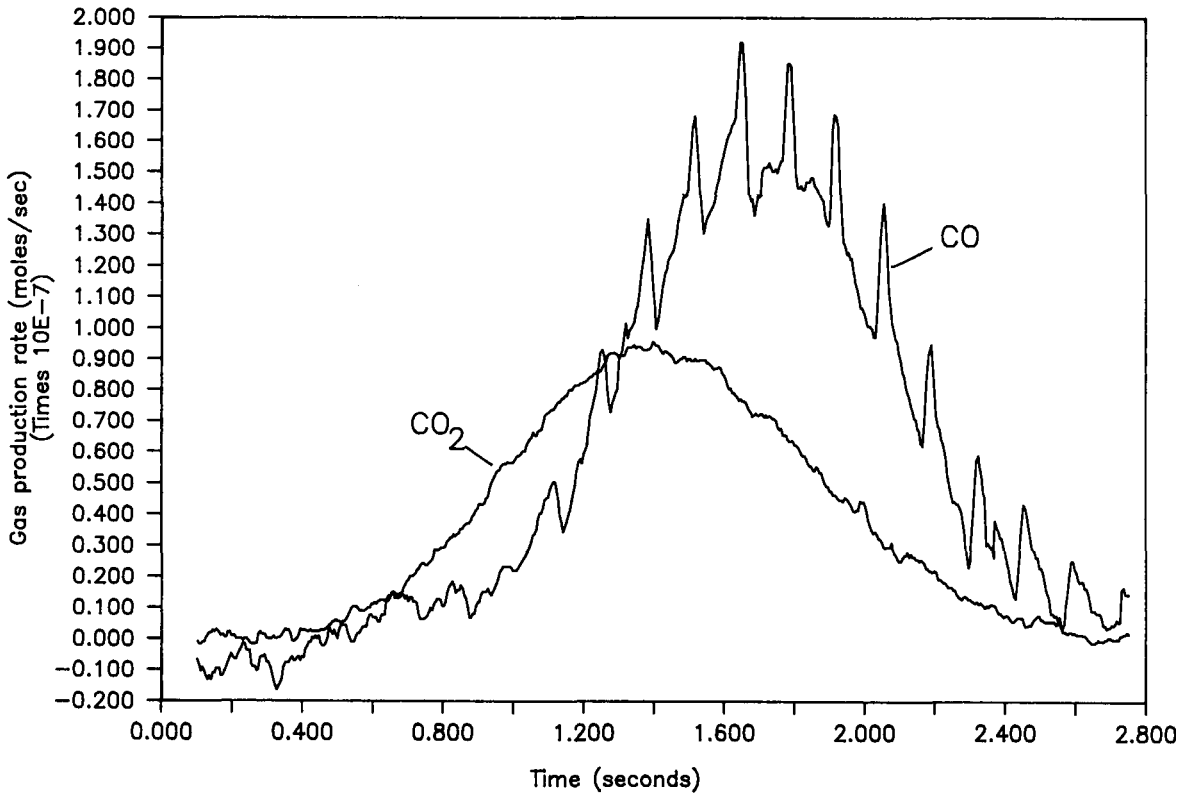

Figure 23. Rates of CO and CO_2 production from dry Beulah lignite vitrain at 650°C.

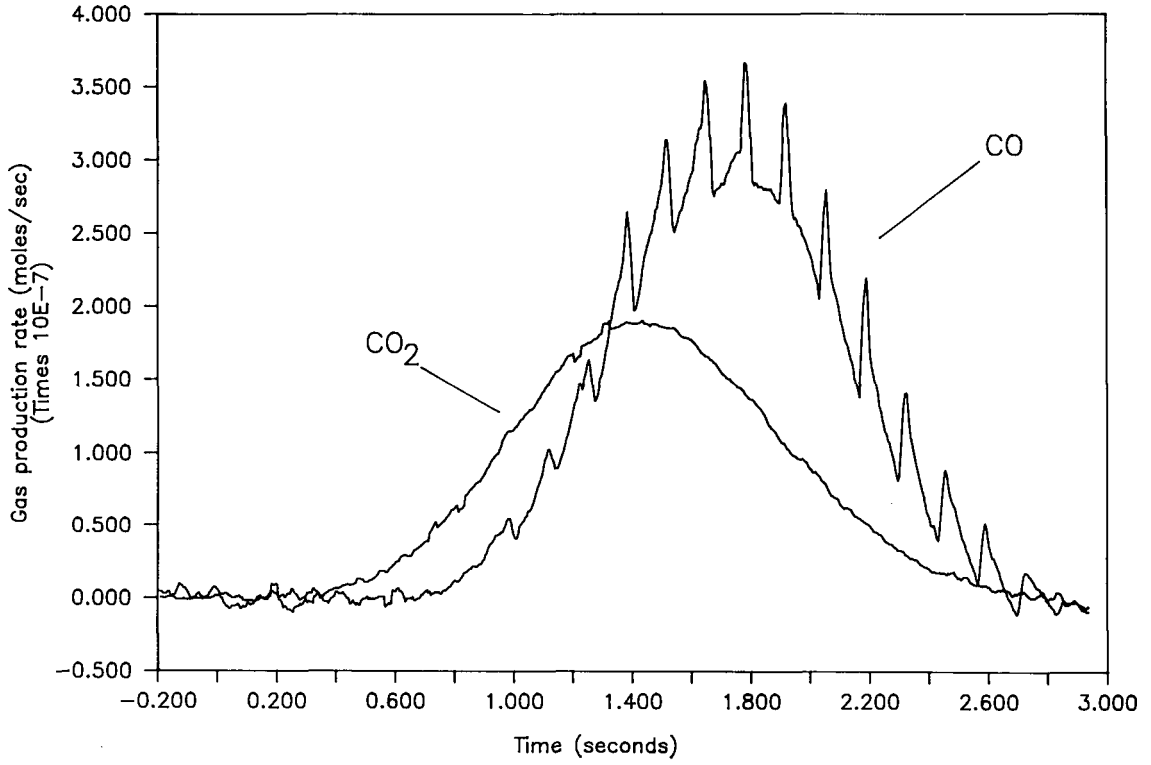

Figure 24. Rates of CO and CO_2 production from dry Beulah lignite fusain at 650°C.

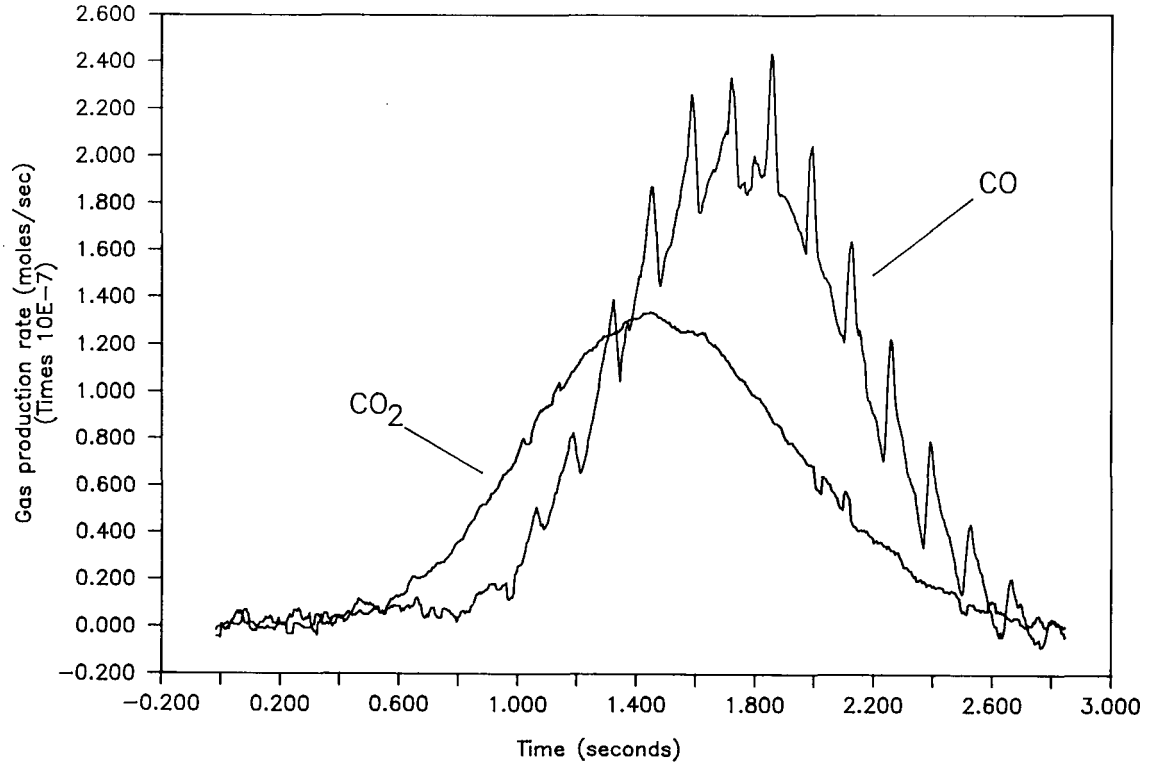

Figure 25. Rates of CO and CO_2 production from dry Beulah lignite attritus at 650°C.

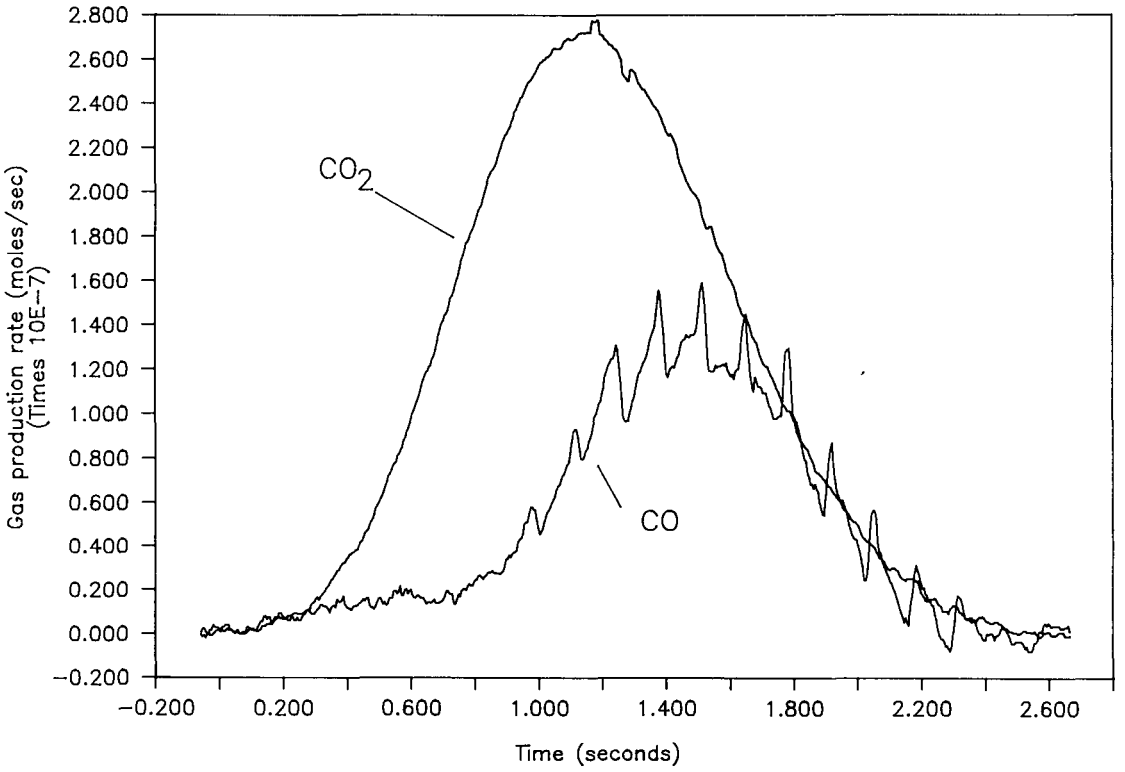

Figure 26. Rates of CO and CO_2 production from dry Beulah lignite vitrain at 1000°C.

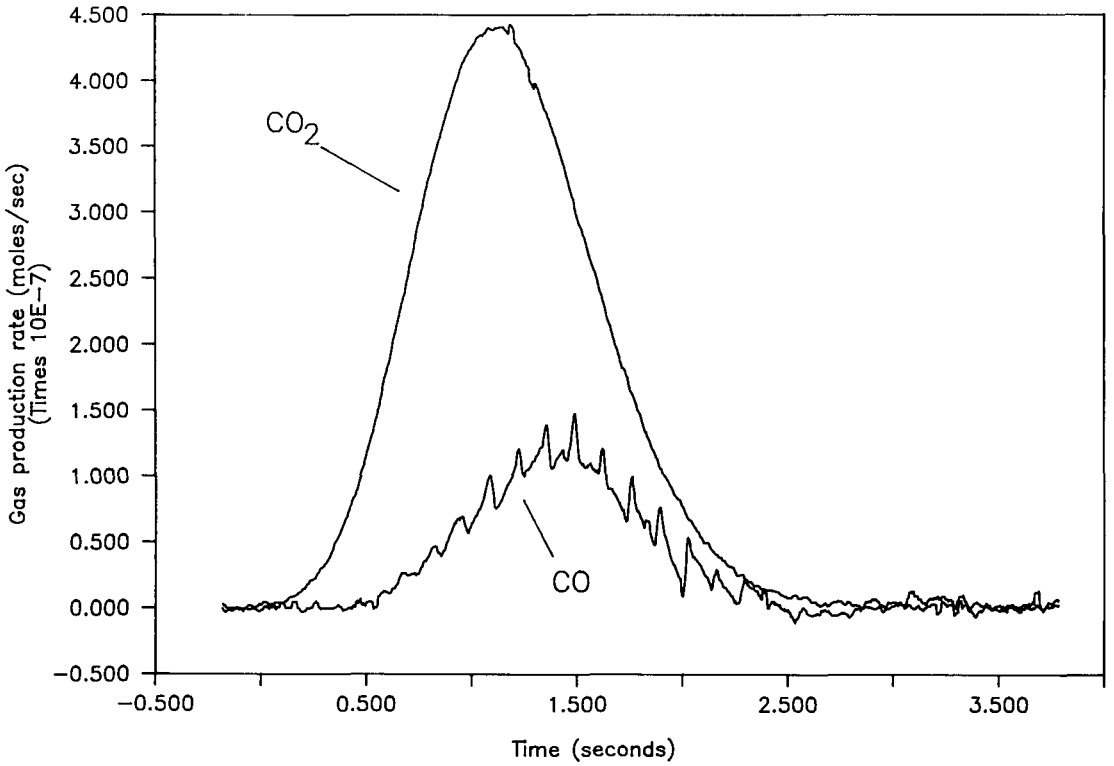

Figure 27. Rates of CO and CO_2 production from dry Pittsburgh #8 vitrain at 1000°C.

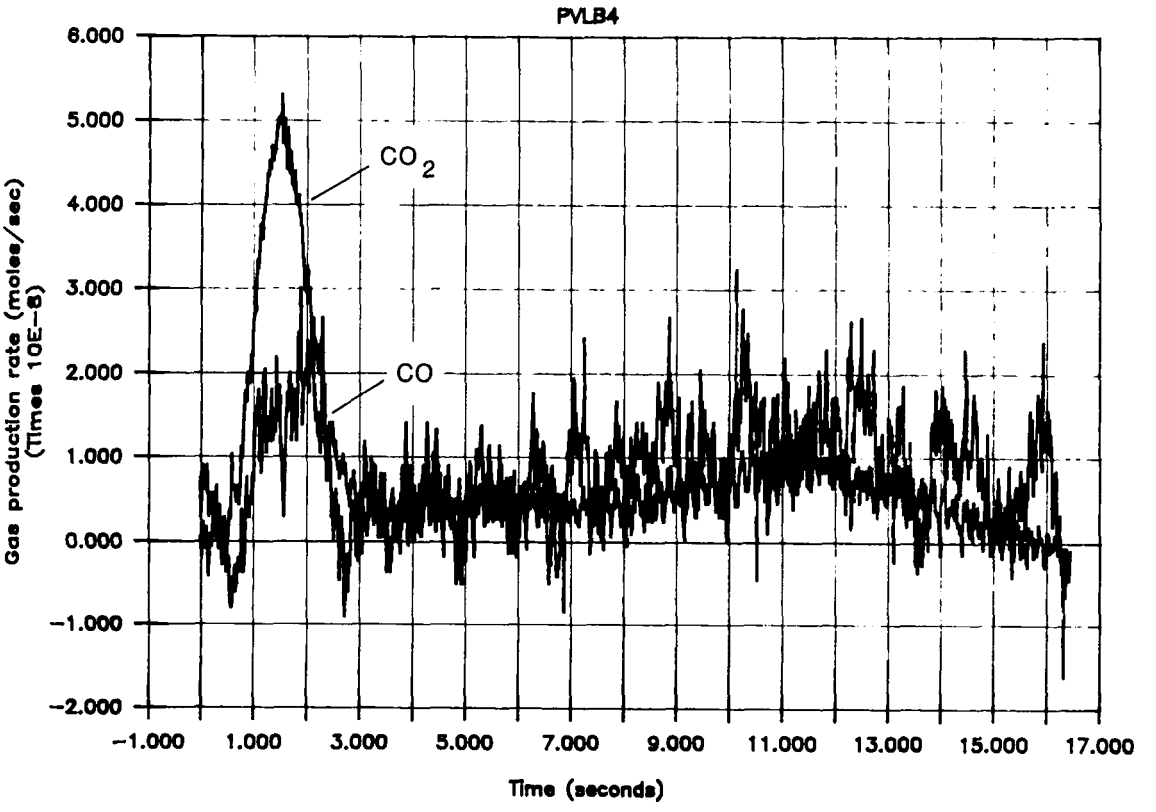

Figure 28. Rates of CO and CO_2 production from dry Pittsburgh #8 vitrain at 650°C.

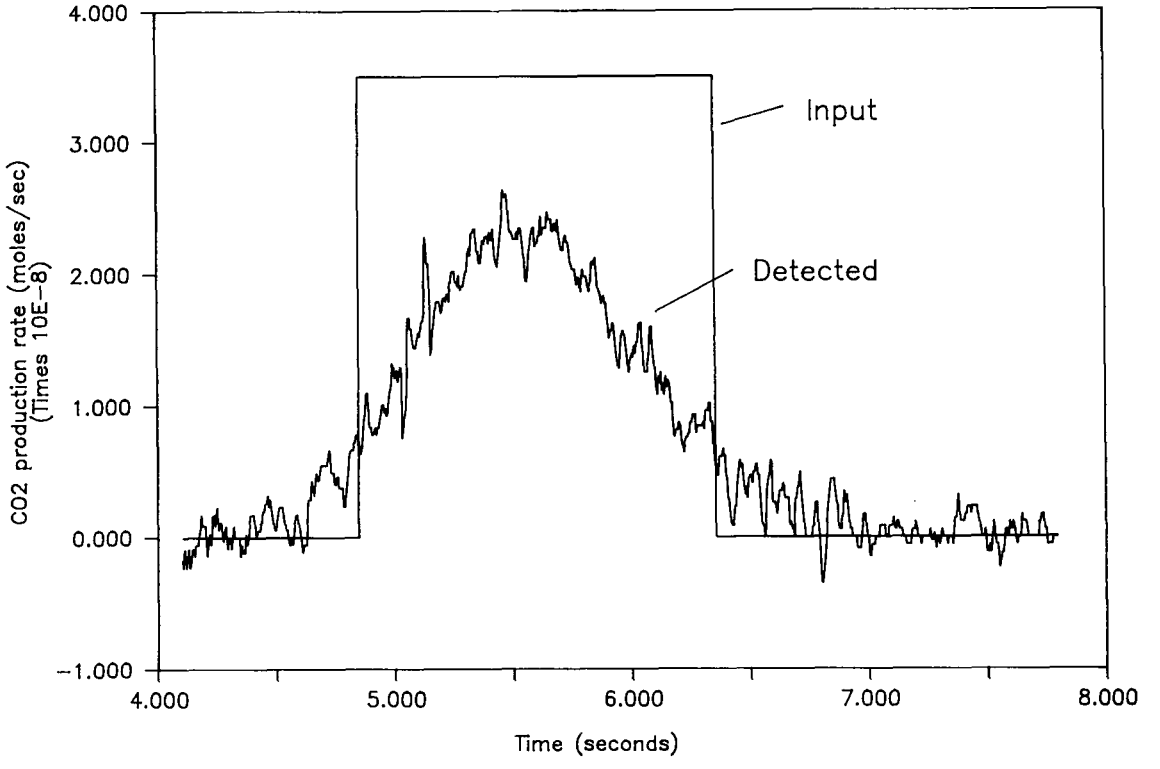

Figure 29. Evaluation of sample distortion.

Three possible mechanisms exist for the formation of CO_2: initial production at the particle surface, oxidation of CO to CO_2 in the boundary layer of the particle where the gas temperature is influenced by the particle, and CO oxidation in the bulk gas phase during the transition of the gas sample through the combustion zone furnace. In order to remove the latter mechanism from consideration, its magnitude was quantitated by introducing CO/air mixtures into the combustion furnace at various temperatures. No significant CO oxidation was observed at or below 825°C. At 1000°C significant conversion was observed, and an overall rate constant was estimated. The CO_2:CO product and rate ratios reported in Table 21 were corrected for conversion of CO to CO_2 in the bulk gas stream.

The Arrhenius activation energies and preexponential factors for both the Beulah lignite and Pittsburgh #8 vitrains are presently being calculated.

4.4 Results and Discussion

The quantitative results of the ignition studies are summarized in Table 21. In Figures 22-28 the differentiated CO_2 and CO analyses, containing no corrections for diffusional distortion or conversion of CO to CO_2 in the bulk gas phase, are presented to show relative differences in particle CO_2 and CO production rates.

The initial tests of the ignition apparatus at 650°, 825°,and 1000°C using Pittsburgh #8 coal produced bimodal distributions of the ignition delays and the maximum combustion rates (32). These responses were, therefore, divided into two groups. Group 1 responses were defined by long ignition delays, slow combustion rates, and poor mass balances. Group 2 particles had shorter ignition delays, faster combustion rates, and good mass balances. Group 1 responses occurred 80% of the time.

In order to determine if these bimodal responses were produced by the apparatus itself or by an uncharacterized parameter of the coal particles, malonic acid particles were studied in the ignition apparatus. This material was chosen because of its uniform composition and its low decarboxylation temperature (140°C). The results of these tests showed standard deviations in the delay between the trigger and initial CO_2 detection of 0.013 sec at 650°C and 0.042 sec at 1000°C. These were much smaller than those previously observed and were not bimodaly distributed.

Repetition of the initial coal data with the stainless steel injector was necessary, since the initial coal tests were performed with a quartz drop tube injector, which attracted and immobilized a large percentage of the coal particles. The malonic acid tests were performed with a stainless steel injection tube, which did not produce particle immobilization. Upon repetition, unimodal distributions of the coal ignition delays, combustion rates, and mass balances were observed. The results were similar to those previously categorized as Group 2. It seems, therefore, that the earlier observed bimodal distribution of combustion behaviors was due to a large portion of the particles being trapped in the drop tube and combusting in this sheltered region, thus producing diluted CO_2/CO gas streams.

A major goal of the initial experiments was to define the lower particle size limit for which ignition delays and combustion behavior could be determined. The average particle employed to date has had a volume of 6.0×10^{-6} cm^3 (the same volume as a 225 micrometer diameter sphere). These particles produced excellent results, from which it was estimated that the 1000°C ignition delays of particles having volumes as small as 5.7×10^{-8} cm^3 (the same volume as a 48-micrometer diameter sphere) could be distinguished from the CO_2 analyzer response.

In order for the future kinetic parameter evaluations to be valid, the ignition delays used must be those of the heterogeneous particle combustion process rather than those of a combusting volatile cloud. A comparison of a coal to its char can be performed in order to determine the effects of volatiles on the measured ignition delay (27,34). Since heterogeneous ignition is usually assumed for char particles, small differences between the ignition characteristics of these two materials indicate the likelihood of heterogeneous coal ignition. Since chars have not yet been examined in the present studies, the only experimental evidence presently available for the occurrence of heterogeneous ignition consists of the observation of rapid single-stage combustion during most of the ignition tests (see Table 21).

Studies have been performed to ascertain the parameters which dictate the limits of heterogeneous and homogeneous ignition. Morrison reviewed the effects of temperature, oxygen concentration, and particle size on the ignition mechanism of Beulah lignite particles (22). These results indicated that heterogeneous ignition should occur for 200-micrometer particles in 20% O_2 at temperatures of approximately 500°C or greater, conditions met in the present study. Chen et al. (35) saw little difference between the ignition temperatures, detected by light emission, of a char and a bituminous coal at particle sizes between 60 and 230 micrometers. Heterogeneous ignition for both materials was concluded. These results indicate that the present experiments are in the region where heterogeneous ignition occurs. Further studies, however, will be performed on coal chars to confirm this mechanism.

The effect of moisture on the combustion of the vitrain lithotype of Beulah lignite at 650°C is shown in Table 21 and Figures 22 and 23. No effect of moisture on the ignition delay, or maximum carbon conversion rate was observed. The CO_2:CO rate ratio was slightly higher for the water-containing runs. Most coal particle moisture is expected to be vaporized during the initial heating of the coal particle and hence affects the ignition delay more than the overall conversion rate. The fact that moisture did not affect the ignition delay indicates that the energy necessary for its devolatilization was small in comparison to that necessary to produce ignition. This result is consistent with those of Harker and Mellor (25) who did not observe a moisture effect on the ignition temperature of a coal. If some moisture did remain until the ignition of the coal particle, its presence would not be expected to significantly affect the carbon conversion rate due to the large exothermicity of the combustion reactions.

The CO_2 and CO production curves seen in Figures 22-28 show a slightly delayed production of CO with respect to CO_2. This same phenomena was reported by Gomez (23) and Gomez and Vastola (27). Insufficient data is presently available to estimate the significance of this result.

The combustion behaviors of the different lithotypes of Beulah lignite were examined (see Table 21 and Figures 23, 24, and 25). These three materials behaved similarly in all respects except for their ignition delays. Fusain had a significantly shorter delay than either vitrain or attritus. Karcz et al. (31) also reported shorter ignition delays for both anthracite and bituminous coal fusains than for their vitrains. This is a somewhat surprising result due to the poor reactivity usually associated with fusinite and semifusinite (36), which are major constituents of fusain (37). The resolution of this anomaly may be in the much higher surface areas of the fusain particles than the vitrain particles (31). Essenhigh (21), citing earlier work (29), suggested that internal surface area has a significant effect on the ignition of char particles. Other workers (4) have emphasized the effects of inherent mineral matter over differing surface areas. Detailed characterization of the mineral matter content in the various lithotypes would help resolve the question.

The effect of temperature on the vitrain lithotypes of both the lignite and bituminous coal was examined (see Table 21 and Figures 23, 26, 27, and 28). For the lignite, increasing the temperature dramatically decreased the ignition delay, slightly increased the CO_2:CO ratios, and had no effect on the maximum carbon conversion rate or combustion time. Examination of Figures 23 and 26 shows that single-stage burning occurred at both temperatures. For the bituminous coal, increased temperature dramatically decreased the ignition delay and total combustion time, increased the maximum carbon conversion rate, and had no effect on the CO_2:CO rate ratio. The mass recovery and CO_2:CO production ratio are underestimated for the 650°C data set since the combustion time exceeded the 6.5-second residence time of the CO_2 analyses. Examination of Figures 27 and 28 shows that two different burning regimes existed for the low-temperature combustion of the bituminous coal.

The decrease in ignition delay with increased temperature is an expected phenomena and results from the more rapid energy transfer rates to the particles at the higher temperatures. The increased carbon conversion rates of the bituminous coal with increased temperature are a result of faster char combustion at the higher temperature and the resulting shift from two- to single-stage combustion. Tsai and Scaroni (28) have reported the effect of gas temperature (723° to 923°C) on the mass loss of combusting bituminous coal particles. These workers reported that increased temperatures: 1) decrease ignition delays, 2) increase char combustion rates, and 3) have little effect on the volatiles combustion rate. These results are consistent with the present findings. The lack of a large effect of gas temperature on the maximum carbon conversion rate of the lignite is perhaps a reflection of having approached a maximum particle temperature.

The effect of rank on combustion behavior is also seen in Table 21 and Figures 23, 26, 27, and 28. Comparison of the Beulah lignite results at 1000°C to those of the bituminous coal shows that these materials behave similarly. At 650°C, these materials have significant differences. The lignite's ignition delay and total combustion time are shorter, its CO_2:CO rate ratio is smaller, and its maximum carbon conversion rate is higher. The lignite has single-stage combustion, while the bituminous coal burns in two stages. The ignition delay and total combustion times, together with the carbon conversion rate, demonstrate that Beulah lignite is a more reactive material than the bituminous coal. The major difference in reactivity seems

to be in the chars of the materials and is highly temperature dependent. The higher reactivity of Beulah lignite char compared with Pittsburgh #8 char was reported by Young and Niksa (4).

4.5 Summary

The ignition apparatus was completed. An initial study of Pittsburgh #8 coal (PSOC-1451) was performed to define the sensitivity of the apparatus and optimum operational procedures. The results demonstrate the ability to determine CO_2 and CO production rates as well as ignition delays for coal particles having volumes of approximately 7.0×10^{-6} cm^3. Extrapolation of these results indicates the ability to measure ignition delays of particles of volumes as small as 5.7×10^{-8} cm^3.

The ignition characteristics of Beulah lignite (PSOC-1507) were defined as a function of moisture content, lithotype, and gas temperature. Moisture had little effect; some variations with lithotype were noted, with fusain appearing to be the most reactive; and increased gas temperature dramatically decreased ignition delays. Comparisons of the lignite runs to those of the bituminous coal showed lignite to be the more reactive material.

4.6 Future Work

The effect of particle size, volatile matter content, and oxygen concentration on the ignition characteristics of Beulah lignite (PSOC-1507) will be examined.

5.0 REFERENCES

1. Tichenor, D.A., Mitchell, R.E., Hencken, K.R., and Niksa, S. Twentieth Symposium (International) on Combustion, Ann Arbor, Michigan, 1985, The Combustion Institute, p. 1213.

2. Schafer, H.N.S. Fuel 1970, **49**, 3.

3. Young, B.C., McCollor, D.P., Weber, B.J., and Jones, M.L. Fuel 1988, **67**, 40.

4. Young, B.C. and Niksa, S. Fuel 1988, **67**, 155.

5. Kleesattel, D., Benson, S.A., Jones, M.L., and McCollor, D.P. "Extended Abstracts," Joint Conf. Western States and Japanese Sections, 1987, The Combustion Institute, p. 122.

6. Benson, S.A., McCollor, D.P., Kleesattel, D., and Grow, D.T. "Coal/Char Reactivity," Final Technical Progress Report for the Period April 1, 1986, to March 31, 1987. University of North Dakota Energy & Mineral Research Center/U.S. Department of Energy Cooperative Agreement No. DE-FC21-86MC10637, April 1987.

7. Stach, E., Taylor, G.H., Mackowsky, M.T., Chandra, D., Teichmuller, M., and Teichmuller, R. 3rd. ed., Coal Petrography, Gerbruder-Borntraegger, Berlin-Stuttgart, 1982, p. 535.

8. Field, M.A., Gill, D.W., Morgan, B.B., and Hawksley, P.G.W. "Combustion of Pulverized Coal," Leatherhead, 1967, p. 191.

9. Frank-Danumetskii, D.A. Diffusion and Heat Transfer in Chemical Kinetics, 2nd ed., Plenum Press, New York, 1969, p. 108.

10. Fletcher, T. Sandia National Laboratories, Stanford, CA, private communication.

11. McCollor, D.P., Sweeny, P.G., Grow, D.T., and Benson, S.A. "Coal/Char Reactivity," Sixth Quarterly Technical Progress Report for the Period July-September 1987. University of North Dakota Energy & Mineral Resarch Center/U.S. Department of Energy Cooperative Agreement No. DE-FC21-86MC10637, October 1987.

12. Hurley, J.P., Steadman, E.N., and Kleesattel, D.R. Distribution of Inorganics Final Report, DOE/FE/60181-2094, June 1986.

13. Laurendeau, N.M. Prog. Energy Sci. 1978, **4**, 221.

14. Henchamps, C. and Duval, X. Carbon 1966, **4**, 223.

15. Walker, P.L. Jr., Mahajan, O.P., and Komatsu, M. Am. Chem. Soc. Div. Fuel Chem. Prepr. 1979, **24**, 10.

16. Amarigilo, H. and Duval, X. Carbon 1966, **4**, 323.

17. McKee, D.W. Chemistry and Physics of Carbon, (Eds. P.L. Walker Jr. and P.A. Thrower), Marcel Dekker, 1981, **16**, 1.

18. Margenav, H. and Murphy, G.M. The Mathematics of Physics and Chemistry, Van Nostrand, Princeton, NJ, 1956.

19. Smythe, W. Static and Dynamic Electricity, McGraw-Hill, New York, 1968.

20. Carslan, H.S. and Jaegar, J.C. Conduction of Heat in Solids, Oxford University Press, 1959.

21. Essenhigh, R.H. in "Chemistry of Coal Utilization -- Second Supplementary Volume" (Ed., M.A. Elliott), John Wiley & Sons, 1981, p. 1153.

22. Morrison, G.F. "Understanding Pulverized Coal Combustion: IEA Coal Research," International Energy Agency Coal Research, London, United Kingdom, 1986, PCA03/MFA01. File number TI87900593, available NTIS.

23. Gomez, C.O. M.Sc. Thesis, Pennsylvania State University, 1982.

24. Bandyopadhyay, S. and Bhaduri, D. Combustion and Flame 1972, **18**, 411.

25. Harker, J.H. and Mellor, N.S. J. Inst. Energy 1986, **59**, 154.

26. Ashu, J.T., Nsakala, N.Y., Mahyjun, O.P., and Walker, P.L. Fuel 1978, **57**, 250.

27. Gomez, C.O. and Vastola, F.J. Fuel 1985, **64**, 558.

28. Tsai, C.Y. and Scaroni, A.W. Energy and Fuels 1987, **1**, 263.

29. Cogoli, J.G., Gray, D., and Essenhigh, R.H. Combustion Science and Technology 1977, **16**, 165.

30. Wall, T.F. and Gururajan, V.S. Combustion and Flame 1986, **66**, 151.

31. Karcz, H.K., Kordylewski, W., and Rybak, W. Fuel 1980, **59**, 799.

32. Seventh Quarterly Technical Progress Report for the Period October-December 1987. University of North Dakota Energy & Mineral Research Center/U.S. Department of Energy Cooperative Agreement No. DE-FC21-86MC10637, January 1988.

33. Deevi, S.C. and Suuberg, E.M. Fuel 1987, **66**, 454.

34. Wall, T.F. Second Australian Coal Science Conference, 1986, 1, 117.

35. Chen, M.R., Fan, L.S., and Essenhigh, R.H. Twentieth Symposium (International) on Combustion/The Combustion Institute, 1984, 1513.

36. Nandi, B.N., Brown, T.D., and Lee, G.K. Fuel 1977, **56**, 125.

37. Kleesattel, D.R. Proceedings from "1984 Symposium on the Geology of Rocky Mountain Coal," Bismarck, ND, 1984 (Ed. Houghton, R.L. and Clausen, E.N.). North Dakota Geological Society Publication 84-1, p. 28.

APPENDIX

BY COAL/CHAR TYPE

STEFAN-CORRECTED CHI AND RHO

CHAR TYPE=B(DEMINERAL-8.0%) AVG SIZE*(MICRONS)=58

(XO2)	VOL.MATTER (%W/W)	GAS TEMP (K)	PARTICLE TEMP (K)	WALL TEMP (K)	NO.DATA USED	TOTAL NO. GATHERED	STD DEV	HEIGHT (MM)	CHI	RHO(g/(cm^2 sec)	TOTAL PRESSURE
0.10	7.1	1006	1531	400	11	18	51	150	0.98	0.0172	0.966
0.15	7.1	1001	1634	400	36	60	53	150	0.80	0.0213	0.970

CHAR TYPE=B(DEMINERAL-8.0%) AVG SIZE*(MICRONS)=69

(XO2)	VOL.MATTER (%W/W)	GAS TEMP (K)	PARTICLE TEMP (K)	WALL TEMP (K)	NO.DATA USED	TOTAL NO. GATHERED	STD DEV	HEIGHT (MM)	CHI	RHO(g/(cm^2 sec)	TOTAL PRESSURE
0.06	6.9	1028	1459	400	23	30	66	150	1.35	0.0122	0.986
0.10	6.9	1013	1508	400	37	57	44	150	0.96	0.0140	0.964
0.15	6.9	1021	1641	400	10	31	58	150	0.81	0.0184	0.976
0.15	6.9	911	1662	400	29	53	58	150	0.96	0.0210	0.965

CHAR TYPE=B(DEMINERAL-8.0%) AVG SIZE*(MICRONS)=82.5

(XO2)	VOL.MATTER (%W/W)	GAS TEMP (K)	PARTICLE TEMP (K)	WALL TEMP (K)	NO.DATA USED	TOTAL NO. GATHERED	STD DEV	HEIGHT (MM)	CHI	RHO(g/(cm^2 sec)	TOTAL PRESSURE
0.1	6.9	1006	1514	400	12	18	57	150	1	0.0124	0.982

CHAR TYPE=B1(CA) AVG SIZE*(MICRONS)=58

(XO2)	VOL.MATTER (%W/W)	GAS TEMP (K)	PARTICLE TEMP (K)	WALL TEMP (K)	NO.DATA USED	TOTAL NO. GATHERED	STD DEV	HEIGHT (MM)	CHI	RHO(g/(cm^2 sec)	TOTAL PRESSURE
0.06	17.4	1011	1418	400	37	59	49	150	1.24	0.0130	0.981
0.10	17.4	1014	1538	400	32	60	45	150	0.97	0.0173	0.981
0.15	17.4	1012	1676	400	14	30	52	150	0.84	0.0227	0.981

CHAR TYPE=B1(CA) AVG SIZE*(MICRONS)=69

(XO2)	VOL.MATTER (%W/W)	GAS TEMP (K)	PARTICLE TEMP (K)	WALL TEMP (K)	NO.DATA USED	TOTAL NO. GATHERED	STD DEV	HEIGHT (MM)	CHI	RHO(g/(cm^2 sec)	TOTAL PRESSURE
0.05	19.5	1001	1400	400	32	60	58	150	1.50	0.0109	0.969
0.10	19.5	1006	1582	400	36	60	48	150	1.08	0.0166	0.991
0.10	19.5	904	1524	400	43	60	62	150	1.14	0.0165	0.977
0.15	19.5	1006	1699	400	29	59	54	150	0.91	0.0207	0.973
0.15	19.5	902	1683	400	35	58	42	150	1.00	0.0219	0.968

CHAR TYPE=B1(CA) AVG SIZE*(MICRONS)=82.5

(XO2)	VOL.MATTER (%W/W)	GAS TEMP (K)	PARTICLE TEMP (K)	WALL TEMP (K)	NO.DATA USED	TOTAL NO. GATHERED	STD DEV	HEIGHT (MM)	CHI	RHO(g/(cm^2 sec)	TOTAL PRESSURE
0.05	18.5	1000	1396	400	40	58	43	150	1.55	0.0094	0.966
0.10	18.5	1002	1578	400	39	60	40	150	1.14	0.0143	0.974
0.15	18.5	1001	1725	400	11	58	41	150	0.98	0.0189	0.974
0.15	18.5	1001	1737	400	19	56	33	150	1.01	0.0192	0.966

CHAR TYPE=B1(DM) AVG SIZE*(MICRONS)=58

(XO2)	VOL.MATTER (%W/W)	GAS TEMP (K)	PARTICLE TEMP (K)	WALL TEMP (K)	NO.DATA USED	TOTAL NO. GATHERED	STD DEV	HEIGHT (MM)	CHI	RHO(g/(cm^2 sec)	TOTAL PRESSURE
0.06	12.1	1002	1440	400	19	30	30	150	1.34	0.0140	0.970
0.10	12.1	1001	1556	400	32	60	52	150	1.03	0.0182	0.970
0.15	12.1	1006	1666	400	36	60	47	150	0.84	0.0225	0.965

BY COAL/CHAR TYPE
STEFAN-CORRECTED CHI AND RHO

CHAR TYPE=B1(DM) AVG SIZE*(MICRONS)=69

(XO2)	VOL.MATTER (%W/W)	GAS TEMP (K)	PARTICLE TEMP (K)	WALL TEMP (K)	NO.DATA USED	TOTAL NO. GATHERED	STD DEV	HEIGHT (MM)	CHI	RHO(g/(cm^2 sec)	TOTAL PRESSURE
0.06	7.9	1009	1427	400	19	30	53	150	1.31	0.0116	0.975
0.10	7.9	1010	1534	400	20	29	41	150	1.02	0.0149	0.956
0.15	7.9	1009	1702	400	7	13	73	150	0.90	0.0207	0.978
0.15	7.9	1010	1694	400	14	32	76	150	0.91	0.0204	0.961

CHAR TYPE=B1(DM) AVG SIZE*(MICRONS)=82.5

(XO2)	VOL.MATTER (%W/W)	GAS TEMP (K)	PARTICLE TEMP (K)	WALL TEMP (K)	NO.DATA USED	TOTAL NO. GATHERED	STD DEV	HEIGHT (MM)	CHI	RHO(g/(cm^2 sec)	TOTAL PRESSURE
0.06	12.5	1024	1400	400	17	25	56	150	1.23	0.0091	0.982
0.10	12.5	999	1531	400	46	60	53	150	1.05	0.0130	0.975
0.15	12.5	1000	1709	400	13	28	41	150	0.96	0.0184	0.975
0.15	12.5	1020	1685	400	20	33	41	150	0.90	0.0173	0.982

CHAR TYPE=B1(HCL) AVG SIZE*(MICRONS)=69

(XO2)	VOL.MATTER (%W/W)	GAS TEMP (K)	PARTICLE TEMP (K)	WALL TEMP (K)	NO.DATA USED	TOTAL NO. GATHERED	STD DEV	HEIGHT (MM)	CHI	RHO(g/(cm^2 sec)	TOTAL PRESSURE
0.06	13.6	998	1417	400	29	45	53	150	1.34	0.0116	0.967
0.10	13.6	1005	1504	400	37	59	43	150	0.95	0.0141	0.976
0.15	13.6	1005	1605	400	18	30	36	150	0.78	0.0174	0.976
0.15	13.6	1009	1616	400	36	58	48	150	0.79	0.0177	0.975

CHAR TYPE=B1(K) AVG SIZE*(MICRONS)=58

(XO2)	VOL.MATTER (%W/W)	GAS TEMP (K)	PARTICLE TEMP (K)	WALL TEMP (K)	NO.DATA USED	TOTAL NO. GATHERED	STD DEV	HEIGHT (MM)	CHI	RHO(g/(cm^2 sec)	TOTAL PRESSURE
0.06	20	1008	1478	400	36	60	37	150	1.43	0.0152	0.971
0.10	20	1005	1616	400	27	54	47	150	1.13	0.0204	0.971
0.15	20	1010	1737	400	17	37	30	150	0.92	0.0253	0.970

CHAR TYPE=B1(K) AVG SIZE*(MICRONS)=69

(XO2)	VOL.MATTER (%W/W)	GAS TEMP (K)	PARTICLE TEMP (K)	WALL TEMP (K)	NO.DATA USED	TOTAL NO. GATHERED	STD DEV	HEIGHT (MM)	CHI	RHO(g/(cm^2 sec)	TOTAL PRESSURE
0.05	23.5	1002	1429	400	27	45	46	150	1.59	0.0118	0.978
0.10	23.5	1004	1642	400	9	30	29	150	1.22	0.0186	0.968
0.10	23.5	1006	1661	400	28	59	32	150	1.25	0.0192	0.974
0.15	23.5	1002	1755	400	15	30	42	150	0.99	0.0228	0.971

CHAR TYPE=B1(K) AVG SIZE*(MICRONS)=82.5

(XO2)	VOL.MATTER (%W/W)	GAS TEMP (K)	PARTICLE TEMP (K)	WALL TEMP (K)	NO.DATA USED	TOTAL NO. GATHERED	STD DEV	HEIGHT (MM)	CHI	RHO(g/(cm^2 sec)	TOTAL PRESSURE
0.05	21.3	999	1425	400	29	60	49	150	1.65	0.0101	0.975
0.10	21.3	999	1635	400	27	60	43	150	1.27	0.0160	0.962
0.15	21.3	993	1762	400	22	60	32	150	1.09	0.0202	0.962

CHAR TYPE=B1(NA) AVG SIZE*(MICRONS)=69

(XO2)	VOL. MATTER (%W/W)	GAS TEMP (K)	PARTICLE TEMP (K)	WALL TEMP (K)	NO. DATA USED	TOTAL NO. GATHERED	STD DEV	HEIGHT (MM)	CHI	RHO(g/(cm^2 sec)	TOTAL PRESSURE
0.05	25.2	1005	1398	400	35	60	43	150	1.47	0.0108	0.977
0.10	25.2	1009	1557	400	21	60	43	150	1.05	0.0157	0.977
0.14	25.2	1008	1671	400	20	59	39	150	0.93	0.0196	0.972
0.15	25.2	1008	1695	400	17	30	63	150	0.90	0.0205	0.972

CHAR TYPE=B1(NA) AVG SIZE*(MICRONS)=82.5

(XO2)	VOL. MATTER (%W/W)	GAS TEMP (K)	PARTICLE TEMP (K)	WALL TEMP (K)	NO. DATA USED	TOTAL NO. GATHERED	STD DEV	HEIGHT (MM)	CHI	RHO(g/(cm^2 sec)	TOTAL PRESSURE
0.05	24.7	1010	1402	400	33	60	53	150	1.52	0.0094	0.981
0.10	24.7	1011	1556	400	9	22	41	150	1.08	0.0136	0.978
0.10	24.7	1008	1540	400	36	59	52	150	1.05	0.0131	0.979
0.15	24.7	1005	1686	400	34	60	39	150	0.92	0.0176	0.981

CHAR TYPE=B1(UT) AVG SIZE*(MICRONS)=58

(XO2)	VOL. MATTER (%W/W)	GAS TEMP (K)	PARTICLE TEMP (K)	WALL TEMP (K)	NO. DATA USED	TOTAL NO. GATHERED	STD DEV	HEIGHT (MM)	CHI	RHO(g/(cm^2 sec)	TOTAL PRESSURE
0.05	15.2	1002	1427	400	21	32	32	150	1.53	0.0135	0.984
0.10	15.2	1004	.	400	2	20	.	150	.	.	0.983
0.10	15.2	1024	1619	400	36	50	44	150	1.11	0.0201	0.969
0.14	15.2	1006	1721	400	15	56	41	150	0.97	0.0247	0.965

CHAR TYPE=B1(UT) AVG SIZE*(MICRONS)=69

(XO2)	VOL. MATTER (%W/W)	GAS TEMP (K)	PARTICLE TEMP (K)	WALL TEMP (K)	NO. DATA USED	TOTAL NO. GATHERED	STD DEV	HEIGHT (MM)	CHI	RHO(g/(cm^2 sec)	TOTAL PRESSURE
0.05	15.7	1000	1403	400	28	50	45	150	1.51	0.0110	0.972
0.10	15.7	1014	1593	400	29	54	44	150	1.11	0.0168	0.971
0.10	15.7	900	1525	400	29	47	42	150	1.16	0.0166	0.971
0.12	15.7	907	1605	400	11	21	68	150	1.09	0.0191	0.976
0.15	15.7	1011	1731	400	11	30	42	150	0.95	0.0217	0.965
0.15	15.7	903	1679	400	12	24	30	150	0.98	0.0217	0.975

CHAR TYPE=B1(UT) AVG SIZE*(MICRONS)=82.5

(XO2)	VOL. MATTER (%W/W)	GAS TEMP (K)	PARTICLE TEMP (K)	WALL TEMP (K)	NO. DATA USED	TOTAL NO. GATHERED	STD DEV	HEIGHT (MM)	CHI	RHO(g/(cm^2 sec)	TOTAL PRESSURE
0.05	14.4	1020	1427	400	42	60	35	150	1.60	0.0098	0.972
0.10	14.4	1020	1586	400	18	36	52	150	1.12	0.0143	0.977
0.15	14.4	1012	1749	400	27	60	38	150	1.00	0.0195	0.973

CHAR TYPE=B2(CA) AVG SIZE*(MICRONS)=69

(XO2)	VOL. MATTER (%W/W)	GAS TEMP (K)	PARTICLE TEMP (K)	WALL TEMP (K)	NO. DATA USED	TOTAL NO. GATHERED	STD DEV	HEIGHT (MM)	CHI	RHO(g/(cm^2 sec)	TOTAL PRESSURE
0.06	23.3	1006	1550	400	25	59	44	150	1.70	0.0155	0.970
0.06	23.3	1006	1433	400	21	30	39	150	1.34	0.0118	0.978
0.10	23.3	1006	1553	400	9	30	49	150	1.04	0.0156	0.978
0.10	23.3	1008	1556	400	29	60	66	200	1.07	0.0157	0.956
0.15	23.2	1005	1677	400	14	28	43	100	0.88	0.0199	0.970
0.15	23.2	1009	1688	400	29	59	43	150	0.88	0.0202	0.979
0.15	23.3	1009	1688	400	29	59	43	150	0.88	0.0202	0.979

CHAR TYPE=B2(CA) AVG SIZE*(MICRONS)=82.5

(XO2)	VOL. MATTER (%W/W)	GAS TEMP (K)	PARTICLE TEMP (K)	WALL TEMP (K)	NO. DATA USED	TOTAL NO. GATHERED	STD DEV	HEIGHT (MM)	CHI	RHO(g/(cm^2 sec)	TOTAL PRESSURE
0.06	23.1	1000	1423	400	22	30	34	150	1.38	0.0101	0.973
0.10	23.1	1002	1574	400	20	30	44	150	1.15	0.0142	0.963

CHAR TYPE=B2(CA-RDM) AVG SIZE*(MICRONS)=82.5

(XO2)	VOL. MATTER (%W/W)	GAS TEMP (K)	PARTICLE TEMP (K)	WALL TEMP (K)	NO. DATA USED	TOTAL NO. GATHERED	STD DEV	HEIGHT (MM)	CHI	RHO(g/(cm^2 sec)	TOTAL PRESSURE
0.06	24.9	1003	1458	400	17	30	48	150	1.47	0.0108	0.960
0.06	23.1	1002	1468	400	18	30	38	150	1.48	0.0112	0.993
0.08	24.9	1005	1542	400	17	30	51	150	1.32	0.0132	0.973
0.08	24.9	1001	1518	400	22	30	32	150	1.27	0.0126	0.973
0.10	24.9	1010	1616	400	18	30	49	150	1.21	0.0153	0.960
0.10	23.1	1010	1584	400	14	29	45	150	1.12	0.0144	0.987

CHAR TYPE=B2(DM) AVG SIZE*(MICRONS)=69

(XO2)	VOL. MATTER (%W/W)	GAS TEMP (K)	PARTICLE TEMP (K)	WALL TEMP (K)	NO. DATA USED	TOTAL NO. GATHERED	STD DEV	HEIGHT (MM)	CHI	RHO(g/(cm^2 sec)	TOTAL PRESSURE
0.05	13.2	1006	1376	400	22	30	35	100	1.39	0.0101	0.981
0.05	13.2	1012	1444	400	13	30	75	150	1.61	0.0120	0.978
0.10	13.2	1006	1617	400	11	30	39	100	1.16	0.0177	0.981
0.10	13.2	1012	1622	400	13	30	32	150	1.16	0.0178	0.978
0.15	13.2	1006	1709	400	15	29	29	100	0.91	0.0210	0.981
0.15	13.2	1012	1736	400	14	30	56	150	0.94	0.0219	0.978

CHAR TYPE=B2(DM) AVG SIZE*(MICRONS)=82.5

(XO2)	VOL. MATTER (%W/W)	GAS TEMP (K)	PARTICLE TEMP (K)	WALL TEMP (K)	NO. DATA USED	TOTAL NO. GATHERED	STD DEV	HEIGHT (MM)	CHI	RHO(g/(cm^2 sec)	TOTAL PRESSURE
0.06	.	1016	1550	400	5	8	40	150	1.73	0.0133	0.978
0.06	.	1003	1440	400	12	28	47	150	1.41	0.0105	0.979
0.08	.	1003	1599	400	18	26	37	150	1.45	0.0149	0.979
0.10	.	1005	1651	400	19	28	46	125	1.32	0.0164	0.947
0.10	.	1005	1656	400	24	30	45	150	1.30	0.0166	0.964
0.10	.	1009	1636	400	19	29	42	150	1.25	0.0159	0.967
0.10	.	1009	1668	400	17	29	45	150	1.32	0.0169	0.967
0.10	.	1005	1666	400	18	30	48	175	1.35	0.0169	0.947
0.10	.	1009	1650	400	11	30	45	200	1.28	0.0163	0.967
0.10	.	1005	1662	400	15	30	39	200	1.34	0.0168	0.949

CHAR TYPE=B2(DM-RDM) AVG SIZE*(MICRONS)=62.5

(XO2)	VOL. MATTER (XW/W)	GAS TEMP (K)	PARTICLE TEMP (K)	WALL TEMP (K)	NO. DATA USED	TOTAL NO. GATHERED	STD DEV	HEIGHT (MM)	CHI	RHO(g/(cm^2 sec)	TOTAL PRESSURE
0.08	.	1003	1584	400	14	28	28	150	1.40	0.0145	0.989
0.10	.	1001	1657	400	17	30	45	150	1.28	0.0167	0.987

CHAR TYPE=B2(K) AVG SIZE*(MICRONS)=69

(XO2)	VOL. MATTER (XW/W)	GAS TEMP (K)	PARTICLE TEMP (K)	WALL TEMP (K)	NO. DATA USED	TOTAL NO. GATHERED	STD DEV	HEIGHT (MM)	CHI	RHO(g/(cm^2 sec)	TOTAL PRESSURE
0.05	22.4	1005	1351	400	15	30	51	100	1.31	0.0094	0.976
0.05	22.4	1004	1411	400	16	29	64	150	1.52	0.0112	0.981
0.10	22.4	998	1599	400	34	60	30	100	1.14	0.0173	0.976
0.10	22.4	1004	1593	400	13	30	29	100	1.12	0.0170	0.975
0.10	22.4	1004	1645	400	9	30	36	150	1.21	0.0187	0.981
0.15	22.4	1004	1694	400	15	30	37	100	0.90	0.0205	0.975
0.15	22.4	1004	1719	400	13	29	62	150	0.93	0.0214	0.981

CHAR TYPE=B2(K) AVG SIZE*(MICRONS)=62.5

(XO2)	VOL. MATTER (XW/W)	GAS TEMP (K)	PARTICLE TEMP (K)	WALL TEMP (K)	NO. DATA USED	TOTAL NO. GATHERED	STD DEV	HEIGHT (MM)	CHI	RHO(g/(cm^2 sec)	TOTAL PRESSURE
0.08	23	1003	1538	400	11	24	42	150	1.33	0.0131	0.983
0.08	23	1012	1523	400	17	30	39	150	1.25	0.0126	0.977
0.10	23	1013	1566	400	14	29	47	150	1.10	0.0138	0.977

CHAR TYPE=B2(K-RDM) AVG SIZE*(MICRONS)=82.5

(XO2)	VOL. MATTER (%W/W)	GAS TEMP (K)	PARTICLE TEMP (K)	WALL TEMP (K)	NO. DATA USED	TOTAL NO. GATHERED	STD DEV	HEIGHT (MM)	CHI	RHO(g/(cm^2 sec)	TOTAL PRESSURE
0.08	21.6	1003	1522	400	17	29	51	150	1.29	0.0127	0.963
0.10	21.6	1004	1542	400	19	28	53	150	1.08	0.0133	0.963

CHAR TYPE=B2(NA) AVG SIZE*(MICRONS)=69

(XO2)	VOL. MATTER (%W/W)	GAS TEMP (K)	PARTICLE TEMP (K)	WALL TEMP (K)	NO. DATA USED	TOTAL NO. GATHERED	STD DEV	HEIGHT (MM)	CHI	RHO(g/(cm^2 sec)	TOTAL PRESSURE
0.06	22.8	1010	1396	400	14	29	39	100	1.23	0.0106	0.967
0.06	22.8	1005	1461	400	34	58	51	150	1.45	0.0127	0.962
0.10	22.8	1010	1569	400	11	29	37	100	1.08	0.0161	0.967
0.10	22.8	1002	1604	400	33	60	34	150	1.16	0.0174	0.961
0.15	22.8	1010	1616	400	8	28	44	100	0.80	0.0177	0.967
0.15	22.8	1002	1701	400	29	61	50	150	0.92	0.0208	0.961

CHAR TYPE=B2(NA) AVG SIZE*(MICRONS)=82.5

(XO2)	VOL. MATTER (%W/W)	GAS TEMP (K)	PARTICLE TEMP (K)	WALL TEMP (K)	NO. DATA USED	TOTAL NO. GATHERED	STD DEV	HEIGHT (MM)	CHI	RHO(g/(cm^2 sec)	TOTAL PRESSURE
0.06	22.4	1004	1458	400	18	30	38	150	1.47	0.0109	0.978
0.08	22.4	1001	1499	400	19	30	59	150	1.62	0.0121	0.978
0.10	22.4	1014	1557	400	20	28	58	150	1.08	0.0135	0.977

CHAR TYPE=B2(NA-RDM) AVG SIZE*(MICRONS)=62.5

(XO2)	VOL. MATTER (%W/W)	GAS TEMP (K)	PARTICLE TEMP (K)	WALL TEMP (K)	NO. DATA USED	TOTAL NO. GATHERED	STD DEV	HEIGHT (MM)	CHI	RHO(g/(cm^2 sec)	TOTAL PRESSURE
0.06	20.1	1005	1418	400	14	22	41	150	1.34	0.0099	0.980
0.08	20.1	1011	1503	400	20	30	60	150	1.23	0.0120	0.962
0.10	20.1	1005	1550	400	22	29	62	150	1.09	0.0135	0.962

CHAR TYPE=B2(UT) AVG SIZE*(MICRONS)=49

(XO2)	VOL. MATTER (%W/W)	GAS TEMP (K)	PARTICLE TEMP (K)	WALL TEMP (K)	NO. DATA USED	TOTAL NO. GATHERED	STD DEV	HEIGHT (MM)	CHI	RHO(g/(cm^2 sec)	TOTAL PRESSURE
0.1	.	1001	1606	400	8	30	46	150	1.09	0.0232	0.976
0.1	.	999	1604	400	12	30	57	150	1.08	0.0232	0.983

CHAR TYPE=B2(UT) AVG SIZE*(MICRONS)=69

(XO2)	VOL. MATTER (%W/W)	GAS TEMP (K)	PARTICLE TEMP (K)	WALL TEMP (K)	NO. DATA USED	TOTAL NO. GATHERED	STD DEV	HEIGHT (MM)	CHI	RHO(g/(cm^2 sec)	TOTAL PRESSURE
0.05	14.7	1013	1416	400	19	30	46	150	1.53	0.0112	0.967
0.10	14.7	1010	1604	400	16	30	29	100	1.13	0.0172	0.975
0.10	14.7	1013	1609	400	17	30	30	150	1.15	0.0173	0.967
0.15	14.7	1010	1704	400	18	29	37	100	0.91	0.0208	0.975
0.15	14.7	1013	1761	400	19	30	69	150	0.99	0.0238	0.967

FUNDAMENTAL COMBUSTION RUN SUMMARY
BY COAL/CHAR TYPE
STEFAN-CORRECTED CHI AND RHO

CHAR TYPE=LNB(DM) AVG SIZE*(MICRONS)=69

(XO2)	VOL. MATTER (%W/W)	GAS TEMP (K)	PARTICLE TEMP (K)	WALL TEMP (K)	NO. DATA USED	TOTAL NO. GATHERED	STD DEV	HEIGHT (MM)	CHI	RHO(g/(cm^2 sec)	TOTAL PRESSURE
0.06	.	1002	1477	400	16	30	44	150	1.49	0.0132	0.967
0.08	.	995	1510	400	17	29	48	150	1.21	0.0144	0.976
0.08	.	1002	1580	400	21	30	48	150	1.37	0.0166	0.967

CHAR TYPE=LNB(UT) AVG SIZE*(MICRONS)=69

(XO2)	VOL. MATTER (%W/W)	GAS TEMP (K)	PARTICLE TEMP (K)	WALL TEMP (K)	NO. DATA USED	TOTAL NO. GATHERED	STD DEV	HEIGHT (MM)	CHI	RHO(g/(cm^2 sec)	TOTAL PRESSURE
0.05	.	1008	1410	400	9	30	50	150	1.53	0.0111	0.959
0.05	.	1016	1387	400	20	43	37	150	1.43	0.0102	0.956
0.05	.	1016	1387	400	20	43	37	150	1.43	0.0102	0.956
0.10	.	1008	1649	400	9	30	28	150	1.24	0.0188	0.959
0.10	.	1016	1594	400	17	44	43	150	1.13	0.0168	0.956
0.10	.	1016	1594	400	17	44	43	150	1.13	0.0168	0.956

CHAR TYPE=LWX(CA) AVG SIZE*(MICRONS)=69

(XO2)	VOL. MATTER (%W/W)	GAS TEMP (K)	PARTICLE TEMP (K)	WALL TEMP (K)	NO. DATA USED	TOTAL NO. GATHERED	STD DEV	HEIGHT (MM)	CHI	RHO(g/(cm^2 sec)	TOTAL PRESSURE
0.06	25.3	1027	1386	400	6	8	44	150	1.16	0.0100	0.961
0.06	25.3	1020	1378	400	8	18	56	150	1.15	0.0099	0.966
0.10	25.3	1017	1511	400	36	58	45	150	0.96	0.0141	0.964
0.10	25.3	1014	1559	400	22	58	47	200	1.05	0.0157	0.973
0.15	25.3	1012	1647	400	15	29	43	150	0.84	0.0187	0.964
0.15	25.3	1024	1655	400	14	28	66	150	0.84	0.0188	0.961
0.15	25.3	1019	1642	400	25	55	48	200	0.82	0.0184	0.972

CHAR TYPE=LWX(DM) AVG SIZE*(MICRONS)=69

(XO2)	VOL. MATTER (%W/W)	GAS TEMP (K)	PARTICLE TEMP (K)	WALL TEMP (K)	NO. DATA USED	TOTAL NO. GATHERED	STD DEV	HEIGHT (MM)	CHI	RHO(g/(cm^2 sec)	TOTAL PRESSURE
0.06	13.5	1016	1444	400	17	30	38	150	1.36	0.0120	0.964
0.06	13.5	1017	1465	400	17	30	37	150	1.40	0.0126	0.980
0.06	13.5	1019	1450	400	28	60	29	200	1.37	0.0121	0.969
0.10	13.5	1030	1622	400	20	60	55	150	1.16	0.0175	0.959
0.10	13.5	1013	1621	400	39	60	39	200	1.16	0.0178	0.973
0.15	13.5	1016	1717	400	32	59	43	150	0.93	0.0211	0.964
0.15	13.5	1028	1690	400	20	44	37	200	0.87	0.0200	0.971

FUNDAMENTAL COMBUSTION RUN SUMMARY
BY COAL/CHAR TYPE
STEFAN-CORRECTED CHI AND RHO

CHAR TYPE=LWX(NA) AVG SIZE*(MICRONS)=69

(XO2)	VOL. MATTER (%W/W)	GAS TEMP (K)	PARTICLE TEMP (K)	WALL TEMP (K)	NO. DATA USED	TOTAL NO. GATHERED	STD DEV	HEIGHT (MM)	CHI	RHO(g/(cm^2 sec)	TOTAL PRESSURE
0.05	23	1017	1389	400	19	30	51	150	1.40	0.0103	0.980
0.10	23	1014	1612	400	24	57	45	150	1.14	0.0174	0.982
0.15	23	1014	1695	400	16	29	50	150	0.88	0.0204	0.982
0.15	23	1027	1711	400	9	28	29	150	0.90	0.0207	0.971

CHAR TYPE=LWX(UT) AVG SIZE*(MICRONS)=69

(XO2)	VOL. MATTER (%W/W)	GAS TEMP (K)	PARTICLE TEMP (K)	WALL TEMP (K)	NO. DATA USED	TOTAL NO. GATHERED	STD DEV	HEIGHT (MM)	CHI	RHO(g/(cm^2 sec)	TOTAL PRESSURE
0.06	18.3	1012	1435	400	13	29	37	100	1.32	0.0118	0.981
0.06	18.3	1022	1438	400	17	28	38	150	1.31	0.0117	0.976
0.06	18.3	1019	1415	400	28	60	45	200	1.26	0.0110	0.969
0.10	18.3	1006	1535	400	23	30	40	100	1.00	0.0150	0.984
0.10	18.3	1011	1579	400	13	29	39	100	1.08	0.0164	0.977
0.10	18.3	1017	1613	400	26	59	36	150	1.14	0.0174	0.980
0.10	18.3	1013	1599	400	20	60	68	200	1.12	0.0170	0.974
0.15	18.3	1011	1656	400	39	58	60	100	0.84	0.0191	0.977
0.15	18.3	1022	1693	400	26	58	46	150	0.88	0.0202	0.976
0.15	18.3	1024	1671	400	18	60	47	200	0.86	0.0194	0.964

CHAR TYPE=NMB(CA) AVG SIZE*(MICRONS)=69

(XO2)	VOL. MATTER (%W/W)	GAS TEMP (K)	PARTICLE TEMP (K)	WALL TEMP (K)	NO. DATA USED	TOTAL NO. GATHERED	STD DEV	HEIGHT (MM)	CHI	RHO(g/(cm^2 sec)	TOTAL PRESSURE
0.06	22.7	1013	1391	400	16	28	27	100	1.20	0.0104	0.968
0.06	22.7	1011	1446	400	35	60	39	150	1.38	0.0121	0.967
0.10	22.7	1014	1574	400	35	58	39	100	1.07	0.0162	0.979
0.10	22.7	1032	1633	400	23	44	26	150	1.16	0.0178	0.976
0.15	22.7	1016	1711	400	15	28	34	100	0.91	0.0209	0.979
0.15	22.7	1011	1729	400	22	60	41	150	0.95	0.0217	0.967

CHAR TYPE=NMB(DM) AVG SIZE*(MICRONS)=69

(XO2)	VOL. MATTER (%W/W)	GAS TEMP (K)	PARTICLE TEMP (K)	WALL TEMP (K)	NO. DATA USED	TOTAL NO. GATHERED	STD DEV	HEIGHT (MM)	CHI	RHO(g/(cm^2 sec)	TOTAL PRESSURE
0.06	54.2	1005	1439	400	12	30	41	150	1.39	0.0120	0.957
0.06	54.2	1022	1463	400	27	57	38	200	1.41	0.0124	0.963
0.06	54.2	1006	1426	400	16	31	44	200	1.33	0.0116	0.965
0.10	54.2	1009	1559	400	22	30	62	100	1.06	0.0158	0.968
0.10	54.2	1011	1540	400	26	30	54	100	1.02	0.0151	0.968
0.10	54.2	1006	1629	400	30	58	43	150	1.19	0.0181	0.972
0.10	54.2	1016	1616	400	30	56	38	200	1.15	0.0175	0.975
0.15	54.2	1011	1685	400	38	71	52	100	0.89	0.0201	0.968
0.15	54.2	1005	1728	400	24	56	28	150	0.96	0.0217	0.957
0.15	54.2	1016	1718	400	15	44	35	200	0.92	0.0212	0.970

CHAR TYPE=NMB(K) AVG SIZE*(MICRONS)=69

(XO2)	VOL. MATTER (%W/W)	GAS TEMP (K)	PARTICLE TEMP (K)	WALL TEMP (K)	NO. DATA USED	TOTAL NO. GATHERED	STD DEV	HEIGHT (MM)	CHI	RHO(g/(cm^2 sec)	TOTAL PRESSURE
0.06	42.3	1008	1403	400	11	29	51	100	1.26	0.0109	0.964
0.06	22.4	987	1451	400	16	29	46	150	1.47	0.0127	0.956
0.06	22.4	1003	1469	400	21	30	40	150	1.49	0.0130	0.956
0.10	42.3	1010	1583	400	30	60	34	100	1.10	0.0165	0.971
0.10	22.4	1011	1594	400	36	57	52	150	1.13	0.0169	0.960
0.10	22.4	1022	1635	400	27	59	34	200	1.18	0.0181	0.972
0.15	42.3	1010	1684	400	34	60	37	100	0.88	0.0201	0.971
0.15	22.4	994	1683	400	15	30	49	150	0.91	0.0203	0.956
0.15	22.4	1010	1725	400	10	29	26	150	0.94	0.0215	0.967

CHAR TYPE=NMB(NA) AVG SIZE*(MICRONS)=69

(XO2)	VOL. MATTER (%W/W)	GAS TEMP (K)	PARTICLE TEMP (K)	WALL TEMP (K)	NO. DATA USED	TOTAL NO. GATHERED	STD DEV	HEIGHT (MM)	CHI	RHO(g/(cm^2 sec)	TOTAL PRESSURE
0.05	18.8	999	1358	400	20	30	37	100	1.36	0.0097	0.969
0.06	18.8	1022	1436	400	18	30	47	150	1.32	0.0116	0.968
0.10	18.8	1006	1527	400	22	35	49	100	1.01	0.0148	0.964
0.10	18.8	993	1604	400	29	58	50	150	1.18	0.0175	0.956
0.10	18.8	1017	1596	400	13	29	66	150	1.13	0.0168	0.956
0.10	18.8	1017	1607	400	17	29	43	150	1.14	0.0172	0.968
0.15	18.8	1002	1686	400	27	55	36	100	0.88	0.0203	0.986
0.15	18.8	1016	1747	400	14	30	38	150	0.96	0.0222	0.968

CHAR TYPE=NMB(UT) AVG SIZE*(MICRONS)=69

(XO2)	VOL.MATTER (%W/W)	GAS TEMP (K)	PARTICLE TEMP (K)	WALL TEMP (K)	NO.DATA USED	TOTAL NO. GATHERED	STD DEV	HEIGHT (MM)	CHI	RHO(g/(cm^2 sec)	TOTAL PRESSURE
0.05	20.5	1009	1386	400	36	57	47	150	1.41	0.0103	0.985
0.10	20.5	1006	1589	400	30	59	31	100	1.12	0.0168	0.968
0.10	20.5	1009	1549	400	47	60	52	150	1.02	0.0154	0.987
0.10	20.5	902	1577	400	33	60	36	150	1.24	0.0182	0.983
0.15	20.5	1005	1682	400	11	30	46	100	0.89	0.0201	0.968
0.15	20.5	1006	1668	400	34	57	44	100	0.87	0.0196	0.970
0.15	20.5	1009	1639	400	22	58	58	150	0.81	0.0185	0.985
0.15	20.5	902	1671	400	32	60	44	150	0.97	0.0214	0.983

CHAR TYPE=PTC(SPECIAL) AVG SIZE*(MICRONS)=69

(XO2)	VOL.MATTER (%W/W)	GAS TEMP (K)	PARTICLE TEMP (K)	WALL TEMP (K)	NO.DATA USED	TOTAL NO. GATHERED	STD DEV	HEIGHT (MM)	CHI	RHO(g/(cm^2 sec)	TOTAL PRESSURE
0.1	.	983	1580	400	15	30	35	150	1.13	0.0169	0.973